

# Fluid Dynamics of Sprays—1992 Freeman Scholar Lecture

**William A. Sirignano**

Department of Mechanical  
and Aerospace Engineering,  
University of California, Irvine,  
Irvine, CA 92717-2700

*Various theoretical and computational aspects of the fluid dynamics of sprays are reviewed. Emphasis is given to rapidly vaporizing sprays on account of the richness of the scientific phenomena and the several, often disparate, time scales. Attention is given to the behavior of individual droplets including the effects of forced convection due to relative droplet-gas motion, Stefan convection due to the vaporization or condensation of the liquid, internal circulation of the liquid, interactions with neighboring droplets, and interactions with vortical eddies. Flow field details in the gas boundary layer and wake and in the liquid droplet interior are examined. Also, the determinations of droplet lift and drag coefficients and Nusselt and Sherwood numbers and their relationships with Reynolds number, transfer number, Prandtl and Schmidt numbers, and spacing between neighboring droplets are extensively discussed. The spray equations are examined from several aspects; in particular, two-continua, multi-continua, discrete-particle, and probabilistic formulations are given. The choice of Eulerian or Lagrangian representation of the liquid-phase equations within these formulations is discussed including important computational issues and the relationship between the Lagrangian method and the method of characteristics. Topics for future research are suggested.*

## 1 Introduction

A spray is one type of two-phase flow. It involves a liquid as the dispersed or discrete phase in the form of droplets or ligaments and a gas as the continuous phase. There are many occurrences of spray phenomena in power and propulsion applications, industrial applications, and nature. A dusty flow is very similar to a spray except that the discrete phase is solid rather than liquid. Bubbly flow is the opposite kind of two-phase flow wherein the gas forms the discrete phase and the liquid is the continuous phase. Generally, the liquid density is considerably larger than the gas density, so bubble motion involves lower kinematic inertia, higher drag force, and different behavior under gravity force than droplet motion.

The fluid dynamics of sprays is a rapidly developing field of broad importance. There are many interesting applications of spray theory related to power, propulsion, heat exchange, and materials processing. Important and intellectually challenging fluid dynamic phenomena can occur in many different ways with sprays. On the scale of an individual droplet in a spray, boundary layers and wakes appear due to relative motion between the droplet center and the ambient gas. Other complicated and coupled fluid dynamic factors are abundant: shear-driven internal circulation of the liquid in the droplet, Stefan flow due to vaporization or condensation, flow modifications due to closely neighboring droplets in the spray, hydrodynamic interfacial instabilities leading to droplet shape distortion and perhaps droplet shattering, and droplet inter-

actions with vortical structures in the gas flow (e.g., turbulence). On a much larger and coarser scale, we have the complexities of the integrated exchanges of mass, momentum, and energy of many droplets in some subvolume of interest with the gas flow in the same subvolume. The problem is further complicated by the strong coupling of the phenomena on the different scales; one cannot describe the mass, momentum, and energy exchanges on the large scale without detailed knowledge of the fine-scale phenomena. Note that in some practical applications, these scales can differ by several orders of magnitude so that a challenging subgrid modeling problem results.

The author's research interests have focused on the theoretical and computational aspects of the spray problem. Therefore, this review will emphasize those aspects. Major, but not total attention, will be given to the research of the author and his co-workers. Also, detailed consideration will be given to applications where the mass vaporization rate is very large since this is the most complex situation and therefore its coverage leads to the most general formulation of the theory. In particular, as the vaporization rate increases, the coupling between the two phases becomes stronger and, as the droplet lifetime becomes as small as some of the other characteristic times, the transient or dynamic character of the problem emerges in a dominant manner.

The fast vaporization rate is especially prominent in situations where the ambient gas is at very high temperatures (of the order of 1000 K or higher). Combustion with liquid fuels is the most notable example here. The spray combustion regime is a most interesting limiting case of the more general field of

Contributed by the Fluids Engineering Division for publication in the JOURNAL OF FLUIDS ENGINEERING. Manuscript received by the Fluids Engineering Division November 20, 1992; revised manuscript received February 18, 1993. Associate Technical Editor: D. P. Telionis.

thermal and dynamic behavior of sprays. In the high temperature domain, rapid vaporization causes droplet lifetimes to be as short as the time for a droplet to heat throughout its interior. It can be shorter than the time for liquid-phase mass diffusion to result in the mixing of various components in a multicomponent liquid. The combustion limit is inherently transient from the perspective of the droplet, richer in terms of scientific issues, and more challenging analytically and numerically than low temperature spray problems.

The spray problem is complicated by the presence of spatial temperature and concentration gradients and internal circulation in the liquid. Interaction amongst droplets is another complication to be treated.

There is a great disparity in the magnitudes of the scales. Liquid-phase mass diffusion is slower than liquid-phase heat diffusion which, in turn, is much slower than the diffusion of vorticity in the liquid. Transport in the gas is faster than transport in the liquid. Droplet diameters are typically of the order of a few tens of microns to a few hundreds of microns in diameter. Resolution of internal droplet gradients can imply resolution on the scale of microns or even on a submicron scale. Combustor or flow chamber dimensions can be five or six orders of magnitude greater than the required minimum resolution. Clearly, subgrid droplet vaporization models are required to make progress on this problem.

Experiments have been successful primarily in resolving the global characteristics of sprays. The submillimeter scales associated with the spray problem have made detailed experimental measurements very difficult. If an attempt is made to increase droplet size, similarity is lost; droplet Reynolds number can be kept constant by decreasing velocity but the Grashof number grows implying that buoyancy becomes relatively more important. Also, Weber number decreases as droplet size increases; surface tension becomes relatively less important and the droplet is more likely to acquire a nonspherical shape. Modern nonintrusive laser diagnostics have made resolution possible on a scale less than one hundred microns so that, in recent years, more experimental information has been appearing. Nevertheless, theory and computation have led experiment in terms of resolving the fluid dynamical characteristics of spray flows.

In Section 2, we shall discuss the vaporization of individual droplets and study the phenomenon on the scale of the droplet

diameter. The theoretical models and correlations of computational results for individual droplets can be used to describe exchanges of mass, momentum, and energy between the phases in a spray flow. The spray with its many droplets is examined in Section 3. Much of the results presented in Sections 2 and 3 can be helpful in engineering practice. Some of the information already appears in computational codes; modification of the codes to address more recent advances should not be difficult. One shortcoming, of course, is the limited experimental verification as previously discussed. Interactions amongst a few droplets and their effects on the modification of the theory are discussed in Section 4. Turbulence-droplet interactions are briefly surveyed in Section 5. Concluding remarks are stated in Section 6. The spray discussion of Section 3 precedes the topics of Sections 4 and 5 because droplet-droplet interactions and turbulence-droplet interactions have not yet been fully integrated into a comprehensive spray theory. These interaction studies are still active research domains and, so far, little application to engineering practice has occurred. Due to length limitations on this article, several important areas of spray phenomena are not discussed. Excluded examples are primary and secondary atomization, slurry sprays, and radiation-droplet interactions.

## 2 Theory of Isolated Droplet Vaporization, Heating and Acceleration

The vaporizing droplet problem is a challenging, multidisciplinary issue. It can involve heat and mass transport, fluid dynamics and chemical kinetics. In general, there is a relative motion between a droplet and its ambient gas. Here, the general aerodynamic characteristics of pressure gradients, viscous boundary layers, separated flows, and wakes can appear for the gas flow over the droplet. Reynolds number based upon the relative velocity, droplet diameter, and gas-phase properties is a very important descriptor of the gaseous flow field. Internal liquid circulation, driven by surface shear forces, is another important fluid dynamic feature of the droplet problem.

These flow features have critical impact on the exchanges of mass, momentum, and energy between the gas and liquid phases. They are important for both vaporizing and nonvaporizing situations. The vaporizing case is complicated by re-gressing interfaces and boundary layer blowing.

### Nomenclature

$a$	= droplet acceleration	$t$	= time
$a$	= constant of curvature in stagnation point flow	$T$	= temperature
$a, b$	= parameters in Section 2.2, Eq. (50)	$u, v$	= velocity
$A$	= constant in Section 2.2	$U$	= free stream velocity
$\bar{A}$	= liquid vortex strength	$v$	= velocity in the argument of distribution function
$B$	= transfer number	$V$	= volume in eight-dimensional phase space
$C_D, C_L$	= drag and lift coefficients	$Q$	= energy per unit mass of fuel
$c_l$	= liquid specific heat	$r$	= spherical radial coordinate
$c_p$	= specific heat at constant pressure	$\tilde{r}$	= cylindrical radial coordinate
$d$	= droplet diameter	$r_f$	= flame radius
$D$	= mass diffusivity, droplet center-to-center spacing	$R$	= droplet radius
$e$	= thermal energy	$R_2$	= droplet radii ratio
$e$	= error	$R$	= gas constant
$e$	= unit vector	$Re$	= Reynolds number
$g_1, g_2$	= functions defined in Section 2.2, Eqs. (46)–(47)	$s$	= nondimensional radius
$f$	= Blasius function	$S$	= weighted area in numerical interpolation schemes
$f$	= droplet distribution func-	$Sh$	= Sherwood number
		$Sc$	= Schmidt number
		$t$	= time
		$T$	= temperature
		$u, v$	= velocity
		$U$	= free stream velocity
		$v$	= velocity in the argument of distribution function
		$V$	= volume in eight-dimensional phase space

There is interest in the droplet vaporization problem from two different aspects. First, we wish to understand the fluid dynamic and transport phenomena associated with the transient heating and vaporization of a droplet. Second, but just as important, we must develop models for droplet heating, vaporization, and acceleration that are sufficiently accurate and simple to use in a spray analysis involving very many droplets. The first goal can be met by examining both approximate analyses and finite-difference analyses of the governing Navier-Stokes equations. The second goal can only be addressed at this time with approximate analyses since Navier-Stokes resolution for the detailed flow field around each droplet is too costly in a practical spray problem. However, correlations from Navier-Stokes solutions provide useful inputs into approximate analyses.

Introductory descriptions of vaporizing droplet behavior can be found in Chigier (1981), Clift et al. (1978), Glassman (1987), Kanury (1975), Kuo (1986), Lefebvre (1989), and Williams (1985). Useful research reviews are given by Faeth (1983), Law (1982), and Sirignano (1983).

In developing the study of the gas flow field surrounding the droplet and of the liquid flow in the droplet, certain assumptions are employed. Small Mach number is considered so that kinetic energy and viscous dissipation are negligible. Gravity effects, droplet deformation, radiation, Dufour energy flux, and mass diffusion due to pressure and temperature gradients are all neglected. (Note, however, that thermophoresis can affect the transport rates for submicron particles: e.g., soot.) The multicomponent gas-phase mixture is assumed to behave as an ideal gas. Phase equilibrium is stated at the droplet-gas interface. Gas-phase density and thermophysical parameters are generally considered variable, unless otherwise stated. Liquid-phase viscosity is generally taken as variable in the finite-difference calculations but density and other properties are typically taken to be constant. The basic equations governing the gas flow are the Navier-Stokes equations for a viscous, variable density, and variable properties multicomponent mixture. The liquid-phase primitive equations are the incompressible Navier-Stokes equations; however, the stream-function, vorticity axisymmetric formulation is typically employed. These equations are described in general form by Williams (1985) and in boundary layer form by Chung (1965). Useful descriptions of the Navier-Stokes equations for single component (variable density and constant den-

sity) flow can be found in many reference books. Landau and Lifshitz (1987), Howarth (1964), Sherman (1990), and White (1991) are recommended. The formulation for the gas and the liquid phases of the axisymmetric droplet problem complete with boundary, interface, and initial conditions can be found in Chiang (1990).

In the limiting case where there is no relative motion between the droplet and the gas, a spherically symmetric field exists for the gas field surrounding the droplet and for the liquid field. If a small relative velocity occurs, the droplet acceleration becomes so large that the relative velocity between the droplet and the surrounding gas immediately goes to zero. Therefore, in this limit, relative velocity remains negligible even as the gas velocity varies. Here, the fluid motion is reduced to a Stefan convection in the radial direction. Although our major interest will be in the forced convection case, it is helpful to discuss briefly this spherically symmetric case. All of the important issues in this case will also appear in the more general case.

**2.1 Spherically-Symmetric Droplet Vaporization and Heating.** Consider the case where a spherical droplet vaporizes with a radial flow field in the gas-phase. The vapor from the droplet convects and diffuses away from the droplet surface. Heat conducts radially against the convection toward the droplet interface. At the droplet surface, the heat from the gas partially accommodates the phase change and the remainder conducts into the liquid interior, raising the liquid temperature at the surface and in the interior of the droplet. This type of convection is named Stefan convection. In case of condensation, the Stefan convective flux becomes negative.

In some cases, the reactant vapor, diffusing away from the vaporizing droplet, can mix in the gas film with the other reactant, diffusing from the ambient gas, and react in an exothermic manner. The energy source enhances the droplet heating and vaporization. This can happen with a fuel droplet vaporizing in an oxidizing environment if the reaction time is not longer than the film diffusion time; otherwise, a flame must envelop many droplets if it is to occur. See Sirignano (1983).

The liquid does not move relative to the droplet center in this spherically symmetric case. Rather, the surface regresses into the liquid as vaporization occurs. Therefore, heat and mass transfer in the liquid occur due only to diffusion with a

## Nomenclature (cont.)

$V$	liquid volume
$\dot{w}$	chemical reaction rate
$W$	molecular weight
$x$	spatial coordinate
$y$	normal coordinate in boundary layer
$Y$	mass fraction
$z$	spatial coordinate

### Greek Symbols

$\alpha$	thermal diffusivity
$\beta$	Shvab Zeldovich variables
$\delta$	distance ratio in Section 3
$\tilde{\delta}$	upstream distance for application of boundary condition
$\epsilon$	species flux fraction
$\epsilon$	correction in Section 3 for application of ambient conditions
$\eta$	Blasius coordinate
$\theta$	void volume fraction

$\lambda$	thermal conductivity
$\mu$	dynamic viscosity
$\nu$	stoichiometric coefficient (mass of fuel per mass of oxygen)
$\rho$	density
$\tau$	nondimensional time
$\tau_H$	droplet heating time
$\tau_L$	droplet lifetime
$\tau^*$	droplet heating time with uniform temperature
$\phi$	normalized streamfunction
$\varphi$	generic variable
$\chi$	ratio of effective thermal diffusivity to thermal diffusivity
$\psi$	liquid volume fraction
$\Psi$	stream function
$\omega$	velocity

### Subscripts

$0$	initial condition
$\infty$	conduction at infinity

$\text{eff}$	effective value
$F$	vapor or fuel vapor
$H$	related to thermal transfer
$i$	index for vectorial component, index for species component
$j$	index for vectorial component
$e$	edge of boundary layer
$L$	lift
$l$	liquid
$M$	related to mass transfer
$n, p$	integers for numerical mesh points
$N$	nitrogen
$O$	oxygen
$p$	particle
$P$	product
$s$	droplet surface condition
$wb$	wet bulb

### Superscript

$k$	index for droplet group
-----	-------------------------

moving boundary but without convection. Here, we present the spherically symmetric isolated droplet equations. A quasi-steady assumption is made for the gas phase because diffusion of heat and mass in the gas is relatively fast compared to the liquid; this assumption weakens as we approach the critical pressure.

#### Continuity

$$\frac{\partial}{\partial r} (\rho u r^2) = 0 \quad \text{or} \quad \rho u r^2 = \text{constant} = \frac{\dot{m}}{4\pi} \quad (1)$$

#### Energy

$$\frac{\partial}{\partial r} (\rho u r^2 h) - \frac{\partial}{\partial r} \left( \lambda r^2 \frac{\partial T}{\partial r} \right) = -\rho r^2 Q \dot{w}_F \quad (2)$$

#### Vapor Species Conservation

$$L(Y_F) = \frac{\partial}{\partial r} (\rho u r^2 Y_F) - \frac{\partial}{\partial r} \left( \rho D r^2 \frac{\partial Y_F}{\partial r} \right) = \rho r^2 \dot{w}_F \quad (3)$$

#### Oxygen Species Conservation

$$L(Y_O) = \rho r^2 \dot{w}_O = \rho r^2 \dot{w}_F / \nu \quad (4)$$

#### Nitrogen Species Conservation

$$L(Y_N) = 0 \quad (5)$$

#### Product Species Conservation

$$L(Y_P) = -\rho r^2 \dot{w}_P \left( \frac{\nu + 1}{\nu} \right) \quad \text{or} \quad Y_F + Y_O + Y_N + Y_P = 1 \quad (6)$$

In these equations, we assume very low Mach number (and therefore uniform pressure) and neglect Soret and Dufour effects and radiation. Also, we assume Fickian mass diffusion, Fourier heat conduction, and one-step chemical kinetics. In the limit of no chemical reaction,  $Y_P = 0$  and  $\dot{w}_P = 0$ . Equations of state for  $\rho$  and  $h$  are also prescribed; in particular, a perfect gas is usually considered.

Typically, ambient conditions at  $r = \infty$  are prescribed for  $Y_O$ ,  $Y_N$ ,  $Y_F$ ,  $Y_P$ , and  $T$ . Interface conditions are also prescribed at the droplet surface. Temperature is assumed to be continuous across the interface. Phase equilibrium is assumed at the interface typically by the use of the Clausius-Clapeyron relation. Mass balance at the interface is imposed for each species.

$$\frac{\dot{m}}{4\pi} Y_{i_s} - \rho D R^2 \frac{\partial Y_i}{\partial r} \Big|_s = \frac{\dot{m}}{4\pi} \delta_{iF}, \quad i = O, F, N, P \quad (7)$$

where  $\delta_{iF}$  is the Kronecker delta function.

For nonvaporizing species, radial convection and diffusion cancel each other. The right-hand side is nonzero only for the vaporizing species.

The energy balance at the interface equates the difference in conductive fluxes to the energy required to vaporize the liquid at the surface.

$$\lambda R^2 \frac{\partial T}{\partial r} \Big|_s = \lambda_e R^2 \frac{\partial T}{\partial r} \Big|_s + \frac{\dot{m}}{4\pi} L = \frac{\dot{m}}{4\pi} L_{\text{eff}} \quad (8)$$

where  $L_{\text{eff}}$  is an effective latent heat of vaporization.

In considering Eqs. (1) through (6), it should be realized that density is immediately related to temperature through an equation of state. Therefore, Eq. (1) can be considered to govern the radial gas velocity. Equations (2) through (6) are the second-order differential equations governing five quantities: temperature and the four mass fractions. Ten boundary or matching conditions would normally be required. We have a total of twelve conditions: five ambient conditions for the five quantities, five interface conditions given by Eqs. (7) and (8), a phase equilibrium condition at the interface, and a continuous temperature condition at the interface. Apparently, two extra conditions are presented that are needed because the problem has an eigenvalue character. The vaporization rate  $\dot{m}$  and the heat entering the liquid phase  $4\pi\lambda_e R^2 (\partial T/\partial r)_{t,s}$  are

unknown a priori. This means that, if  $T_s$  were known, the gas-phase problem could readily be solved without examining the details of the liquid phase. Another valid viewpoint is that, if the heating rate of the liquid were known, the gas-phase problem including the interface temperature could be readily determined without consideration of the liquid-phase details. However, in the general problem, neither the surface temperature nor the liquid heating rate are known a priori. An analysis of heat diffusion in the liquid phase is required in order to provide an additional relationship between the liquid heating rate and the interface temperature.

In the special case of very fast chemistry, constant specific heat and unitary Lewis number ( $\rho D = \lambda/c_p$ ) for the gas-phase, the gas-phase equations can be reduced to certain algebraic relations.

$$\dot{m} = 4\pi \left[ \int_R^\infty \frac{dr}{\rho D r^2} \right]^{-1} \log(1 + B) \quad (9)$$

where

$$B = \frac{h_\infty - h_s + \nu Q Y_{O\infty}}{L_{\text{eff}}} = \frac{\nu Y_{O\infty} + Y_{F\infty}}{1 - Y_{F\infty}} \quad (10)$$

Note that  $Y_{F\infty}$  is a function of  $T_s$  through the phase equilibrium relation. Therefore, Eqs. (8) and (10) relate interface temperature to liquid heating rate. When heating rate becomes zero,  $L_{\text{eff}} = L$ , and Eq. (10) yields the wet bulb temperature for the droplet.

In the special case under consideration, it is convenient to present the solution in terms of Shvab-Zeldovich variables  $\beta$  which satisfy  $L(\beta) = 0$ . In particular, we have

$$\begin{aligned} \beta_1 &\equiv Y_O - Y_F / \nu; \quad \beta_2 \equiv Y_O + Y_P / (1 + \nu); \\ \beta_3 &\equiv Y_O + h / \nu Q; \quad \beta_4 \equiv Y_N \end{aligned} \quad (11)$$

It is found that Eqs. (2) through (6) yield

$$\beta - \beta_\infty \sim \exp \left[ -\frac{m}{4\pi} \int_r^\infty \frac{dr'}{\rho D(r')^2} \right] - 1 \quad (12)$$

In the limit of negligible Stefan convection, the first derivative terms in Eqs. (2) through (6) can be neglected yielding

$$\beta - \beta_\infty \sim -\frac{m}{4\pi} \int_r^\infty \frac{dr'}{\rho D(r')^2} \quad (13)$$

Note that the same result can be found by a series expansion of Eq. (12) whereby the first term in the expansion gives the results with neglected Stefan flow. The constants of proportionality in Eqs. (12) and (13) are different for each of the four  $\beta$  functions and are determined from the interface conditions.

Equation (12) indicates a monotonic behavior with radius for the  $\beta$  functions. In the case where no exothermic reaction occurs in the gas film, a monotonic behavior for temperature and vapor mass fraction results. With chemical reaction, we have a peak in temperature and in product concentration occurring at the flame position. An infinitesimally thin flame assumption leads to certain simplifications in the determination of the profile in the reaction case. Without the thin flame assumption, the reacting case requires the integration of Eq. (4) coupled with Eqs. (11) and (12).

For very fast oxidation chemical kinetics, the reaction zone reaches the limit of zero thickness. Then  $\beta_1 = Y_O$  and  $Y_F = 0$  outside of the flame zone while  $\beta_1 = -Y_P/\nu$  and  $Y_O = 0$  inside the flame zone and  $Y_F = Y_O = 0$  at the flame zone. Now, determinations of  $Y_P$  and  $T$  from Eqs. (11) and (12) readily follow once the surface temperature is determined from the coupled liquid-phase solution.

The position of the flame zone can be determined for the thin flame case as

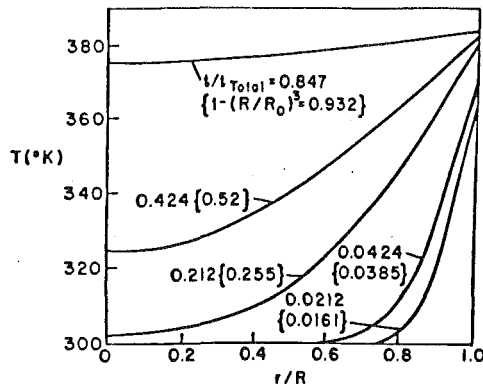


Fig. 1 Temporal and spatial variations of liquid temperature for spherically symmetric droplet vaporization. Temperature versus nondimensional radial coordinate for fixed fraction of droplet lifetime (or fixed vaporized fraction of original mass).

$$\frac{r_f}{R} = \frac{\log \left( \frac{1 + \nu Y_{O\infty}}{1 - Y_{Fs}} \right)}{\log(1 + Y_{O\infty})} \quad (14)$$

Now, the solution of the equation for heat diffusion through the liquid phase can be considered to provide the necessary relation between the interface temperature and the liquid heating rate. That equation is written in spherically symmetric form

$$\frac{\partial T_\ell}{\partial t} = \alpha_\ell \left( \frac{\partial^2 T_\ell}{\partial r^2} + \frac{2}{r} \frac{\partial T_\ell}{\partial r} \right) \quad (15)$$

The time derivative is considered in the liquid phase although it is neglected in the gas phase because the liquid thermal diffusivity at subcritical conditions is much smaller than the gas-phase diffusivity. Gas-phase time derivatives are retained at near critical and supercritical conditions. In the most general case, Eq. (15) can be solved by finite-difference techniques although approximate techniques (Law and Sirignano, 1977; Sirignano, 1983) have been employed. The coupled solutions of Eqs. (11), (12), and (15) yield the final results.

The liquid heating time  $\tau_H$  is defined as the time required for a thermal diffusion wave to penetrate from the droplet surface to its center and is of the order of  $R_0^2/\alpha_\ell = \rho c_\ell R_0^2/\lambda_\ell$ . From Eq. (9) with a constant value of  $\rho D$  and from a relationship between the initial liquid droplet mass and its initial radius, the droplet lifetime  $\tau_L$  can be estimated as  $\rho_\ell R_0^2/[2\rho D \log(1+B)]$ . The ratio of heating time  $\tau_H$  to lifetime  $\tau_L$  is estimated by

$$\frac{\tau_H}{\tau_L} = \frac{2\rho D c_\ell}{\lambda_\ell} \log(1+B) = 2 \frac{\lambda_\ell}{\lambda_\ell c_p} \log(1+B) \quad (16)$$

The most interesting effect appears through the temperature dependence of the parameter  $B$ . The transient behavior is found to persist over a large portion of the droplet lifetime when the ambient temperatures are high, especially for higher molecular weight liquids.

Typical results from Law and Sirignano (1977) for the liquid-phase temperature are found in Fig. 1 which portrays a thermal wave diffusing from the droplet surface toward its center. The surface regression is shown in Fig. 2.

There are several special cases of interest. In the first case, we consider that the droplet heating time is short compared to the lifetime. This implies that the droplet interior is quickly heated since a thermal wave diffuses from the droplet surface to its center in a short time compared to the lifetime. As a consequence, a nearly uniform liquid temperature is established quickly. Many authors have employed the simplifications of this case, sometimes beyond its range of validity. See Law (1976) and El-Wakil et al. (1956), for example. Equation (16) shows that this case can occur if  $\lambda \ll \lambda_\ell$ ,  $c_\ell \ll c_p$ , or  $B$  is

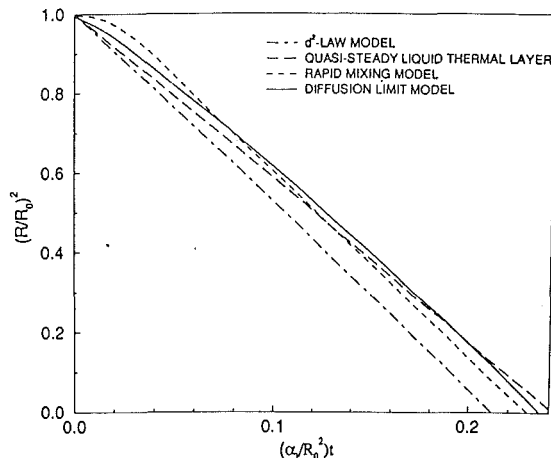


Fig. 2 Comparison of four models for spherically symmetric droplet vaporization. Nondimensional radius squared versus nondimensional time.

small. Ambient temperatures of a few hundred degrees centigrade can lead to a small  $B$  value.

For this case, further classification can be made with regard to the temporal behavior of the liquid temperature. Equation (15) can be integrated over the droplet volume accounting for the zero gradient at the droplet center and for the regressing surface. Furthermore, it can be assumed in this case that surface temperature is approximately equal to the volumetric average liquid temperature. As a result, we have that the heat flux entering the liquid is

$$\dot{q}_\ell = mc_\ell \frac{dT_\ell}{dt} \quad (17)$$

where  $m$  is the instantaneous droplet mass,  $T_\ell$  is the average liquid temperature, and  $\dot{q}_\ell = 4\pi R^2 \lambda_\ell (\partial T / \partial r)_{\ell,s}$ . This indicates that the liquid temperature would continue to rise until the heat flux  $\dot{q}_\ell$  became zero, i.e., the wet bulb temperature  $T_{wb}$  is reached. The characteristic time  $\tau^*$  for this heating depends upon the magnitudes of the thermal inertia  $mc_\ell$  and the heat flux  $\dot{q}_\ell$ . There can be shown to be two possibilities; either  $\tau^* < \tau_H$  or  $\tau^* > \tau_H$  for Eq. (17). However, if  $\tau^* < \tau_H$ , Eq. (17) is not valid because the temperature remains nonuniform on that time scale. Equation (17) is only valid and interesting if  $\tau^* > \tau_H$ .

An estimate for  $\tau^*$  can be obtained by using Eqs. (8) and (10) to yield  $\dot{q}_\ell$  which is then substituted in Eq. (17). In particular,  $\dot{q}_\ell$  is represented by a truncated Taylor series expansion about the wet bulb temperature point. The result is

$$\frac{\tau^*}{\tau_H} = \frac{1}{3} \frac{\lambda_\ell}{\lambda} \left[ \frac{1}{\log \frac{1 + \nu Y_{O\infty}}{1 - Y_{Fs}}} \right] \times \left[ \frac{\nu Y_{O\infty} + Y_{Fs}}{1 - Y_{Fs} + \frac{L^2}{c_p R} \frac{Y_{Fs}}{T_S^2} \left( \frac{1 + \nu Y_{O\infty}}{1 - Y_{Fs}} \right)} \right] \quad (18)$$

where  $Y_{Fs}$  is evaluated at the wet bulb temperature. A Clausius-Clapeyron relationship has been assumed to describe phase equilibrium. Furthermore, it can be shown from Eqs. (8) and (10) that, at the wet bulb temperature,

$$Y_{Fs} = \frac{\frac{h_\infty - h_{wb} + \nu Q Y_{O\infty}}{L} - \nu Y_{O\infty}}{1 + \frac{h_\infty - h_{wb} + \nu Q Y_{O\infty}}{L}} \quad (19)$$

which can be substituted above.

It can be concluded that the characteristic time  $\tau^*$  is bounded below by a quantity of order  $\tau_H$ . Therefore, this case can be

divided into two subcases. In one situation, the wet bulb temperature is reached in a time of the same order of magnitude as the heating time which is very short compared to the lifetime. Here, liquid temperature can be considered constant with  $L_{\text{eff}} = L$ . Then, Eqs. (9) and (10) and the phase equilibrium relation for  $Y_{F_5}(T_s)$  immediately yield the vaporization rate  $\dot{m}$  and the droplet temperature  $T_s = T_{wb}$ . When  $\rho D$  is constant, integration of Eq. (9), where  $m = 4\pi R^3 \rho / 3$ , yields the well-known  $d^2$  law. That is,

$$(R/R_0)^2 = 1 - t/\tau_L \quad (20)$$

Note that the previously given estimate for  $\tau_L$  is exact here with  $B$  calculated using  $L_{\text{eff}} = L$ .

The second subcase involves a characteristic time  $\tau^*$  substantially larger than  $\tau_H$  and perhaps comparable to  $\tau_L$ . This requires the integration of Eq. (17) (coupled with Eq. (10) that relates  $\dot{q}_L$  to  $T_L = T_s$ ). The results for such an integration are shown in Fig. 2. The use of an average temperature tends to underestimate the surface temperature during the early vaporization period because the thermal energy is artificially distributed over the droplet interior. As a result, the early vaporization rate for this subcase is less than found in the general case by solving the diffusion equation (15). However, because the surface temperature is artificially low at first, more heat enters the droplet and ultimately it vaporizes faster than the general case as shown in Fig. 2.

Another interesting case occurs when the heating time is much longer than the lifetime. Then, a thin thermal layer is maintained in the liquid near the surface; the regression rate is too large for the thermal wave to penetrate faster than the regressing surface. This case can occur if  $\lambda_f$  is small or if  $c_f$  or  $B$  is large. Very large ambient temperatures of a few thousand degrees Kelvin can lead to this situation. The thin thermal layer can be considered quasi-steady so that the conductive heat flux through the surface balances the liquid convective rate toward the surface. (Convection here is measured relative to the regressing surface.) We have therefore the approximation that

$$\lambda_f \frac{\partial T_f}{\partial r} \Big|_s = \rho_f U_f c_f (T_s - T_{\infty}) \quad \text{or} \quad L_{\text{eff}} = L + c_f (T_s - T_{\infty}) \quad (21)$$

Equations (10) and (21) together with the phase equilibrium relation yield  $T_s$  (which here is constant with time). Then Eq. (9) yields  $\dot{m}$  and subsequently  $R(t)$ . Since  $L_{\text{eff}}$  is here a constant with larger positive value than  $L$ , another  $d^2$  relationship results but with a lower absolute value of the slope on a time plot. Equation (17) can be employed with  $\tau_L$  now calculated using Eq. (18).

The two  $d^2$ -law results are also plotted in Fig. 2 for the purpose of comparison with the general case. The general case is the only one of the three cases discussed so far that considers an initial transient. The first (well-known)  $d^2$ -law neglects the initial thermal diffusion across the droplet interior while the other  $d^2$ -law neglects the initial diffusion across the thin layer.

Note that the droplet lifetimes vary little from model to model in Fig. 2. However, the local slope of the curves (related to instantaneous vaporization rates) do vary more significantly. This variation implies that the vaporization rate as a function of spacial position for a droplet moving through a volume can depend significantly upon the particular model.

There are various complications that occur when a multicomponent liquid is considered (Landis and Mills, 1974 and Sirignano and Law, 1978). Different components vaporize at different rates, creating concentration gradients in the liquid phase and causing a liquid-phase mass diffusion. The theory requires the coupled solutions of liquid-phase species continuity equations, multicomponent phase equilibrium relations (typically Raoult's law), and the gas-phase multicomponent energy and species continuity equations. Liquid-phase mass diffusion is commonly much slower than liquid-phase heat

diffusion so that thin diffusion layers can occur near the surface especially at high ambient temperatures where the surface regression rate is large. The more volatile substances tend to vaporize faster at first until their surface concentrations values are diminished and further vaporization of those quantities becomes liquid-phase-mass-diffusion controlled.

Liquid-phase mass diffusion also becomes important at pressures near or above the critical pressure of the liquid even if it initially is a pure component. Ambient gases dissolve in the liquid to a significant extent as the critical pressure is approached; then mass diffusion occurs in the liquid phase. It is noteworthy that the actual critical pressure and temperature vary spatially with composition. Typically, the dependence on composition is very nonlinear and the critical pressure for a mixture can be greater than the critical pressure of any component. Therefore, subcritical conditions can exist at an interface with a distinct discontinuity between liquid and gas even if the pressure is above the critical pressure of the original pure component in the droplet. See Sheun et al. (1992) and Delplanque and Sirignano (1993) for detailed analyses of these problems.

The spherically symmetric droplet problem introduces many fundamental physical issues that remain in the problem as the flow field becomes more complex due to the relative motion between the gas and the droplet. The effects of transient heat conduction and mass diffusion, phase equilibrium at the interface, and the regressing liquid surface remain as the relative flow is introduced. The effects of relative motion are discussed in the following subsection.

**2.2 Convective Droplet Vaporization.** In most applications, droplets in a spray will be moving at some relative velocity to the surrounding. The Reynolds number based upon the relative velocity, droplet radius, and gas properties can be as large as the order of one hundred. Convective boundary layers and separated near wakes can therefore surround the droplet. For a liquid-gas (or liquid-liquid) interface, shear stress and tangential velocity do not generally become zero at the same point; the separation point is defined as the zero velocity point where the streamline actually leaves the surface. The boundary layer enhances the heat and mass transport rates over the values for the spherically symmetric droplet. Furthermore, the shear force on the liquid surface causes an internal circulation that enhances the heating of the liquid. As a result, vaporization rate increases with increasing Reynolds number.

One commonly used empirical result is the Ranz and Marshall (1952) correlation that corrects the spherically symmetric vaporization rate  $\dot{m}_{ss}$  as follows:

$$\dot{m} = \dot{m}_{ss} (1 + 0.3 \text{Pr}^{1/3} \text{Re}^{1/2})$$

This formula is based upon certain quasi-steady, constant radius, porous wetted sphere experiments. A similar correlation is reported by Frossling (1938). Those experiments do not account for transient heating, regressing interface, and internal circulation. There is a need for more fundamental experimental and theoretical analyses.

The calculations for a vaporizing droplet that is moving through a gas require the solution of a complex set of nonlinear coupled partial differential equations. The problem is inherently unsteady since droplet size is continually changing due to vaporization; relative velocity is also changing due to droplet drag; and temperatures are varying on account of droplet heating. The problem can be considered to be axisymmetric for a spherical droplet. Since the boundary is moving due to droplet vaporization, adaptive gridding is required for finite-difference computations.

The configuration to be studied for an isolated droplet is an axisymmetric flow as depicted in Fig. 3. Droplet can turn in a flow or the gas flow can change direction but typically

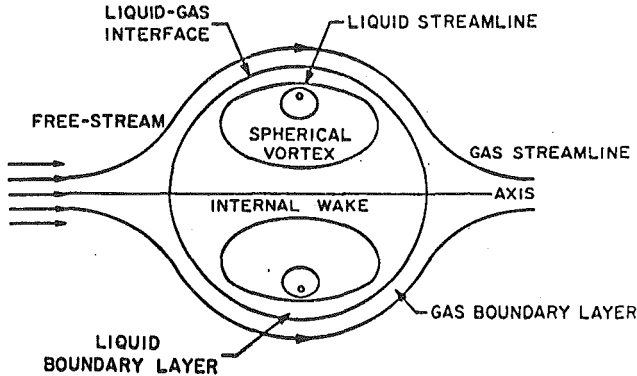


Fig. 3 Vaporizing droplet with relative gas-droplet motion and internal circulation

the characteristic time for a change of vectorial direction of the relative velocity is long compared to the residence time for an element of gas to flow past the droplet. Therefore, axisymmetry is a very good approximation. The droplet still retains a spherical shape provided that the Weber number remains of order unity or less.

The evaluations of the vaporization rate and heating rate have been performed by both approximate analyses and exact solution of the coupled gas and liquid flow equations by finite-difference calculations. These analyses and their results will be discussed in the following sections.

**Approximate Analyses for Gas-Phase Boundary Layer.** There exist various analyses that describe the behavior of a quasi-steady, laminar, gas-phase boundary layer that exists at the interface of a droplet with Reynolds number (based upon relative velocity) that is larger than unity. The earliest studies were performed by Prakash and Sirignano (1978, 1980) for single component liquids and Lara-Urbaneja and Sirignano (1981) and Law et al. (1977) for multicomponent liquids. Prakash and Sirignano (1978, 1980) and Lara-Urbaneja and Sirignano (1981) used integral boundary layer techniques to analyze the gaseous flow over a vaporizing droplet surface. These works were the first to identify the essential physics of the convective droplet vaporization problem. The analyses were made earlier to those to be described in this subsection and also were more complex without offering clear advantages. They were not yielding as complete and as detailed information as the finite-difference solution of the Navier-Stokes elliptic flow equations. At the same time, the integral techniques were too complex to incorporate into extensive spray computations.

Later analyses that will be examined more closely here were developed by Sirignano (1979), Tong and Sirignano (1982a, 1982b, 1983, 1986a, 1986b), and Abramzon and Sirignano (1989). These analyses are strictly limited to boundary layers and do not predict the behavior in the near wake. Some of the analyses can predict the point of separation on the droplet surface. They use either integral techniques or local similarity assumptions for the analysis. Since most of the heat and mass transport for the Reynolds number range of interest (order one hundred and less) occurs before the point of separation, vaporization, and droplet heating rates can be well predicted. However, since form drag is competitive in magnitude with friction drag, and drag coefficient cannot even be approximated by these analyses; input is needed for these values.

Under the assumption that the droplet Reynolds number is large compared to unity (but not so large that instability or turbulence occurs), a thin, gas-phase boundary layer exists on the surface of the droplet. In our application, we can reasonably neglect kinetic energy and viscous dissipation. Also,  $Pr = Sc = 1$  and one-step chemistry can be assumed following Tong and Sirignano. The  $x, y$  coordinates are tangent and

normal to the droplet surface, respectively, with  $r$  representing the distance from the axis of symmetry. The governing equations in quasi-steady form are

*Continuity*

$$\frac{\partial(\rho u r)}{\partial x} + \frac{\partial(\rho v r)}{\partial y} = 0 \quad (22)$$

*x-Momentum*

$$L \left( \frac{u}{u_e} \right) = \rho u \frac{\partial}{\partial x} \left( \frac{u}{u_e} \right) + \rho v \frac{\partial}{\partial y} \left( \frac{u}{u_e} \right) - \frac{\partial}{\partial y} \left( \mu \frac{\partial}{\partial y} \left( \frac{u}{u_e} \right) \right) \\ = \left[ \frac{\rho_e}{\rho} - \frac{u}{u_e} \right]^2 \rho \frac{du_e}{dx} \text{ where } \frac{dp_e}{dx} = \rho_e u_e \frac{du_e}{dx}. \quad (23)$$

Note that  $u_e(x)$  is the potential flow velocity immediately external to the boundary layer. The  $y$ -momentum equation states that pressure gradients in the  $y$  direction are negligible.

*Energy*

$$L(h) = -Q \dot{w}_F \quad (24)$$

*Species Conservation*

$$L(Y_i) = \dot{w}_i \quad i = O, F, P, N \quad (25)$$

The  $x$ -momentum equation can be further simplified as the ambient temperature is much higher than the surface temperature and the ambient velocity is much higher than the tangential surface velocity. The right-hand side of Eq. (23) goes to zero at the outer edge of the boundary layer; also, it becomes very small at the droplet surface. The ad hoc assumption can be made following Lees (1956) that the right-hand side is everywhere zero because the quantity in square brackets is negligibly small. Note that the pressure gradient can still be nonzero; it is the transverse variation of the dynamic pressure that is small.

Two interesting cases are readily studied: the stagnation point flow ( $r=x$  and  $u_e=ax$ ) and the shoulder region ( $\theta=\pi/2$ ,  $r=R$ ,  $u_e=(3/2)U_\infty$ ) where the pressure gradient is zero and the flow locally behaves like a flat plate flow. That is, because the right-hand side of Eq. (23) is negligible, local similarity is believed to be a very good approximation. The well-known similarity solution

$$u = u_e(x) \frac{df}{d\eta}(\eta) \equiv u_e(x)f'(\eta)$$

is found where  $f(\eta)$  satisfies the Blasius equation and

$$\eta = \frac{ru_e \int_0^y \rho dy'}{\left[ \int_0^x \rho_e \mu_e u_e r^2 dx' \right]^{1/2}}$$

The vaporization rate per unit area is given by

$$(\rho v)_s = -A f'(0) \quad (26)$$

Note that  $A = (2\rho_e \mu_e)^{1/2}$  for the stagnation point and  $\rho_e \mu_e [u_e / 2 \int_0^x \rho_e \mu_e dx']^{1/2}$  for the shoulder region.

Two of the three boundary conditions for the third-order, nonlinear ordinary differential equation governing  $f(\eta)$  are

$$\frac{df}{d\eta}(0) = u_s/u_e; \quad \frac{df}{d\eta}(\infty) = 1 \quad (27)$$

The third boundary condition will be developed from Eq. (26) and requires a coupling with the solution of the energy equation.

The definitions given in Eq. (11) can be used to solve Eqs. (24) and (25) for the case of rapid chemical kinetics. With the simplified version of Eq. (23) discussed above, it can be shown that for all of the  $\beta$  functions

$$\beta = \beta_s + \frac{u - u_s}{u_e - u_s} (\beta_e - \beta_s) = \beta_s + \frac{f'(\eta) - f'(0)}{1 - f'(0)} (\beta_e - \beta_s) \quad (28)$$

Equations (24) and (25) are second-order partial differential equations normally associated with five boundary conditions at the outer edge of the boundary layer and five boundary conditions at the droplet surface. The ambient conditions for temperature (or enthalpy) and mass fractions are provided. Five boundary conditions at the droplet surface are given by conservation of energy and species mass flux as follows

$$\lambda \frac{\partial T}{\partial y} \Big|_{g,s} = \lambda_f \frac{\partial T}{\partial y} \Big|_{l,s} + \rho v)_s L \equiv \rho v)_s L_{\text{eff}} \quad (29)$$

$$\rho v)_s Y_{F_s} - \rho D \frac{\partial Y_F}{\partial y} \Big|_s = \rho v)_s \quad (30)$$

and

$$\rho v)_s Y_{i,s} - \rho D \frac{\partial Y_i}{\partial y} \Big|_s = 0; \quad i = O, P, N \quad (31)$$

In addition, we have a phase equilibrium relation and a continuity condition on the temperature at the interface. The extra two conditions are required because the vaporization rate (per unit area)  $\rho v)_s$  and the liquid heating rate (per unit area)  $\lambda_f (\partial T / \partial y)_s$  are not given a priori. They are eigenvalues of the problem. Complete determination requires the coupling with the heat transport problem in the liquid phase.

From these boundary conditions, Eq. (28), and Eq. (10), we can develop the third boundary condition for the Blasius differential equation. We find that

$$\frac{f''(0)}{[f'(0)][1-f'(0)]} = \frac{1}{B} \quad (32)$$

Actually, the Blasius function depends upon  $\eta$ ,  $B$ , and  $u_s/u_e$  since  $B$  and  $u_s/u_e$  appear in the boundary conditions (27) and (32). So  $f(0)$  implies  $f(0, B, u_s/u_e)$ . Furthermore,  $f(0)$  is negative for the vaporization conditions. It can also be shown that

$$\lambda_f \frac{\partial T}{\partial y} \Big|_{l,s} = -Af(0) \left[ \frac{h_e - h_s + Q\nu Y_{O_\infty} - L}{\frac{1 + \nu Y_{O_\infty}}{1 - Y_{F_s}} - 1} \right] \quad (33)$$

An interesting comparison is made between this convective case and the spherically symmetric case. Equations (26), (29), and (33) can be combined to reproduce an equation exactly like Eq. (10) except that  $h_e$  appears instead of  $h_\infty$ . This demonstrates a great similarity in the physics of the two cases. Furthermore, the same formula for the wet bulb temperature results in the spherically symmetric case and for the stagnation point and shoulder region under similarity conditions.

The flow is expected to separate shortly after the point of zero pressure gradient. Therefore, most of the heat and mass transport occurs on the forward side or the "shoulders" of the droplet; little occurs on the downstream side. The above analyses for the stagnation region and for the shoulder region can be used to construct a reasonable estimate for the global liquid heating rate and vaporization rate.

From this analysis, Sirignano (1979) has shown that the Nusselt number Nu follows a certain relationship. In particular,

$$Nu = \frac{k[-f(0)]}{B} Re^{1/2} \quad (34)$$

where  $k$  is a positive nondimensional coefficient of order unity which is determined by averaging the heat flux over the droplet surface in an approximate manner (based upon the two local solutions discussed above). Again,  $f(0)$  is negative with vaporization. Also, we have the global vaporization rate via a similar averaging process

$$\dot{m} = \mu_e R [-f(0)] Re^{1/2} \quad (35)$$

The results (34) and (35) are based upon an analysis limited

to high droplet Reynolds number. There exists an important domain between the spherically symmetric case (zero Reynolds number case) and the thin laminar boundary layer case (high Reynolds number case). A more robust vaporization model that covers a wide range of Reynolds number is needed. This is especially important since a given droplet can experience a range of Reynolds number during its lifetime. Typically, the droplet Reynolds number will decrease with time as the droplet diameter and the relative velocity decrease. There are exceptions to the monotonic behavior; e.g., oscillatory ambient flow where large fluctuations of relative velocity (including change in direction) can occur.

One ad hoc method for developing a more robust model was presented by Abramzon and Sirignano (1989). The Nusselt number and the vaporization rate are each given by a composite of two asymptotes (zero Reynolds number limit and large Reynolds number limit). We have that

$$Nu = \frac{2 \log(1+B)}{B} \left[ 1 + \frac{k}{2} \frac{[-f(0)]}{2 \log(1+B)} Re^{1/2} \right] \quad (36)$$

$$\dot{m} = 4\pi\rho DR \log(1+B) \left[ 1 + \frac{k}{2} \frac{[-f(0)]}{\log(1+B)} Re^{1/2} \right] \quad (37)$$

Note that  $f(0) = f(0, u_s/u_e, B)$  reaches a finite limit as  $B$  becomes large. The above results therefore disagree strongly with the Ranz-Marshall or Frossling correlations. The problems with those correlations are that they were developed for only a very narrow range of  $B$  values.

Abramzon and Sirignano actually made two further extensions. First, they considered general values for Schmidt, Prandtl, and Lewis numbers, relaxing the unitary conditions and allowing for variable properties. Second, they considered a range of Falkner-Skan solutions to develop the average transport rates across the gas boundary layer on the droplet surface. With the definitions

$$B_H = \frac{h_e - h_s}{L_{\text{eff}}} \quad \text{and} \quad B_M = \frac{Y_{F_s} - Y_{F_\infty}}{1 - Y_{F_s}} \quad (38)$$

they demonstrated that

$$\begin{aligned} Nu &= 2 \frac{\log(1+B_H)}{B_H} \left[ 1 + \frac{k}{2} \frac{Pr^{1/3} Re^{1/2}}{F(B_H)} \right]; \\ Sh &= 2 \frac{\log(1+B_M)}{B_M} \left[ 1 + \frac{k}{2} \frac{Sc^{1/3} Re^{1/2}}{F(B_M)} \right] \\ \dot{m} &= 4\pi \frac{\lambda R}{c_p} \log(1+B_H) \left[ 1 + \frac{k}{2} \frac{Pr^{1/3} Re^{1/2}}{F(B_H)} \right] \\ &= 4\pi\rho DR \log(1+B_M) \left[ 1 + \frac{k}{2} \frac{Sc^{1/3} Re^{1/2}}{F(B_M)} \right] \end{aligned} \quad (39)$$

Note that, when  $Pr = Sc = 1$ , we have that  $B_M = B_H$ . Otherwise,

$$B_H = (1 + B_M)^a - 1 \quad \text{where} \quad a \equiv \frac{c_{pF}}{c_p} \frac{1}{Le} \frac{1 + \frac{k}{2} \frac{Re^{1/2}}{F(B_M)}}{1 + \frac{k}{2} \frac{Re^{1/2}}{F(B_H)}} \quad (40)$$

A correlation of numerical results shows that

$$\begin{aligned} F(B) &= (1 + B)^{0.7} \frac{\ln(1+B)}{B} \\ \text{for } 0 \leq B_H, B_M \leq 20 \text{ and } 1 \leq Pr, Sc \leq 3. \end{aligned} \quad (41)$$

Other approximate or asymptotic techniques have been utilized to solve related problems. Hadamard (1911) and Rybczynski (1911) solved for the creeping flow around a nonvaporizing liquid droplet. Acrivos and Taylor (1962) and Acrivos and Goddard (1965) analyzed the heat transfer for this type of flow and estimated the Nusselt number. Harper

and Moore (1968) and Harper (1970) solved the high Reynolds number nonvaporizing droplet; boundary layers on both sides of the droplet interface were analyzed. Rangel and Fernandez-Pello (1984) studied the high Reynolds number vaporizing droplet with an isothermal liquid assumption. Chung et al. (1984a, 1984b) and Sundararajan and Ayyaswamy (1984) studied condensing droplets by perturbation and numerical methods.

In the case where many components exist in the liquid phase, it is necessary to track the vapor components individually as the species advect and diffuse through the gas phase. If there are  $n$  vaporizing components in the liquid, an additional  $n - 1$  field equations of the form of Eq. (25) and an additional  $n - 1$  boundary conditions of the form of Eq. (30) must be added to the system. Also, a phase equilibrium relationship is required for each component and the chemical source term in the energy equation (24) must be modified.

The gas-phase equations are strongly coupled to the liquid-phase equations through the continuity of velocity and temperature and the balances of mass, force, and energy. See, for example, Eqs. (27), (29), (30), and (32).

**Liquid-Phase Flows.** The jump in shear stress across a liquid-gas interface equals the gradient of surface tension (Levich, 1962). Sirignano (1983) argues that generally, the temperature and composition variations along the surface of a droplet are too small to cause a significant gradient of surface tension. Therefore, we consider a continuity of shear stress across the interface.

The liquid-phase responds to the viscous shear force at the interface by circulating within the droplet. Toroidal stream surfaces in the liquid result with low velocities. Due to the larger liquid density, the Reynolds number for the internal circulation (based upon droplet diameter, maximum liquid velocity, and liquid properties) can be of the same order of magnitude as or higher than the Reynolds number for the gas flow over the droplet. Peclet numbers are even higher in the liquid because of the large Prandtl and Schmidt numbers. Heat and mass transport in the liquid will therefore behave in a highly dissimilar fashion to the transport of momentum or vorticity. The analysis of the hydrodynamics in the approximate models differs substantially from the analyses of heat and mass transport on account of the large Prandtl and Schmidt numbers.

It is convenient to address the incompressible, liquid-phase hydrodynamics by the use of the vorticity-stream-function formulation. The vorticity equation can be developed by taking the curl of the momentum equation. For an incompressible fluid, we have

$$\frac{D\omega}{Dt} = \boldsymbol{\omega} \cdot \nabla \mathbf{u} + \nu \nabla^2 \boldsymbol{\omega} \quad (42)$$

In a planar flow,  $\boldsymbol{\omega}$  and  $\mathbf{u}$  are orthogonal. So, the first term on the right-hand side becomes zero in that case. Therefore, in the inviscid limit, the vorticity vector,  $\boldsymbol{\omega}$ , is constant along a particle path. In the case of a non-swirling axisymmetric flow,  $\boldsymbol{\omega}$  is always directed in the local  $\theta$  direction. Then, it can be shown that

$$\boldsymbol{\omega} \cdot \nabla \mathbf{u} = \frac{\omega v}{\tilde{r}} \mathbf{e}_\theta \quad (43)$$

where  $v$  is the radial component of velocity and  $\tilde{r}$  is the radial coordinate in cylindrical coordinates. In the inviscid limit, it follows that  $\omega/\tilde{r}$  is constant along a particle path with magnitude of  $\omega/\tilde{r}$ . In the steady (or quasi-steady) liquid flow, the particle path is a closed streamline so that  $\omega/\tilde{r}$  is a function of the streamfunction  $\psi$ . Note that the Prandtl number and the Schmidt number for a typical liquid are large compared to unity. Diffusion of heat and mass are slow, therefore, compared to diffusion of vorticity in the liquid. A quasi-steady

hydrodynamic behavior is established in a short time compared to the transient time for heating or mixing. It is also assumed that the transient time is sufficiently short so that the hydrodynamics instantaneously adjusts to droplet diameter changes resulting from vaporization. In our simplified models, quasi-steady hydrodynamic behavior is assumed, while transient heating is allowed.

The Hill's spherical vortex (Lamb, 1945; Batchelor, 1990) is a well-known solution of Eqs. (42) and (43) in the inviscid limit that also satisfies matching interface conditions with an external potential flow. In this special case,  $\omega/\tilde{r}$  has the same constant value for all values of the stream function. It has been shown that

$$\omega = 5\tilde{A}\tilde{r} \sin \theta = 5\tilde{A}\tilde{r} \quad (44)$$

$$\psi = -\frac{1}{2}\tilde{A}\tilde{r}^2(R^2 - r^2)\sin^2 \theta = -\frac{1}{2}\tilde{A}\tilde{r}^2(R^2 - (\tilde{r}^2 + z^2)) \quad (45)$$

$$= -\frac{3}{4}U\frac{\tilde{r}^2}{R^2}(R^2 - \tilde{r}^2 - z^2) \quad (46)$$

Note that  $U$  is the instantaneous relative velocity between the droplet and the ambient gas. The maximum potential flow velocity at the interface is  $3/2$  times that value. We will not assume in our analysis that a potential flow exists immediately near the surface; rather, allowance is made for a viscous boundary layer. So, we consider  $\tilde{A}$  to be the liquid vortex strength and relate it simply to the maximum velocity at the liquid surface which can be an order of magnitude less (depending upon density and viscosity) than the extrapolated potential flow velocity value. In particular,

$$\tilde{A} = U_{\max}/R \quad (47)$$

Therefore, Eq. (46) is neglected when the viscous boundary layer is considered. Rather, Eqs. (45) and (47) are employed.

It is convenient to define the nondimensional variables  $\phi = (8\psi\tilde{A}R^4) + 1$  and  $s = r/R$ . Then

$$\phi = 1 - 4s^2(1 - s^2)\sin^2 \theta \quad (48)$$

Note that  $\phi = 1$  at the interface ( $s = 1$ ) and at the center of the internal wake ( $\theta = 0, \theta = \pi$ ) and that  $\phi = 0$  at the vortex center ( $s = 1/\sqrt{2}$  and  $\theta = \pi/2$ ).

The above solution has been established effectively as a high Reynolds number limiting behavior. That is, the viscous term has been neglected in the derivation so that an inviscid solution for the internal liquid flow results. The low Reynolds number quasi-steady limiting behavior is given by the Hadamard-Rybczynski solution (Hadamard, 1911; Rybczynski, 1911; Batchelor, 1990; Lamb, 1945). There, the inertial term in both the surrounding gas and the interior liquid is neglected. The remaining linear system is solved by separation of variables. The solution in external phase differs significantly from the high Reynolds number solution. The most interesting result is that the Hill's spherical vortex solution given by Eqs. (44), (45) or (48), and (47) applies for the Hadamard-Rybczynski low Reynolds number solution. This can be explained by the fact that the vector  $\boldsymbol{\omega} = \omega \mathbf{e}_\theta = 5\tilde{A}\tilde{r}\mathbf{e}_\theta$  actually satisfies Laplace's equation, so that the viscous term in Eq. (42) goes to zero without assuming zero viscosity. (Note the scalar  $\omega$  is not harmonic, however.) Viscosity only affects the value of the constant  $\tilde{A}$  through the interface matching process. Hill's spherical vortex solution actually applies over a wide range of Reynolds number; in the vorticity equation, both the inertial (nonlinear) terms and the diffusion (viscous) term are individually equal to zero. In the original momentum equation, the viscous term balances exactly the pressure gradient term and the inertial (nonlinear) terms are identically zero. This fortuitous character is shared with Couette and Poiseuille flows. This low Reynolds solution has not been extended to the case of vaporizing droplets where it might provide the basis for an interesting perturbation on the spherically symmetric vaporization case.

In a large Peclet number situation, heat and mass transport within the droplet will involve a strong convective transfer along the streamline with conduction primarily normal to the stream surface. In the limit of zero Peclet number, only conduction occurs. Over the full range of Peclet number, the heat and mass transport problems are axisymmetric and unsteady. With a certain coordinate transformation, the large Peclet number problem can be cast as a one-dimensional, unsteady problem.

In place of the spherical coordinates  $r$  and  $\theta$ , we can use the streamfunction  $\psi$  (a measure of distance normal to the stream-surface) and  $\xi$  (a measure of distance in the local flow direction). The azimuthal coordinate  $\eta$  is maintained in the transformation. There is no variation in the  $\eta$  direction due to the axisymmetric and, for rapid circulation (high Peclet number), the variation in the  $\xi$  direction is negligible. The only variation therefore comes due to conduction in the  $\psi$  direction. Transforming the coordinates and averaging temperature along the streamsurface, we find that the liquid-phase energy equation becomes

$$F(\psi) \frac{\partial T}{\partial t} = \alpha_t \frac{\partial}{\partial \psi} \left( G(\psi) \frac{\partial T}{\partial \psi} \right) \quad (49)$$

where the following definitions have been made for integrals over the closed fluid path.

$$F(\psi) = \oint \frac{h_\xi d\xi}{u_\ell} = \frac{8}{\tilde{A}R} g_1(\phi) \text{ and } G(\psi) = \oint \frac{h_\eta h_\xi}{h_\psi} d\xi = \frac{\tilde{A}R^5}{8} g_2(\phi) \quad (50)$$

Note that  $h_\eta$ ,  $h_\xi$ , and  $h_\psi$  are scale factors of the transformation and  $u_\ell(\psi, \xi)$  is the local velocity which is tangential to the stream surface (Prakash and Sirignano, 1978, 1980). The differential  $h_\xi d\xi$  is an element of length along the streamline and  $(h_\xi/u_\ell)d\xi$  is a differential Lagrangian time; the cyclic integral  $F(\psi)$  is therefore the circulation time. It can be shown that

$$V(\psi) = 2\pi \int_0^\psi F(\psi') d\psi' \text{ and}$$

$$V(\phi, t) = 2\pi R^3(t) \int_0^\phi g_1(\phi') d\phi' \quad (51)$$

gives the volume enclosed by the stream surface  $\psi$ . Note that here  $\psi$  is referenced to the vortex center where its value is set to zero, with the maximum value at the droplet surface. Using  $\phi$  as defined by Eq. (48), we can state that

$$V(\psi) = V(R(t), \phi) = V(t, \phi) \text{ and } \frac{\partial \phi}{\partial t}_\psi = - \frac{\frac{\partial V}{\partial t}}{\frac{\partial V}{\partial \phi}}_t$$

It follows that

$$\frac{\partial T}{\partial t}_\psi = \frac{\partial T}{\partial t}_\phi - \frac{\frac{\partial V}{\partial t}}{\frac{\partial V}{\partial \phi}}_t \frac{\partial T}{\partial \phi} \quad (52)$$

Combination of Eqs. (49), (50), and (52) leads to the following one-dimensional form of the diffusion equation

$$\frac{\partial T}{\partial \tau} = a(\phi, \tau) \frac{\partial^2 T}{\partial \phi^2} + b(\phi, \tau) \frac{\partial T}{\partial \phi} \quad (53)$$

where

$$\tau = \alpha_t t / R_0^2; \quad a(\phi, \tau) = (R_0/R)^2 g_2(\phi) / g_1(\phi)$$

and

$$b(\phi, \tau) = (R_0/R)^2 g'_2(\phi) / g_1(\phi) + (3/R) (dR/dt) \int_0^\phi g_1(\phi') d\phi' / g_1(\phi)$$

where  $g'_2(\phi)$  is the derivative and  $\phi'$  is a dummy variable.

Then Eq. (53) can be solved with proper matching conditions at the interface, i.e., Eqs. (30), (31), and (33) plus the phase-equilibrium condition and continuity of temperature. A boundary condition at  $\phi=0$ , the vortex center, prescribes that the heat flux goes to zero there.

The liquid transient heating phenomenon with internal circulation then involves unsteady heat conduction from  $\phi=1$  (the warm droplet surface and the warm axis of symmetry) toward  $\phi=0$  (the relatively cool vortex center). Temperature is a monotonically increasing function of  $\phi$  with the gradient diminishing with time. The limit of uniform but time-varying temperature results as the liquid thermal diffusivity goes to infinity. Contrary to earlier beliefs by some investigators, the uniform temperature limit does not result from infinitely rapid internal circulation. As shown above, infinitely fast circulation or infinite liquid Peclet number results in the finite temperature gradients becoming oriented normal to the stream surfaces. Note that the averaging of the temperature over the stream surface eliminated the convection term from Eq. (53); only conduction is represented therein. Furthermore, the transformation from  $\psi$  to  $\phi$  modified the vaporizing droplet problem from a moving boundary problem to a fixed boundary problem. The effect of the regressing interface appears in the coefficient of that diffusion equation.

It has been shown by Tong and Sirignano (1982a, 1982b, 1983, 1985, 1986) and Sirignano (1993) that the liquid-phase heat diffusion equation (53) and its counterpart mass diffusion equation can be simplified when the change in droplet radius due to vaporization occurs slowly compared to changes in liquid temperature. Under that assumption, the nonlinearities introduced by the coefficients in Eq. (53) can be modified to give an approximate piecewise linear behavior for the equation. A Green's function analysis reduces the equation to an integral form whereby a quadrature gives the liquid temperature at any point as a function of the surface heat flux. An integral equation results that relates surface temperature to surface heat flux. The Green's function (which is the kernel function in the integral equation) is obtained as an eigenvalue expansion. Tong and Sirignano (1986b) showed that the problem could be reduced to a system of ordinary differential equations, thereby improving computational efficiency at a given accuracy.

An alternative approach to the analysis of the liquid-phase heat diffusion was proposed by Abramzon and Sirignano (1989). In particular, an effective thermal diffusivity  $\alpha_{\text{eff}}$  was employed wherein

$$\alpha_{\text{eff}} = \chi \alpha_t \text{ and } \chi = 1.86 + 0.86 \tanh[2.225 \log_{10}(\text{Pe}_t/30)] \quad (54)$$

Equation (54) results from the fitting of numerical results by Johns and Beckmann (1966) for mass transfer between a droplet with internal circulation and a moving external immiscible liquid. The liquid-phase Peclet number,  $\text{Pe}_t$ , depends upon liquid properties, droplet radius, and the maximum liquid velocity. Here, a "spherically symmetric" pseudo-temperature field is solved using the diffusion equation

$$\frac{\partial T}{\partial t} = \frac{\alpha_{\text{eff}}}{r^2} \frac{\partial}{\partial r} \left( r^2 \frac{\partial T}{\partial r} \right) \quad (55)$$

The use of the effective thermal diffusivity presents an accurate description of the characteristic heating time and thermal inertia of the liquid. Via Eq. (54), the effective diffusivity monotonically increases with the maximum liquid velocity. It is bounded below by the molecular diffusivity and above by 2.72 times that finite value. It is expected therefore that the surface

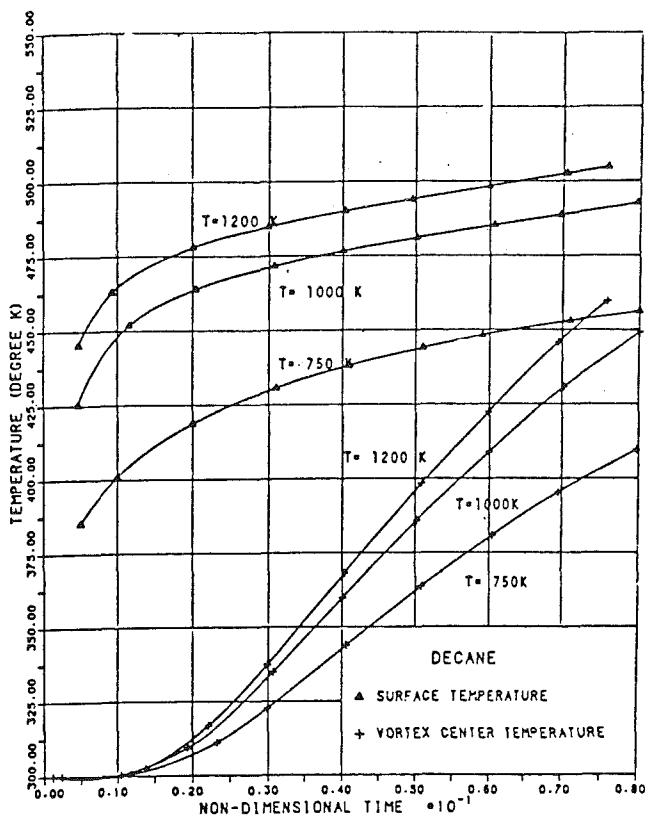


Fig. 4 Surface and vortex center temperature variation for decane liquid droplet at droplet Re = 100 and various ambient temperatures

temperature history will be portrayed with only a small error by this ad hoc analysis. The details of the internal temperature field can be grossly in error. For example, the pseudo-temperature will be a minimum at the center of the droplet while the actual temperature is a minimum at the vortical center.

In the case of a multicomponent liquid fuel, mass diffusion in the liquid phase becomes important. As the more volatile substance is vaporized faster from the surface, more of that substance will diffuse from the interior of the droplet to the surface to vaporize. For  $n$  liquid components,  $n-1$  liquid-phase mass diffusion equations must be solved for  $n-1$  mass fractions; the other mass fraction can immediately be deduced since the mass fractions sum to unity. The mass diffusion equations can be placed in forms equivalent to Eq. (49) or Eq. (53). These equations have been solved by approximate and exact methods (Lara-Urbaneja and Sirignano, 1981; Tong and Sirignano, 1986a, 1986b; Continillo and Sirignano, 1988, 1991; and Megaridis and Sirignano, 1991, 1992). The problem is especially interesting and challenging because the liquid mass diffusivity is typically an order of magnitude smaller than the liquid thermal diffusivity so that a new time scale and a greater degree of "stiffness" are created.

**Results From Approximate Analyses.** The high Reynolds number, quasi-steady, gas-phase boundary-layer analysis coupled with the model of heat diffusion in the internal vortical flow gives a reasonable representation of the quantitative behavior of the velocity and thermal fields in the gas boundary layer and in the liquid. Figure 4 shows results by Tong and Sirignano for surface temperature versus time and for temperature at the vortical center versus time. Spatial variations in the liquid temperature are seen to occur. The surface temperature gradually increases with time toward the wet bulb temperature while the lower vortical center temperature increases at a faster rate, thereby decreasing the spatial variance.

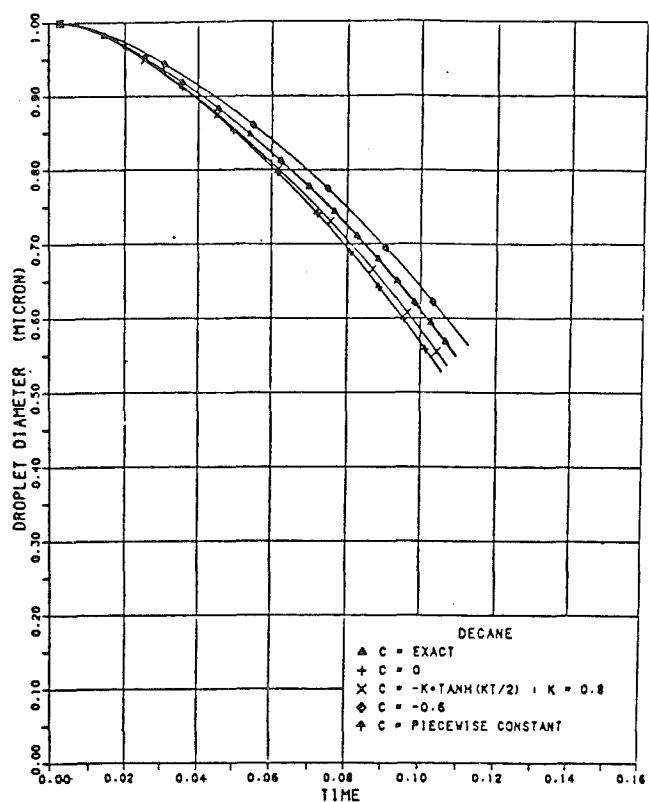


Fig. 5 Droplet diameter versus time for decane. C is a parameter describing surface regression rate.

Figure 5 shows that the rate of change of the radius (which is related to the vaporization) is slower at first and later increases, giving a clear indication of important transient effects.

The gas-film model coupled with the effective liquid conductivity allows for coverage of a much wider range of Reynolds number. This ability makes the model of Abramzon and Sirignano more practical for use in a spray calculation, where even the droplets that begin with a large relative velocity and large Reynolds number witness a deceleration that eventually gives them lower values of the relative velocity and Reynolds number. Figures 6 and 7 show typical variations of the gas-phase Reynolds number, liquid-phase Reynolds number, and liquid-phase Peclet number with time. The Peclet number strongly influences the effective conductivity through Eq. (54); it is seen that it can vary over several orders of magnitude in the droplet lifetime. The high Peclet number assumption that leads to the establishment of Eqs. (49) and (53) and the high gas-phase Reynolds number assumption that allows for thin boundary layers are not valid over the complete lifetime of the droplet.

Figures 8, 9, and 10 compare droplet radius, surface temperature, and vaporization rate variations during the droplet lifetime for several liquid-phase models. The most accurate model is the "extended" model which yields the solution for the liquid-phase axisymmetric energy equation with the velocity field determined by the Hill's spherical vortex solution. See Abramzon and Sirignano (1989) for details. The effective conductivity model is seen to agree very well in terms of these results which are sufficient to give a useful coupling with the gas phase in spray calculations. The Abramzon and Sirignano model does provide a uniformly good description of the internal liquid temperature; it is better at very small Peclet numbers where its spherically symmetric structure is closer to the real situation. Figures 8, 9, and 10 show that the effective thermal conductivity model results and the actual thermal con-

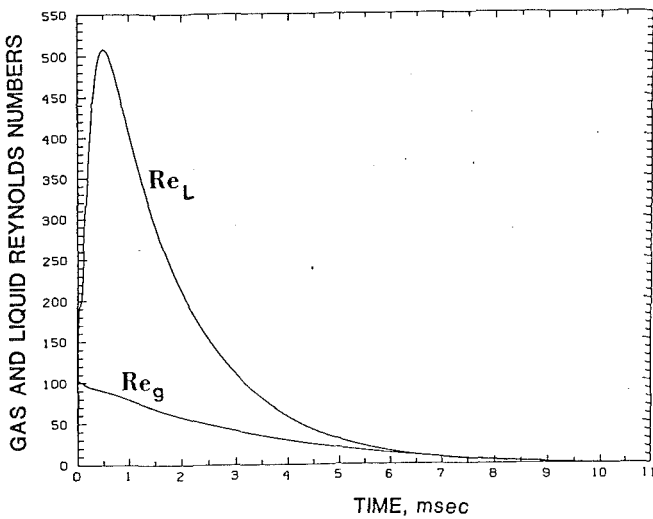


Fig. 6 Gas-phase Reynolds number,  $Re_g$ , and liquid-phase Reynolds number,  $Re_L$  versus time

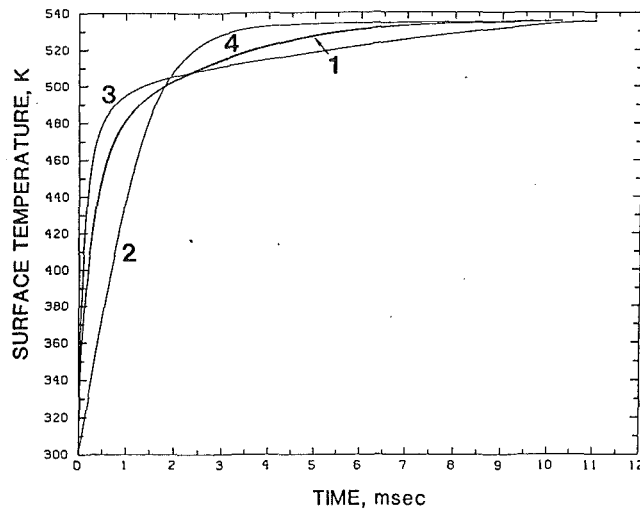


Fig. 9 Surface temperature (K) versus time: various models

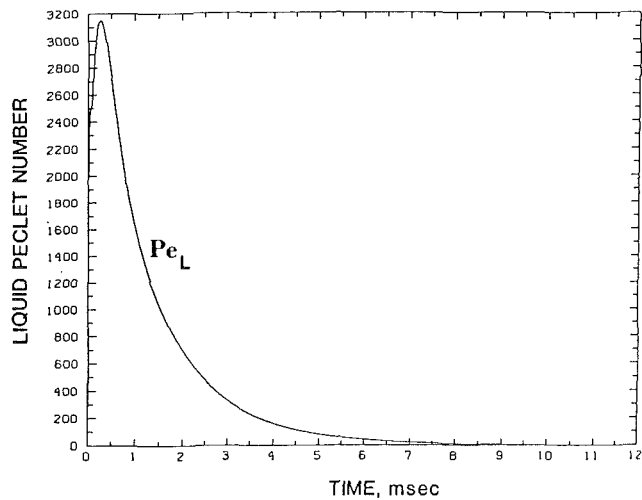


Fig. 7 Liquid-phase Peclet number versus time

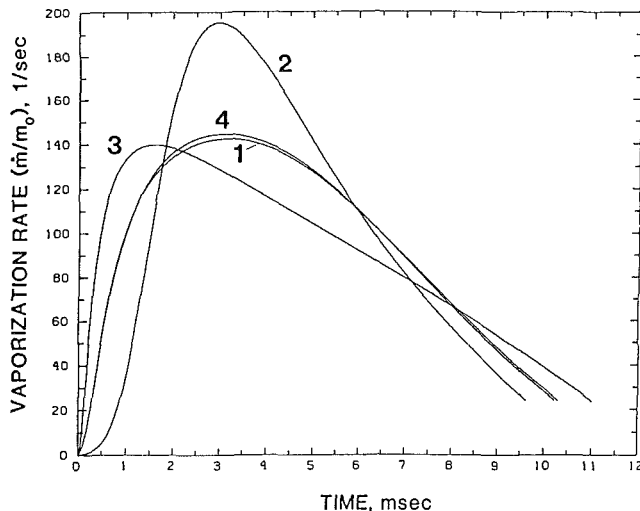


Fig. 10 Vaporization rate versus time: various models

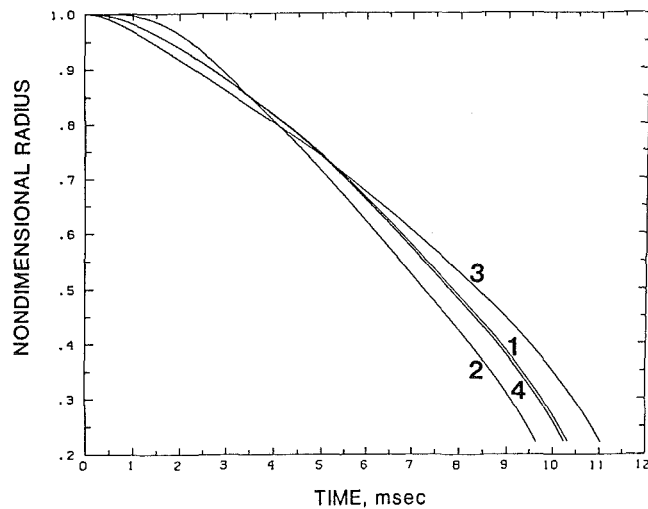


Fig. 8 Nondimensional droplet radius versus time: extended model (curve 1), infinite conductivity model (curve 2), finite conductivity model (curve 3), and effective conductivity model (curve 4)

ductivity model results are significantly different, implying that internal liquid convection is very important. The infinite conductivity model also produces very different results. It is noteworthy that small differences in the droplet radius and surface temperature curves of Figs. 8 and 9 relate to much larger differences in vaporization rate as shown in Fig. 10. Talley and Yao (1986) developed a semi-empirical effective conductivity model that produced good agreement with experiments. Furthermore, it predicted faster liquid-phase mixing than the Tong and Sirignano model.

None of these approximate models addresses the separated, elliptic flow region. Typically, heat and mass transfer are substantially reduced in that region for the Reynolds number range of interest, so that the droplet heating rate and vaporization rate can still be predicted satisfactorily. The pressure or form drag is a major portion of the total droplet drag at velocities above the creeping flow range. Therefore, drag coefficients cannot be predicted well by these models. Either correlations for the drag coefficients obtained from experiment or correlations obtained from finite difference computations can be utilized in principle as inputs to these approximate models. Experiments have generally only yielded correlations that do not account for vaporization (blowing); it is known that solid

sphere data, for example, results in overprediction of the drag if employed for vaporizing droplets. One exception is the experimental work of Renksizbulut and Yuen (1983) where the influence of transfer number was determined. In the next subsection, computational solution of the Navier-Stokes equation and derived correlations are discussed. The correlation for the drag coefficient can be employed in the simplified model although the first uses of these models preceded the availability of the correlation.

Both Tong and Sirignano (1989) and Abramzon and Sirignano (1989) studied the convecting vaporizing droplet under ambient oscillatory conditions. The major conclusion is that oscillations of the vaporization rate have sufficiently large amplitude and sufficiently small phase lag with the pressure to be a plausible mechanism for combustion instability in rockets and ramjets.

**Exact Analyses for Gas-Phase and Liquid-Phase Flow.** Exact analyses for gaseous flows over liquid droplets and internal liquid flows have been performed by several investigators. These Navier-Stokes computations resolve the inviscid flow outside of the boundary layer and wake, as well as the viscous, thermal, and diffusive layers, the recirculating near wake and part of the far wake. The shear-driven internal liquid circulation and transient heating are also resolved. Therefore, elliptic flow regions as well as the hyperbolic and parabolic regions are analyzed in detail. In addition to the global and local heat and mass exchange between the gas and liquid (which is primarily determined by the solution of the parabolic flow regions), these computations yield the drag force on the droplet (which requires resolution of the elliptic near wake as well as the other flow regions).

Exact calculations of the flow around and within vaporizing droplets serve several purposes. First, they provide detailed insight to the phenomena of heat, mass, and momentum transport for the droplet field. Second, these calculations provide a basis for comparison and verification of the simplified models that can be employed in spray calculations. Finally, the calculations can be made for a range of parameters yielding correlations for lift coefficient, drag coefficient, Nusselt numbers, Sherwood numbers, and other similarity parameters that can be employed in the simplified models.

Generally, implicit finite difference techniques are employed and the gas-phase primitive variables (velocity components, temperature, pressure, and mass fractions) are calculated directly, without transformation to other variables. The axisymmetric, unsteady form of the governing equations is solved with stiff upstream boundary conditions and zero-derivative downstream boundary conditions. The liquid and gas flows are coupled at the spherical droplet surface by conditions of continuity on temperature, species and global normal mass fluxes and tangential shear force and balance of normal momentum and normal heat flux. The stream-function-vorticity method is typically employed for the incompressible liquid. Chiang (1990) provides details of the most recent numerical methodology with adaptive nonuniform numerical grids.

Conner and Elghobashi (1987) considered the Navier-Stokes solution for laminar flow past a solid sphere with surface mass transfer. Dwyer and Sanders (1984a,b,c) performed finite-difference calculations assuming constant properties and constant density. Patnaik et al. (1986) relaxed the density assumption in their calculations but considered other properties to be constant. These calculations were made for a hydrocarbon fuel droplet vaporizing in high temperature air so that the heating and vaporization were highly transient. Haywood and Renksizbulut (1986), Renksizbulut and Haywood (1988), and Haywood et al. (1989) solved the problem of a fuel droplet vaporizing into a fuel vapor environment at moderate temperature and the problem of a fuel droplet vaporizing in air at 800 K and one atmosphere of pressure. They considered

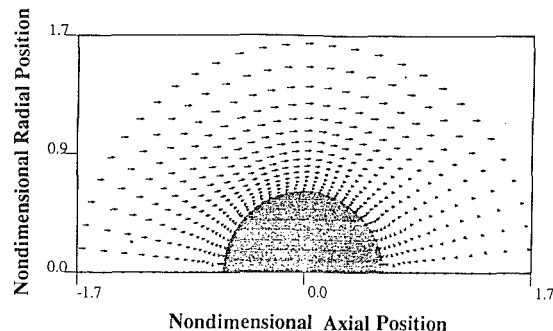


Fig. 11 Gas-phase velocity vectors at nondimensional time of 25.0 and Reynolds number of 23.88

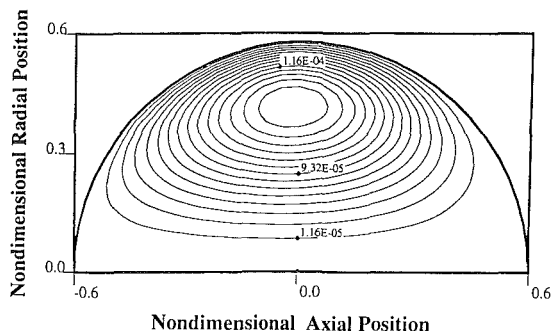


Fig. 12 Liquid-phase stream function contours at nondimensional time of 25.0 and Reynolds number of 23.88. Contour interval:  $1.16 \times 10^{-5}$

variable properties and variable density. Chiang et al. (1992) extended the computational theory to high temperature and high pressure air environments with fuel droplets allowing for variable properties and variable density with multicomponent gaseous mixtures. They showed by comparison that the constant property calculations of Raju and Sirignano (1990) and Patnaik et al. (1986) could overpredict drag coefficients by as much as 20 percent. Of course, appropriate averaging of the properties (between free stream values and droplet interface values) to determine the constant property for the calculation could reduce the error. They also calculated the deceleration of the droplet accounting for the noninertial frame of reference.

The results of Chiang (1990) and Chiang et al. (1992) are shown in Figs. 11 through 17. Figures 11 and 12 show the instantaneous gas-phase velocity field and the liquid-phase streamlines, respectively, at a time when the Reynolds number is 23.88. The decrease in relative droplet-gas velocity due to drag and the decrease in droplet radius due to vaporization imply that the droplet Reynolds number is decreasing with time. Features such as the near-wake separation and recirculation and the internal liquid circulation are clearly seen. Figure 13 shows the liquid-phase isotherms at three points in time as the droplet decelerates from an initial Reynolds number of 100. High Peclet number behavior dominates in the early period but later conduction in the streamwise direction competes with convection. Figures 14 and 15 provide typical results for the drag coefficient and Nusselt number. Figure 16 shows the drag coefficient as a function of instantaneous Reynolds number which is decreasing with time. The drag coefficient is not monotonically decreasing with increasing Reynolds number because of the dependence upon the transfer number. There is a weak sensitivity to the initial liquid temperature but a strong sensitivity to the model for droplet heating and vaporization. These nondimensional numbers are reduced substantially below the values for nonvaporizing spheres due to the blowing effect in the boundary layer. The contributions of the

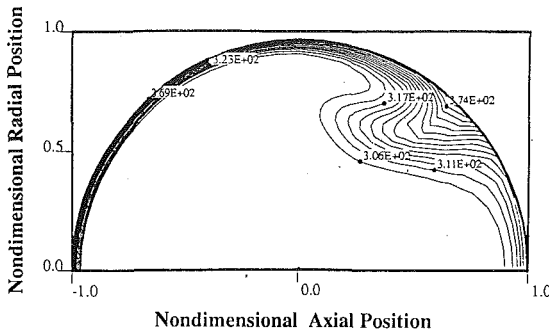


Fig. 13(a)

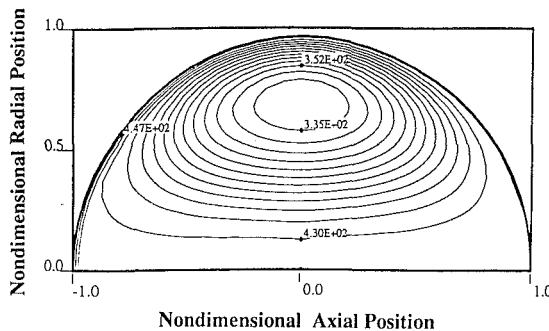


Fig. 13(b)

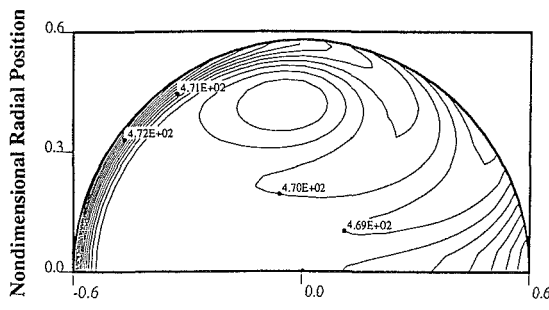


Fig. 13(c)

Fig. 13 Transient history of droplet heating. Liquid-phase isotherms at three nondimensional times and corresponding instantaneous Reynolds number: (a) time = 0.50 and  $Re = 96.45$ ; (b) time = 5.00 and  $Re = 76.06$ ; (c) time = 25.00 and  $Re = 23.88$

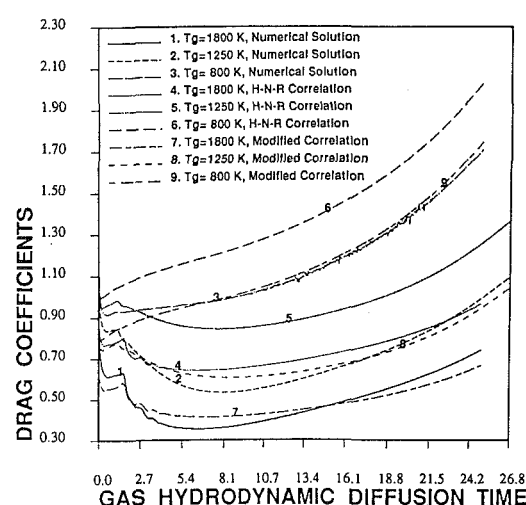


Fig. 14 Drag coefficients versus nondimensional time for different ambient temperatures: numerical results and correlations

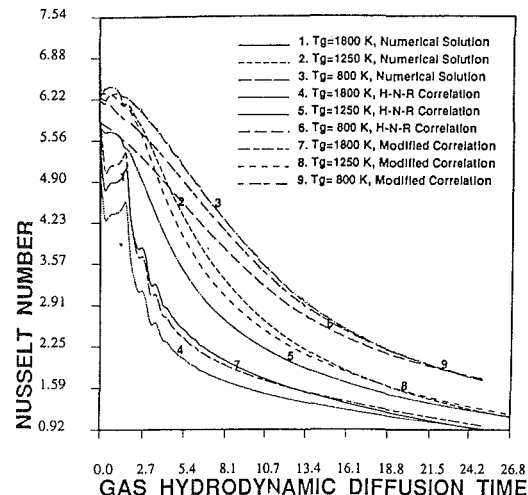


Fig. 15 Nusselt number versus nondimensional time for different ambient temperatures: numerical results and correlations

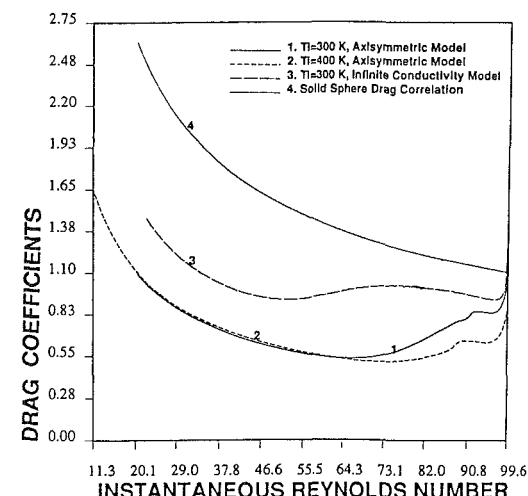


Fig. 16 Drag coefficient versus instantaneous Reynolds number: different models and initial liquid temperature

friction drag, pressure drag, and thrust (due to vaporization) are compared to each other in Fig. 17. Clearly, friction drag is affected the most by ambient temperature and heating rate through the modification of the vaporization (blowing) rate. The impact of blowing rate (through the ambient temperature variation), displayed by Figs. 14 and 15, is observed to be very strong.

Correlations of the numerical results have been obtained by Chiang et al. (1992) relating these nondimensional groupings to the instantaneous Reynolds number and transfer number  $B$ . They are:

$$C_D = (1 + B_H)^{-0.27} \frac{24.432}{Re_m^{0.721}}; \\ Nu = 1.275(1 + B_H)^{-0.678} Re_m^{0.438} Pr_m^{0.619} \\ Sh = 1.224(1 + B_M)^{-0.568} Re_m^{0.385} Sc_m^{0.492} \quad (56)$$

where  $Re_m$ ,  $Pr_m$ , and  $Sc_m$  are based upon average gas film values (except for the use of free-stream density in  $Re_m$ ) and varied from 30 to 200, 0.7 to 1.0, and 0.4 to 2.2, respectively. Also,  $B_H$  and  $B_M$  are given by Eq. (38) and cover the ranges 0.4 to 13 and 0.2 to 6.5, respectively. These correlations are shown by Figs. 14 and 15 to fit the high temperature, multi-component gas situation much better than the previously de-

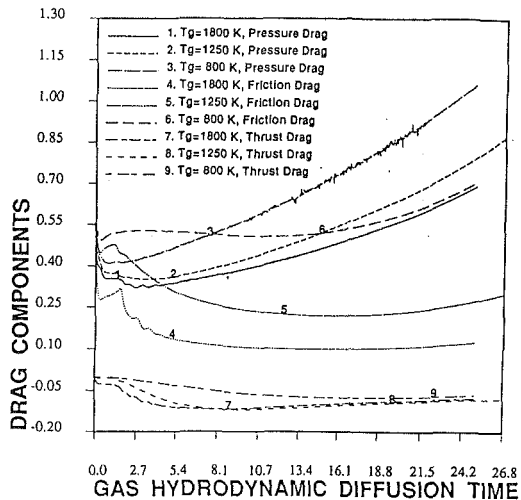


Fig. 17 Three drag coefficient components versus time for different ambient temperatures

veloped (*H-N-R*) correlations of Haywood et al. (1989). The Chiang et al. correlations can be employed for gas film model development without use of any of the models previously discussed. Note that vaporization rate can be readily related to Sherwood number. Model development for the liquid phase is still necessary since many parameters in the correlations introduce surface values. An alternate approach would be to use only the drag coefficient correlation with the approximate model. Under the implied condition of quasi-steady behavior in the gas film, the correlations describe the exchanges of mass, momentum, and energy between the two phases. The transient heating of the liquid phase must be analyzed in the simplified model in order to obtain the surface temperature and liquid heating rate for input to the transfer number which appears in the correlations.

In some recent calculations for droplets near the critical temperature, liquid density variations are taken into account. Specifically, Chiang and Sirignano (1991) replaced the liquid-phase stream function and vorticity calculations with a velocity and pressure calculation. In current research, a cubic equation of state is applied for the liquid and gas. Also, dissolving and diffusion of the ambient gas components in the liquid are considered near the critical point.

### 3 Spray Equations

We will focus here on the formulation of the describing equations for the dynamics of a spray, considering the discrete phase to be strictly a liquid and the continuous phase to be strictly a gas. Of course, it is simple to generalize the formulation to include dusty flows and bubbly flows.

The spray equations will be presented in three different but related constructions: the two-continua or multicontinua formulation, the discrete particle formulation, and the probabilistic formulation. Both Lagrangian and Eulerian methods will be examined. The relationships amongst these various formulations and methods will be emphasized and will be a major contribution here. Previous research on the multicontinua formulation is reported by Sirignano (1972, 1986, 1993), Crowe et al. (1977), Crowe (1978, 1982), and Ducowicz (1980). The discrete particle method is discussed by Sirignano (1986, 1993) while the probabilistic formulation is discussed by Williams (1985) and Sirignano (1986, 1993). The extensions of the current treatise beyond those previous formulations will be identified as we proceed.

In developing the spray equations, it is convenient to define various density functions. Let  $\rho$  be the material density of the

gas which is the mass per unit volume in a volume that includes only gas.  $\bar{\rho}$  is the gas bulk density which is the mass of the gas in a volume that includes both gas and liquid. Similarly,  $\rho_l$  and  $\bar{\rho}_l$  are the material density and the bulk density of the liquid. Furthermore,  $\theta$  is defined as the void fraction of the gas which is the ratio of the equivalent volume of gas to a given volume of a gas and liquid mixture. Obviously,  $1 - \theta$  is the void fraction of liquid. In our terminology, void fraction simply means  $\theta$ .

It follows that

$$\bar{\rho} = \theta \rho \quad \text{and} \quad \bar{\rho}_l = (1 - \theta) \rho_l$$

For very dilute sprays,  $\theta \rightarrow 1$  and  $\bar{\rho} \approx \rho$ . However, because  $\rho_l \gg \rho$  in typical cases, it could be poor in that limit to declare that  $\bar{\rho}_l$  is negligible compared to  $\rho$ . Note that  $\rho_l$  will be considered to be constant although  $\bar{\rho}_l$  can vary spatially and temporally.

There are various types of spray calculations that can be of interest. A most important issue involves the length scale of resolution. First, there is the question of whether droplets can be viewed as point sources with respect to gas-phase consideration. This can be a valid approximation in a domain if the collective volume of all liquid droplets and of all of their immediate gas films in that domain is small compared to the total gas volume in that same domain. The approximation can fail locally in regions of dense spray even if the above criteria is met globally. Only in the limiting case of a spherically symmetric transport field around the droplet does the point source approximation give the exact influence on the far gas field. We almost always make the point source approximation.

Another issue concerns the desired resolution compared to the average spacing between droplets. If the resolution is smaller than that spacing, we must account for each droplet physically present in the flow. This clearly limits the total number of droplets that can be considered. Since droplets are considered here as discrete particles, a numerical method that uses an Eulerian scheme for the gas phase and a Lagrangian scheme for the liquid phase is utilized.

If resolution on a scale larger than the droplet spacing is sufficient, only average droplets in each neighborhood need to be considered. Then, we can obviously consider domains that include a much larger number of droplets. Eulerian calculations are employed for the gas phase and either an Eulerian or Lagrangian scheme can be used for the dispersed liquid phase. The Lagrangian scheme is preferred because it reduces numerical error due to artificial diffusion.

**3.1 Two-Continua and Multicontinua Formulations.** Let us develop the governing equations beginning with the conservation of mass statement. Each dependent variable at any spatial point is an instantaneous average over a neighborhood (of that point) that includes both liquid and gas. Therefore, both liquid properties and gas properties exist at a point regardless of whether that point is actually in a gas or in a liquid at that instant. This method is a two-continua approach since both a continuum of gas properties and a continuum of liquid properties are defined. The gas-phase continuity equation is

$$\frac{\partial \bar{\rho}}{\partial t} + \frac{\partial}{\partial x_j} (\bar{\rho} u_j) = \dot{M} \quad (57)$$

while the liquid-phase continuity equation is

$$\frac{\partial \bar{\rho}_l}{\partial t} + \frac{\partial}{\partial u_j} (\bar{\rho}_l u_j) = -\dot{M} \quad (58)$$

where  $\dot{M}$  is the mass vaporization rate per unit volume. Models for evaluating the vaporization rate are discussed in other sections.

The mixture continuity equation is given by

$$\frac{\partial(\bar{\rho} + \bar{\rho}_v)}{\partial t} + \frac{\partial}{\partial x_j} (\bar{\rho} u_j + \bar{\rho}_v u_{vj}) = 0 \quad (59)$$

The above equations can be obtained by a control volume approach under the assumption that, as the volume shrinks to zero, the limiting value of the volume void fraction  $\theta$  is identical to the limiting value of the void fraction of the bounding surface area. Clearly, only two of the three above equations are independent.

Equation (58) can be recast as an equation governing  $\theta$  instead of  $\bar{\rho}_v$ . It becomes

$$\frac{\partial \theta}{\partial t} + \frac{\partial}{\partial x_j} (\theta u_{vj}) = \frac{\dot{M}}{\rho_v} + \frac{\partial u_{vj}}{\partial x_j} \quad (60)$$

The nonzero right-hand side indicates that  $\theta$  is not conserved for two reasons: (1) vaporization (or condensation) changes the liquid volume and (2) droplet trajectories diverge (or converge) thereby increasing (or decreasing) the distances between droplets.

Often, it is convenient to divide the droplets into many classes according to initial values of velocity, position, diameter, and/or composition. Then, our two-continua approach is expanded to a multicontinua approach. In such a case, it is not usually convenient to solve Eqs. (58) or (60) for  $\bar{\rho}_v$  or  $\theta$ . Rather, we distinguish each class of droplets according to an integer value  $k$  and set

$$n = \sum_k n^{(k)}; \quad \dot{M} = \sum_k \dot{M}^{(k)} = \sum_k \dot{m}^{(k)} n^{(k)} \quad (61)$$

where  $\dot{m}^{(k)}$  is the vaporization rate of an average droplet in the  $k$ th class,  $n^{(k)}$  is the number density of droplets in that  $k$ th class, and  $n$  in the global droplet number density. The methods discussed in Section 2 can be employed to determine  $\dot{m}^{(k)}$ . The determination of  $n^{(k)}$  will be discussed later in this section. In the limit of a very large number of different droplet classes, the summation of Eq. (61) can be replaced by an integral. This extension to a multicontinua approach was first suggested by Ducowicz (1980) and pursued by Sirignano (1986); it allows for better resolution of the variations amongst the many droplets that can be present in a spray calculation. Note that while Ducowicz (1980) refers to his method as a discrete particle method, it does not meet the discrete particle definition employed here. It is a multicontinua method.

We can define  $\psi^{(k)}$  as the liquid volume fraction of the  $k$ th class of droplets and  $\bar{\rho}_v^{(k)}$  as the bulk liquid density of that class. Then

$$1 - \theta = \sum_k \psi^{(k)}; \quad \bar{\rho}_v^{(k)} = \psi^{(k)} \rho_v^{(k)} = n^{(k)} \frac{4\pi}{3} (R^{(k)})^3 \rho_v^{(k)} \quad (62)$$

Note that we are allowing for the possibility that different droplet classes can possess different material densities. The effects of different liquid material densities and the effect of void volume were considered by Ducowicz (1980) but not contained in the original presentations by Sirignano (1972, 1986, 1993). Crowe (1977) did consider the effect of void volume but did not consider separate classes of droplets.

It follows that

$$\frac{\partial \bar{\rho}_v^{(k)}}{\partial t} + \frac{\partial}{\partial x_j} (\bar{\rho}_v^{(k)} u_{vj}^{(k)}) = -n^{(k)} \dot{m}^{(k)} = -\dot{M}^{(k)} \quad (63)$$

where

$$u_{vj} = \sum_k \frac{\bar{\rho}_v^{(k)}}{\bar{\rho}_v} u_{vj}^{(k)}$$

is a mass-weighted average liquid droplet velocity. When the material density is the same for all droplet classes, it also becomes a volume-weighted average velocity. Furthermore, we have

$$\frac{\partial \psi^{(k)}}{\partial t} + \frac{\partial}{\partial x_j} (\psi^{(k)} u_{vj}^{(k)}) = -\frac{\dot{M}^{(k)}}{\rho_v^{(k)}} \quad (64)$$

We can solve either Eq. (63) or (64) simultaneously with other equations to be discussed later in this section and then use Eq. (62) to get both  $\psi^{(k)}$  and  $\bar{\rho}_v^{(k)}$ . However, we still require either  $n^{(k)}$  or  $R^{(k)}$  to determine the right-hand side of Eq. (63) or (64). Realizing that

$$\dot{m}^{(k)} = -\frac{4\pi}{3} \rho_v^{(k)} \frac{d}{dt} (R^{(k)})^3$$

where the time derivative is taken in the Lagrangian sense following the droplet, we can manipulate Eqs. (62) and (63) to obtain

$$\frac{\partial n^{(k)}}{\partial t} + \frac{\partial}{\partial x_j} (n^{(k)} u_{vj}^{(k)}) = 0 \quad (65)$$

which is a conservation equation for droplet number for each class. A global conservation equation is obtained by summing Eq. (65) over all classes. Then

$$\frac{\partial n}{\partial t} + \frac{\partial}{\partial x_j} (n \tilde{u}_{vj}) = 0 \quad (66)$$

where

$$\tilde{u}_{vj} = \sum_k \frac{n^{(k)} u_{vj}^{(k)}}{n}$$

is a number-weighted average velocity.

It is now seen that the two Eqs. (62), Eq. (63) [or (64)], and Eq. (65) provide four (two differential plus two algebraic) equations that will yield  $\bar{\rho}_v^{(k)}$ ,  $\psi^{(k)}$ ,  $n^{(k)}$ , and  $R^{(k)}$ . Necessary inputs are  $u_{vj}^{(k)}$  which will come from the solution of the momentum equation and a mathematical model for the vaporization rate  $\dot{m}^{(k)}$ .

Consider now the species conservation equations for the gas. The integer index  $m$  represents the particular species. The mass fraction  $Y_m$  is prescribed by

$$\begin{aligned} \frac{\partial}{\partial t} (\bar{\rho} Y_m) + \frac{\partial}{\partial x_j} (\bar{\rho} u_j Y_m) - \frac{\partial}{\partial x_j} \left( \bar{\rho} D \frac{\partial Y_m}{\partial x_j} \right) \\ = \dot{M}_m + \bar{\rho} \dot{w}_m = \sum_k n^{(k)} \dot{m}^{(k)} + \bar{\rho} \dot{w}_m \end{aligned} \quad (67)$$

where

$$\dot{M} = \sum_m \dot{M}_m = \sum_m \epsilon_m \dot{M}; \quad \dot{m}^{(k)} = \sum_k \dot{m}_m^{(k)}; \quad \sum_m \dot{w}_m = 0$$

In Eq. (67), the mass diffusivity is assumed to be the same for all species.  $\epsilon_m$  is a species flux fraction. Obviously,

$$\sum_m \epsilon_m = 1.$$

Summation over all components in Eq. (67) yields the continuity Eq. (57). Therefore, if we have  $N$  different species, only  $N-1$  species conservation equations need to be solved together with Eq. (57). Note that Eqs. (57) and (67) can be combined to yield a nonconservative form

$$\bar{\rho} \left[ \frac{\partial Y_m}{\partial t} + u_j \frac{\partial Y_m}{\partial x_j} \right] - \frac{\partial}{\partial x_j} \left( \bar{\rho} D \frac{\partial Y_m}{\partial x_j} \right) = (\epsilon_m - Y_m) \dot{M} + \bar{\rho} \dot{w}_m \quad (68)$$

Generally, the conservative form of the equations are preferred for computation. Note that here the "conservative" Eq. (11) still has source terms.

Now, let us consider the gas-phase momentum equation.

$$\begin{aligned} \frac{\partial}{\partial t} (\bar{\rho} u_i) + \frac{\partial}{\partial x_j} (\bar{\rho} u_j u_i) + \frac{\partial p}{\partial x_i} - \frac{\partial}{\partial x_j} (\theta \tau_{ij}) - \frac{\partial}{\partial x_j} [(1-\theta) \tau_{ij}] \\ = \sum_k n^{(k)} \dot{m}^{(k)} u_{vj}^{(k)} - F_{Di} + \bar{\rho} g_i \end{aligned} \quad (69)$$

where

$$F_{Di} = \sum_k n^{(k)} F_{Di}^{(k)} \quad \text{and} \quad \tau_{ij} = \mu \left( \frac{\partial u_i}{\partial x_j} + \frac{\partial u_j}{\partial x_i} \right) - \frac{2}{3} \delta_{ij} \frac{\partial u_i}{\partial x_j}$$

The assumption is made in the momentum equation that the gradient of the pressure force is continuous across liquid-gas interfaces, but differences are allowed in the viscous stress imposed on the mixture through the different phases. The above equation was derived with the same control volume and bounding surface as described for the continuity equation. In this momentum equation, we first note the uncertainty created by a lack of rigor. On the one hand, we are averaging gas and liquid properties over many droplet spacings so that both liquid and gas properties exist at any point. On the other hand, we shrink the control volume to zero in our calculus and, in that limit, we attempt to distinguish between gas and liquid boundary forces. The statement that the volume void fractions serve as weighting factors for liquid viscous stress and gaseous viscous stress is no better than a reasonable assumption since clarity in the limit of shrinking the volume to zero is really lost in the averaging process. The above equation also includes momentum sources and sinks due to droplet vapor mass sources, reaction to droplet drag, and body forces on the gas.

Combination of Eqs. (57) and (69) yields another nonconservative form of the momentum equation

$$\bar{\rho} \left[ \frac{\partial u_i}{\partial t} + u_j \frac{\partial u_i}{\partial x_j} \right] + \frac{\partial p}{\partial x_i} - \frac{\partial}{\partial x_i} [\theta \tau_{ij} + (1-\theta) \tau_{ij}] = \sum_k n^{(k)} \dot{m}^{(k)} (u_{\ell}^{(k)} - u_i) - F_{Di} + \bar{\rho} g_i \quad (70)$$

The liquid-phase momentum equation can be written as

$$\frac{\partial}{\partial t} (\bar{\rho}_\ell u_\ell) + \frac{\partial}{\partial x_j} (\bar{\rho}_\ell u_j u_\ell) = - \sum_k n^{(k)} \dot{m}^{(k)} u_\ell^{(k)} + F_{Di} + \bar{\rho}_\ell g_i \quad (71)$$

Actually, it is preferably to avoid Eq. (71) and to use a separate momentum equation for each class of droplets. In particular, we have

$$\frac{\partial}{\partial t} (\bar{\rho}_\ell u_\ell^{(k)}) + \frac{\partial}{\partial x_j} (\bar{\rho}_\ell^{(k)} u_j^{(k)} u_\ell^{(k)}) = - n^{(k)} \dot{m}^{(k)} u_\ell^{(k)} + n^{(k)} F_{Di}^{(k)} + \bar{\rho}_\ell g_i \quad (72)$$

or, combining with Eq. (58), we obtain

$$\bar{\rho}_\ell^{(k)} \left[ \frac{\partial u_\ell^{(k)}}{\partial t} + u_{\ell,j}^{(k)} \frac{\partial u_\ell^{(k)}}{\partial x_j} \right] = n^{(k)} F_{Di}^{(k)} + \bar{\rho}_\ell^{(k)} g_i \quad (73)$$

Note that Eqs. (69) and (71) could be added to yield a mixture momentum equation that eliminates all right-hand-side source terms except for the body forces.

In the development of the energy equation, only low Mach number equations are considered so that kinetic energy and viscous dissipation terms are neglected in the formation. Note that the perfect gas law yields

$$\theta p = \bar{\rho} RT \quad \text{and} \quad \bar{\rho} e = \bar{\rho} h - \theta p \quad (74)$$

Then the energy equation can be written as

$$\begin{aligned} \frac{\partial}{\partial t} (\bar{\rho} h) + \frac{\partial}{\partial x_j} (\bar{\rho} u_j h) - \frac{\partial}{\partial x_j} \left( \theta \lambda \frac{\partial T}{\partial x_j} \right) \\ - \frac{\partial}{\partial x_j} \left[ (1-\theta) \lambda_\ell \frac{\partial T}{\partial x_j} \right] - \frac{\partial}{\partial x_j} \left( \sum_m \bar{\rho} h_m D \frac{\partial Y_m}{\partial x_j} \right) = \frac{d}{dt} (\theta p) \\ + \sum_m \bar{\rho} \dot{w}_m Q_m - \sum_k n^{(k)} \dot{m}^{(k)} L_{\text{eff}}^{(k)} + \sum_k n^{(k)} \dot{m}^{(k)} h_s^{(k)} \end{aligned} \quad (75)$$

It can be noted that

$$h = \int_{T_{\text{ref}}}^T c_p dT' = \int_{T_{\text{ref}}}^T \left( \sum_m Y_m c_{pm}(T') \right) dT'$$

Furthermore, we can combine the continuity equation (57) with (75) to obtain a nonconservative form

$$\begin{aligned} \bar{\rho} \left[ \frac{\partial h}{\partial t} + u_j \frac{\partial h}{\partial x_j} \right] - \frac{\partial}{\partial x_j} \left( \theta \lambda \frac{\partial h}{\partial x_j} \right) \\ + \frac{\partial}{\partial x_j} \left[ \bar{\rho} D (Le-1) \sum_m h_m \frac{\partial Y_m}{\partial x_j} \right] - \frac{\partial}{\partial x_j} \left[ (1-\theta) \lambda_\ell \frac{\partial T}{\partial x_j} \right] \\ = \frac{d(\theta p)}{dt} + \sum_m \bar{\rho} \dot{w}_m Q_m - \sum_k n^{(k)} \dot{m}^{(k)} (h - h_s^{(k)} + L_{\text{eff}}^{(k)}) \end{aligned} \quad (76)$$

Note that the chemical source terms would be eliminated from Eqs. (75) and (76) if the enthalpy were redefined to include the summation of the mass fraction times the heat of formation over all species.

The liquid-phase temperature will generally vary spatially and temporally within the liquid droplet. A Navier-Stokes solver or some approximate algorithms as described in Section 2 by Eqs. (49) and (53) can be employed to determine the temperature field in the droplet including the surface temperature. In the special case of a uniform but time varying liquid temperature in the droplet, an equation for the thermal energy contained in the droplet can be useful. If  $e_\ell$  is the liquid internal energy per unit mass, then  $\bar{\rho} e_\ell$  is the liquid internal energy per unit volume of mixture. In the case where a spatial variation of temperature occurs in the droplet,  $e_\ell$  could be considered as the average over the droplet. However, an equation for  $e_\ell$  would not be so useful here since the difference between the average value and the surface value is not specified but yet the results are most sensitive to the surface temperature. The liquid energy equation can be rewritten for each class of droplets

$$\begin{aligned} \frac{\partial}{\partial t} (\bar{\rho}_\ell^{(k)} e_\ell^{(k)}) + \frac{\partial}{\partial x_j} (\bar{\rho}_\ell^{(k)} u_j^{(k)} e_\ell^{(k)}) \\ = n^{(k)} \dot{q}_\ell^{(k)} - n^{(k)} \dot{m}^{(k)} e_{\ell,s}^{(k)} \end{aligned} \quad (77)$$

This equation can be combined with Eq. (63) to yield an alternative form

$$\bar{\rho}_\ell^{(k)} \left[ \frac{\partial e_\ell^{(k)}}{\partial t} + u_{\ell,j}^{(k)} \frac{\partial e_\ell^{(k)}}{\partial x_j} \right] = n^{(k)} \dot{m}^{(k)} \left( e_\ell^{(k)} - e_{\ell,s}^{(k)} + \frac{\dot{q}_\ell^{(k)}}{\dot{m}^{(k)}} \right) \quad (78)$$

where  $\dot{q}_\ell^{(k)}$  is the conductive heat flux from the liquid interface of a droplet toward its interior. Note that during droplet heating, we expect that  $e_\ell^{(k)} - e_{\ell,s}^{(k)}$  is negative (maximum liquid temperature is at the interface) or zero so that energy is lost from the liquid phase on account of this effect.

The liquid-phase equations form a hyperbolic subsystem of partial differential equations. In particular, we define the operation

$$\frac{d^{(k)}}{dt} = \frac{\partial}{\partial t} + u_{\ell,j}^{(k)} \frac{\partial}{\partial x_j}$$

This is a Lagrangian time derivative following an average droplet in the  $k$ th droplet class. Then mass conservation states that the droplet radius is described by

$$\frac{d^{(k)} R^{(k)}}{dt} = - \frac{\dot{m}^{(k)}}{4\pi \bar{\rho}_\ell^{(k)} (R^{(k)})^2} \quad (79)$$

The droplet position is governed by

$$\frac{d^{(k)} x_i^{(k)}}{dt} = u_{\ell,i}^{(k)} \quad (80)$$

while Eq. (73) governs the droplet velocity

$$\bar{\rho}_\ell^{(k)} \frac{d^{(k)} u_{\ell,i}^{(k)}}{dt} = n^{(k)} F_{Di}^{(k)} + \bar{\rho}_\ell^{(k)} g_i \quad (81)$$

The energy Eq. (78) can be written as

$$\bar{\rho}_l^{(k)} \frac{de_l^{(k)}}{dt} = n^{(k)} \dot{m}^{(k)} \left( e_l^{(k)} - e_{ls}^{(k)} + \frac{\dot{q}_l^{(k)}}{\dot{m}^{(k)}} \right) \quad (82)$$

Equations (81) and (82) are the characteristic equations for the hyperbolic partial differential equations (72) and (78). Equation (80) describes the characteristic lines through space for those hyperbolic equations. The Lagrangian method for the averaged liquid properties is therefore fully equivalent to the method of characteristics as explained by Sirignano (1986, 1993). The Ducowicz (1980) analysis is actually a method of characteristic approach to the multicontinua formulation rather than the type of discrete-particle formulation discussed in the next subsection. This method of characteristics allows the partial differential equations to be converted to ordinary differential equations that are solved more readily with a reduction in the numerical error due to integration. Specifically, the solution of the partial differential equations can produce artificial diffusion through the difference equation approximation; this type of error does not occur with the differencing of the ordinary differential equations.

These equations are solved simultaneously with the gas-phase equations (57), (67) or (68), (69) or (70), and (75) or (76) together with the equation of state (74). These gas-phase equations are typically solved by finite-difference methods on an Eulerian mesh that is either fixed or defined through some adaptive grid scheme. The terms representing exchanges of mass, momentum, and energy between the two phases appear as source and sink terms in both the gas-phase and liquid-phase equations. They provide the mathematical coupling between the two subsystems of equations representing the two phases. The liquid Lagrangian equations are effectively solved on a different grid from the gas-phase equations so that interpolation is continually used in the evaluation of the source and sink terms. Care must be taken in avoiding other numerical errors of the same order as the artificial diffusion that has been eliminated; these other errors can be created by a low order interpolation scheme. Details about the method and analyses of its performance can be found in Aggarwal et al. (1981, 1983, 1985).

The Lagrangian or characteristic path is the trajectory of an average droplet that represents a group of droplets that (at least initially) are in the same neighborhood. The droplet number density can vary along this path but the number of droplets represented remains fixed (in the absence of droplet shattering or coalescence).

In this two-continua method, two distinct characteristic lines (from the same or different droplet classes) can intersect without implication of a collision. The characteristic lines or trajectories represent the paths of average droplets; each average droplet represents a beam or moving cloud of droplets. If average spacing between neighboring droplets is sufficiently large, two beams can pass through each other without any collisions. An important implication here is that multivalued liquid properties can occur; at a given point in space and time, more than one value of a liquid property for a given class of droplets can exist. Note that the direct solution of hyperbolic partial differential equations for the liquid properties will smear any multivalued solutions upon numerical integration. In this regard, the Lagrangian method is substantially more powerful and reliable.

In the Lagrangian method, we bypass the use of Eq. (65) for the droplet number conservation. We must still evaluate the droplet number density which appears in source and sink terms in Eqs. (57), (58), (60), (63), (64), (67) through (73), (75), and (76) through (78). Typically, we determine number density locally in a two-continua finite-difference computation by: (i) determining the number of average droplets for each droplet class in each computational cell at each temporal point in the calculation, (ii) determining, based upon the initial con-

dition for each average droplet, the total number of actual droplets of each class present in the computational cell, and (iii) dividing this total number by the volume of the computational cell to obtain the number density.

The gas-phase and liquid-phase equations described in this section can be applied to turbulent flows, but first, Reynolds averaging or Favre averaging of the equations should be performed. Also, some approximations are required to close the equations. As a result of this process, averaged forms of the previous equations plus additional equations for the turbulent kinetic energy and other second-order quantities result. See Elghobashi and coworkers (1983, 1984, 1991, 1992) for details on these turbulent spray analyses.

Initial conditions are required for the solution of the unsteady form of the equations. Often, the unsteady form is employed even when we wish to obtain the steady-state solution. For example, if the system of differential equations (57), (67), (69), (75), (79), (80), (81), and (82) were to be solved, initial conditions would be required for the gas-phase velocity, density, mass fractions, and enthalpy and for the velocities, positions, radii, and thermal energies of the average droplets in each class.

Boundary conditions are also required. Equations (67), (69), and (75) have elliptic spatial operators so that, for velocity, mass fractions, and enthalpy, conditions on the quantities or their gradients are required for every boundary point. Equation (57) is a first-order hyperbolic equation so that density needs to be specified only at the inflow boundaries. Boundary conditions on Eqs. (79), (80), (81), and (82) for the average droplet properties are only required for inflow. When the droplet passes through an open boundary, we discontinue the calculation for that particular droplet. When a droplet strikes a solid wall, there are several options: (i) the wall can be assumed to be so cold that the droplet sticks to the wall and no further vaporization occurs (effectively removing the droplet from the field of computation), (ii) the wall is so hot that the droplet immediately vaporizes providing a local gaseous mass source, and (iii) the droplet rebounds, perhaps shattering into a number of small droplets. Clearly, the last condition is the most difficult to implement in a calculation. Naber and Reitz (1988) have claimed that better agreement with experimental data can be obtained for some calculations if the droplet is assumed to flow along the wall with the local gas velocity near the wall.

**3.2 Discrete-Particle Formulation.** The two-continua or multicontinua approach allows resolution only on a scale larger than the average spacing between neighboring droplets. Often, however, we must resolve a spray behavior on a finer scale. In combustion applications, ignition and flame structure are examples where that level of resolution is required. An alternative to the two-continua approach is the discrete particle approach that serves the purpose of higher resolution. This method follows each individual droplet and resolves the liquid field within each droplet and the gas field surrounding each droplet. Obviously, it is limited to a smaller number of droplets and to a smaller volume of mixture than the two-continua approach. Since the discrete phase is being resolved here, only gas properties or only liquid properties exist at a given point in space or time. The hyperbolic partial differential equations or their characteristic differential equations have no meaning in this approach. Although the droplet trajectories are not characteristic lines in this approach, certain ordinary differential equations are still written along these trajectory lines so that we have a Lagrangian method here, albeit of another type than previously discussed. Here, we do not distinguish droplets by class because, obviously, each droplet forms its own class.

The governing equations for each droplet are

$$\frac{dR}{dt} = \frac{\dot{m}}{4\pi\rho_l R^2} \quad (83)$$

$$\frac{dx_i}{dt} = u_{ii} \quad (84)$$

$$\frac{du_{ii}}{dt} = \frac{3\tilde{F}_{Di}}{4\pi\rho_i R^3} + g_i \quad (85)$$

and

$$\frac{de_i}{dt} = \frac{3\dot{m}}{4\pi\rho_i R^3} \left( e_i - e_{is} + \frac{\dot{q}_i}{\dot{m}} \right) \quad (86)$$

Often, Eq. (86) is replaced by the energy function for the liquid which governs diffusion and convection in the droplet.

The gas-phase equations must be solved simultaneously with the above droplet equations. The discrete-particle approach is only sensible when resolution is finer than the spacing between neighboring droplets. Therefore, the computational mesh size must be significantly smaller (by at least an order of magnitude) than the spacing. In the dilute (or nondense) sprays, this interdroplet spacing is also much greater than the average droplet diameter so therefore we expect the computational mesh size to be comparable to or greater than the droplet diameter. Here, we expect most computational cells will not contain a droplet but only gas; only a small fraction of the cells will contain a droplet, and typically only one droplet each, since average spacing is so large. Equations (57), (67) or (68), (69) or (70), (74), and (75) or (76) describe the gas phase and can be placed into finite-difference form. Here,  $\theta = 1$  and  $\bar{\rho} = \rho$  is taken. Also, the source terms representing exchanges of mass, momentum and energy between phases go to zero in those equations for these cells. This is definitely accurate for the great majority of cells which do not contain any droplet. In the cells containing droplets, we can allow  $\theta$  to deviate from unity to account for the droplet volume. Whenever the droplet diameter is small compared to the mesh size,  $\theta$  can be assumed to be unity neglecting droplet volume from the perspective of the coupling with the gas phase.

**3.3 Computational Issues.** The analyses for the discrete particle method and for the two-continua (or multi-continua) method as outlined herein are built on the premise that subgrid modeling of the behaviors of the liquid in the droplet interior and of the gas in the boundary layer and wake of the droplet will be employed. These subgrid models are discussed in Section 2. This is sensible when the droplet diameter is much smaller than the interdroplet spacing and smaller than or comparable to the mesh size needed to resolve the gas phase. Then, the subgrid modeling avoids the costly solution of complex equations on a grid size smaller than the droplet diameter. In the case of a dense spray, the droplet diameter becomes comparable to the spacing and, therefore, resolution of the gas phase and resolution of the liquid phase are just as costly. It makes much less sense to use the discrete-particle method with its inherent sub-grid modeling for these dense sprays. If fine resolution is required, solution of the Navier-Stokes equations with account for phase boundaries is suggested. Complexity of the problem will limit the total volume of mixture that can be treated. If average properties were sufficient, the two-continua method can be used for these dense sprays. Note that the equations formulated in this section do not account for collisions that might occur in very dense sprays.

In both the multicontinua method and the discrete-particle method, a phase-exchange source term value for the gas phase is generally not immediately given at a gas-phase mesh point. Rather, it is presented at the instantaneous position of the droplet. Its value must be extrapolated to the mesh points. The lowest-order approximation involves simply transferring the value from the droplet location to the nearest mesh point. This produces numerical errors of the same first order as numerical diffusion errors that are avoided for the liquid phase by the Lagrangian method. It is superior therefore to distribute the source term in a weighted manner to the neighboring mesh

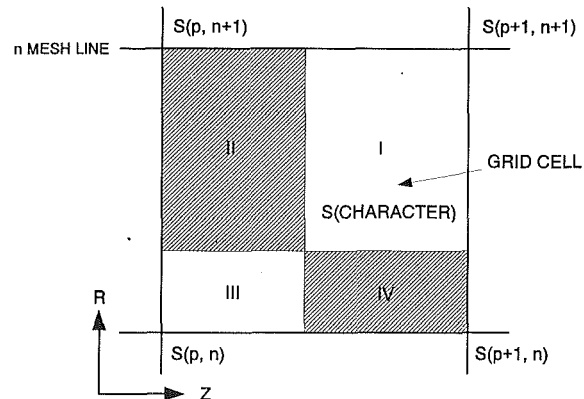


Fig. 18 Graphical display of weighting factors for two dimensional Eulerian-Lagrangian spray calculations

points. There will be two, four, or eight neighboring mesh points depending upon whether we have a one, two, or three-dimensional calculation. The droplet or average droplet under consideration is within a rectangle defined by the corners at the four mesh points  $(p, n)$ ,  $(p+1, n)$ ,  $(p+1, n+1)$ , and  $(p, n+1)$ . Consider that the nearest mesh point is  $(p, n)$ . The lowest-order approximation merely transfers the source term  $S$  to the mesh point  $(p, n)$  with resulting first-order accuracy. The second-order scheme divides the source term  $S$  into four parts, each associated with a mesh point and weighted inversely to proximity of that mesh point to the droplet position. Namely

$$S_{p,n} = \frac{A_{p,n}}{A} S; \quad S_{p+1,n} = \frac{A_{p+1,n}}{A} S;$$

$$S_{p+1,n+1} = \frac{A_{p+1,n+1}}{A} S; \quad S_{p,n+1} = \frac{A_{p,n+1}}{A} S$$

where  $A$  is the area of the original rectangle and  $A_{p,n}$ , etc., are the areas of the subdivided rectangles shown in Figure 18. Note that the extension to three dimensions involves eight subdivided rectangular volumes.

Note that the source point is taken as the center of the droplet. Furthermore, in the multicontinua approach, many droplets can be represented by each average droplet. Also, any given mesh point can be a corner point for several cells (four in two dimensions), each of which can contain droplets and transfer portions of the source terms to the mesh point. These source contributions from various droplets are simply additive. Finally, note that the same geometrical weighting factors should be employed to evaluate gas properties at the droplet position (for input as source terms to the liquid-phase equations) given the properties at the neighboring mesh points.

In the discrete-particle method, we must present ambient gas conditions for the droplet in order to determine the droplet vaporization rate, heating rate, drag, and trajectory. In a finite difference scheme, the gas properties at immediately neighboring mesh points to the instantaneous droplet position are employed as the ambient conditions on the subgrid droplet model. Theoretically, these ambient conditions should exist at the edge of the gas film (boundary layer and wake) surrounding the droplet; in practice, however, the neighboring mesh points might be in the gas film leading therefore to errors in the matching of the subgrid droplet model to the gas phase. These errors and their corrections were addressed by Rangel and Sirignano (1989b) and Sirignano (1993).

The surprising result is that as the gas-phase grid is refined, the error increases; the neighboring mesh points to the droplet actually move closer to the droplet and into the surrounding gas film. In the case where the droplet moves with the surrounding gas, we can assume that the gas film is spherically symmetric with respect to the droplet center. In that case,

Rangel and Sirignano have shown that mass vaporization rate given by Eq. (9) should be multiplied by the factor  $1 + \epsilon$  to correct for the error in application of the ambient boundary condition on the droplet model. For the case where the gas-phase grid size is smaller than the droplet radius, it is found that

$$\epsilon = -\frac{1}{1+\delta}$$

where  $\delta$  is the ratio of the distance between the mesh point (where ambient conditions are applied) and the droplet center to the droplet radius. This analytical solution of Rangel and Sirignano considers the ambient gas conditions as given and only addresses errors associated with the location of the application of these conditions. It does not address the compounding of this error in a coupled gas-liquid calculation by the modification of the ambient values because of the modified vaporization rate; it is assumed that, as one problem is corrected, the other problem is automatically corrected in the coupled calculation.

It should be noted that, for this case where the relative velocity between the droplet and the ambient gas is zero, the droplet can be accurately considered as a point source from the gas perspective. That is, the point-source approximation has been shown by Rangel and Sirignano (1989b) to predict exactly the gas film properties surrounding the droplet. While the droplet size affects the vaporization rate, the ambient gas is only affected by the vaporization rate and, in other ways, it is not affected by the droplet size. This simplification does not apply exactly to the case where a finite relative velocity exists.

Rangel and Sirignano (1989b) have shown for the convective case that a point-source approximation plus a free stream does not provide an accurate velocity field around the droplet (even in the inviscid limit). A point-source, doublet, and free stream combination provides a much more accurate description. In this case, the flow field around the droplet depends upon both the vaporization rate and the droplet diameter. There are still inaccuracies besides the viscous effects on the velocity field. For example, with the point source approximation, the vaporization mass flux is assumed to be uniform over the droplet surface, which is not accurate.

The gas film or boundary layer thickness in the convective case will decrease as the droplet Reynolds number increases. The strategy proposed by Rangel and Sirignano is that the ambient conditions are applied at a position upstream of the droplet by a distance  $\tilde{\delta}$  given by

$$\tilde{\delta} = \left(1 + \frac{5}{Re^{0.6}}\right) (1 + B_M)^{0.17}$$

The upstream direction is determined by the relative velocity vector between the gas and the liquid; the value of  $\tilde{\delta}$  then determines the position where the ambient conditions are applied. The values at the neighboring mesh points (that form the corners of a cell in which the determined point lies) are averaged, in a weighted manner, to provide the ambient conditions. The transfer number  $B_M$  above is calculated using the ambient conditions at this point. Errors are significantly reduced by evaluating the transfer number at this upstream position versus evaluating it at the droplet position. At large grid size to droplet diameter ratio, the error decreases as droplet Reynolds number increases or as the grid size to droplet diameter ratio increases.

Certain studies have been performed to address the issue of optimizing the numerical calculations for sprays. Axisymmetric sprays were studied by Aggarwal et al. (1985) and Sirignano (1993). Laminar, nonreacting situations were considered. Turbulence and chemical reactions would modify characteristic length and time scales, thereby affecting the optimal numerical scheme. Two problems were considered: (i) an axisymmetric,

steady jet flow and (ii) an unsteady, axisymmetric confined model flow.

In both cases, an Eulerian mesh was used for the parabolic gas-phase equations. Note that in the model problem, the spatial differential operator is elliptic. A Lagrangian scheme was used for the hyperbolic equations describing the vaporizing liquid phase. All hydrodynamic and thermal interactions between the two phases were considered. Generally, with one exception, consistent second-order-accurate numerical schemes were considered.

In the first problem, the subset of gas-phase equations has been attacked by four numerical methods: a predictor-corrector explicit method, a sequential implicit method, a block implicit method, and a symmetric operator-splitting method. The computations predicted the hydrodynamics and transport in the gas phase as well as the droplet trajectories. The size, temperature, and velocity of each droplet group were also predicted. Time for computation as a function of the error bound was determined. At low error tolerances, the sequential implicit method gave the best results; at large error tolerances, the explicit and operator-splitting methods gave better results. The block implicit scheme was least effective at all accuracies. Further information can be found in Aggarwal et al. (1985) and Sirignano (1993).

In the second problem, a set of model equations was studied but the technique applies very well to a more general and more physically-accurate set of equations as well. The integration scheme and the scheme for interpolation between the Lagrangian and Eulerian meshes were demonstrated to be second-order accurate. Effects of mesh size, number of droplet characteristic, time step, and the injection pulse time were determined via a parametric study. The results indicated slightly more sensitivity to grid spacing than to the number of droplet characteristics. Still further information is given in Aggarwal et al. (1983) and Sirignano (1993).

**3.4 Applications.** The spray equations have been studied and solved for many applications: single-component and multicomponent liquids, high temperature and low temperature gas environments, monodisperse and polydisperse droplet size distributions, steady and unsteady flows, one-dimensional flows, laminar and turbulent regimes, and recirculating (strongly elliptical) and nonrecirculating (hyperbolic, parabolic, or weakly elliptic) flows. The references cited here will not be totally inclusive of all of the interesting analyses that have been performed; rather, only a selection will be presented here. Overviews of the relationships between the developments of the subgrid vaporization models and the spray calculations can be found in Sirignano (1985a, 1988).

Some of the earlier research employed an Eulerian description of the two-continua formulation. For example, Seth et al. (1978) and Aggarwal and Sirignano (1984) performed one-dimensional analyses of flames propagating through fuel sprays. They did not resolve flame structure to a scale smaller than the average spacing between droplets and suffered some artificial diffusion associated with the Eulerian formulation. Sirignano (1985b) considered a very simple vaporizing spray to develop integral solutions. Other research has addressed the two-continua problem with a Lagrangian description. Aggarwal et al. (1981, 1983, 1985) studied axisymmetric idealized two-continua problems to establish some of the computational foundations and performance analyses for the Lagrangian method. They determined the trade-offs between computational time and accuracy. Among other issues, some guidance is given concerning the number of characteristics (or, equivalently, average particles) that should be selected to yield consistent accuracy with the Eulerian mesh selection for the gas-phase equations. Bhatia and Sirignano (1991) considered oscillatory vaporization and combustion in a one-dimensional simulation of a ramjet combustor.

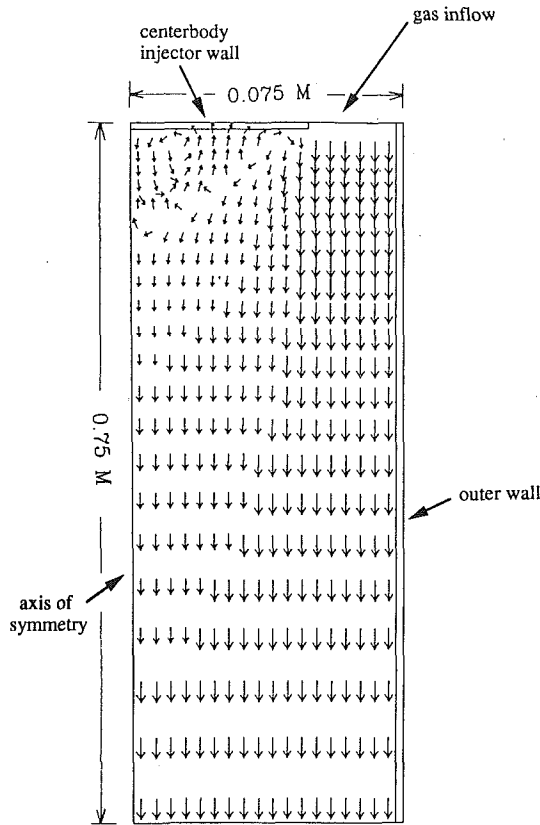


Fig. 19 Gas velocity vectors for centerbody injector configuration. Schematic of axisymmetric chamber showing outer wall, centerbody wall, gas inflow, and axis of symmetry

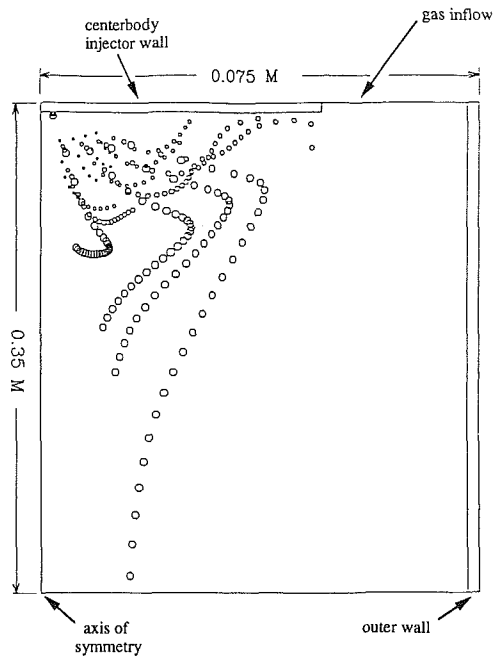
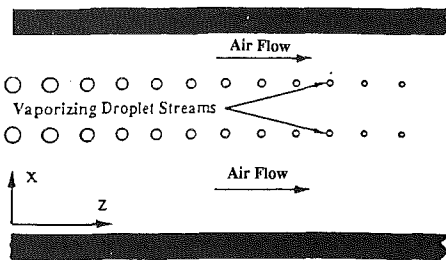


Fig. 20 Droplet trajectories and sizes for polydisperse spray with centerbody injector configuration shown in Fig. 19

The multicontinua formulation has been extended to turbulent domains with the works of Raju and Sirignano (1989, 1990) and of Molavi and Sirignano (1988). Here, the gas-phase equations accounted for the averaged effects of turbulent fluctuations of the gas field but no fluctuations in the droplet



Idealized combustor

Fig. 21 Two-dimensional, planar, parallel droplet stream configuration

behavior were considered. A development of the theory with coupled gas and liquid fluctuations made by Elghobashi and co-workers (1983, 1984, 1985, 1989, and 1991) will be discussed in Section 5. Raju and Sirignano and Molavi and Sirignano considered axisymmetric and planar two-dimensional idealized configurations related to center-body and dump combustors. Single component and multicomponent fuels were considered. Gas velocity directions in Fig. 19 indicate a recirculating flow field near the centerbody injector. Figure 20 shows some vaporizing droplet trajectories and sizes calculated by Raju and Sirignano for a polydisperse spray; the larger droplets are seen to penetrate further than the smaller droplets. Smaller droplets are more likely to become entrained in the recirculating flow field.

One-dimensional, planar unsteady spray configurations have been studied extensively using the discrete particle Lagrangian methodology. Various subgrid vaporization models were studied by Aggarwal et al. (1984) who found that substantial global differences in the two-phase flow can result from different vaporization models; it is clear that accurate subgrid modeling of vaporization is required. Other one-dimensional planar studies based upon the discrete particle formulation include Aggarwal and Sirignano (1985a,b, 1986). They found that ignition delays for sprays could be less than for gas mixtures at the same stoichiometric ratio. Similarly, spray flame speeds could exceed the premixed flame speed at the same stoichiometry. Continillo and Sirignano (1988) extended the study to a spherically symmetric spray configuration. Aggarwal (1987, 1988) and Continillo and Sirignano (1991) considered multi-component liquid sprays in one-dimensional, planar and spherically symmetric configurations. Generally, vaporization rates, ignition delays, and flame propagation rates were predicted.

Studies have been performed on two-dimensional planar flows with parallel streams of droplets. The basic configuration is displayed in Fig. 21. Steady-state calculations that approximate the droplet streams to be continuous liquid streams have been performed by Rangel and Sirignano (1986, 1988b, 1989a). The continuity and momentum equations for the gas flow are not solved in these analyses; rather, the pressure and gas velocity are assumed to be uniform. The droplet velocities are determined by conservation of momentum principles. These studies actually lie between two-continua formulations and discrete-particle formulations. They resolve the flow in one transverse direction on a scale smaller than the spacing between droplets; however, the properties are not resolved on the scale of the droplet spacing in the liquid-stream direction. Averaging of liquid properties occurs in one of the two spacial directions thereby yielding a steady flow result that integrates implicitly over time to remove the effect of the inherent intermittency associated with the spacing between the droplets in the stream. (Averaging in the third direction is implicit since the problem *ab initio* was reduced to a two-dimensional statement.) Certain important phenomena can still be identified even though properties are smoothed to eliminate the intermittency. Figure 22

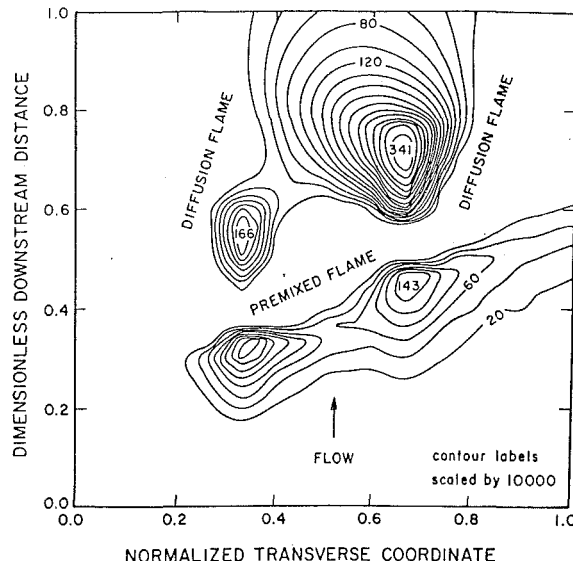


Fig. 22 Fuel vapor mass fractions in the two parallel droplet stream configuration

shows fuel vapor mass fraction in a two-droplet-stream configuration. A multiple flame is portrayed since regions of large fuel vapor mass fraction are separated. Early vaporization and mixing of the fuel vapor with the air together with the introduction of an ignition source allow a premixed flame to occur. The droplets penetrate the premixed flame before complete vaporization has occurred; therefore, continued vaporization in the presence of a hot gas with excess air is sustained. This causes diffusion flames to be established around each stream of droplets. Delplanque and Rangel (1991) performed a related analysis for one stream of droplets flowing through the gaseous viscous boundary layer near a hot wall. They include the important effect of gaseous thermal expansion which created a gas motion and droplet drag that moved the droplet stream away from the wall as it flowed downstream.

The intermittent effects have been addressed in the unsteady analyses of Delplanque et al. (1990) and Rangel and Sirignano (1988a, 1991). These studies are fully in the domain of discrete particle formulations (with the understanding that any two-dimensional representation involves averaging in the third dimension). The inclusion of the intermittent effects yields results that support the general conclusions of the steady-state analyses. Figure 23 shows that both diffusion-flame and premixed-flame structures exist. Furthermore, it is seen that the diffusion flame can envelop more than one droplet. Delplanque et al. also studied the effect of the point source approximation correction discussed in Section 3.3. Figure 24 shows the importance of the correction for the prediction of droplet temperature and droplet mass in the regions where those quantities are rapidly varying with time.

Continillo and Sirignano (1990) studied a counterflow spray problem using a two-continua formulation. They considered two opposed air streams with normal octane liquid droplets injected with the left-hand-side stream. Figure 25 shows that two flames occur in the stagnation region. They are primarily fed by fuel vapor diffusing from vaporizing droplets that have penetrated to the zone between the two flames. Some vaporization occurs before the droplets penetrate the left-hand flame; therefore, that flame has a combined premixed and diffusion character. Figure 25 also shows the effect of varying strain on the behavior of the flow. Increasing the strain results in narrowing the two reaction zones and causing them to approach each other and the stagnation plane. Ultimately, the increasing strain rate causes the two reaction zones to merge and only one temperature peak is seen in Fig. 25(c). Other recent studies

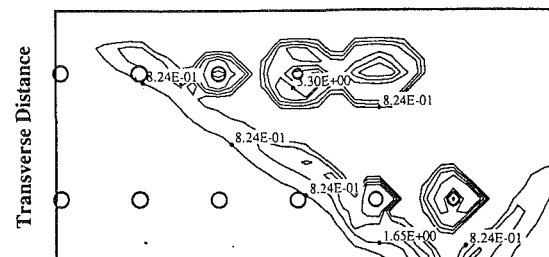


Fig. 23(a)

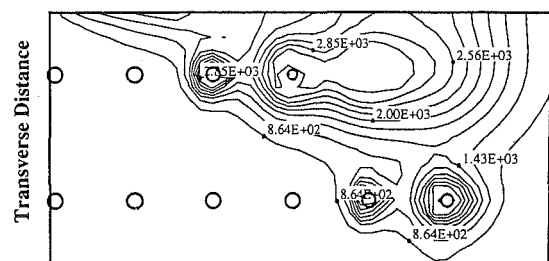


Fig. 23(b)

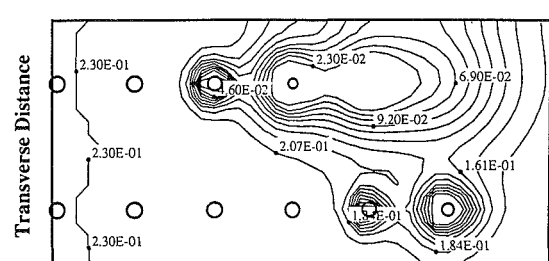


Fig. 23(c)

Fig. 23 Unsteady, two parallel droplet stream configuration contour plots at nondimensional time = 0.016: (a) reaction rate with contour intervals of 0.824, (b) gas temperature with contour intervals of 283 K, and (c) oxygen mass fraction with contour intervals of 0.023

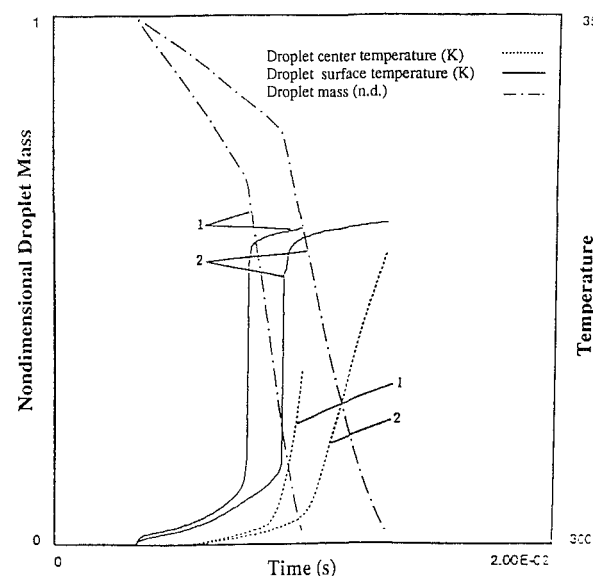


Fig. 24 Droplet temperature and mass versus time for the second droplet in the stream nearest the ignition source in a parallel stream configuration. Point source approximation correction for Curve 1. No correction for Curve 2.

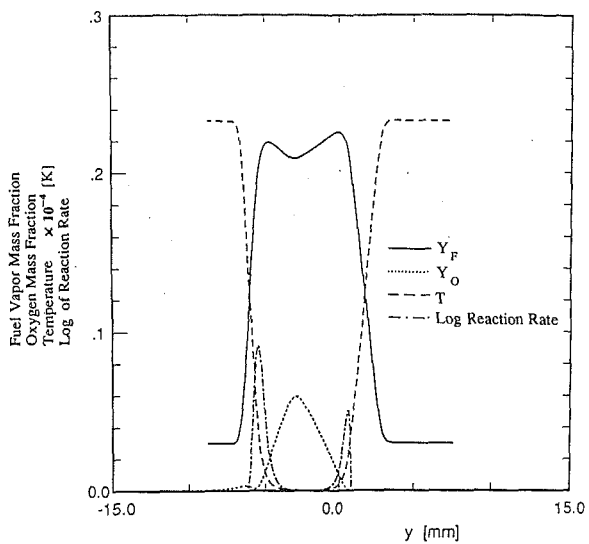


Fig. 25(a)

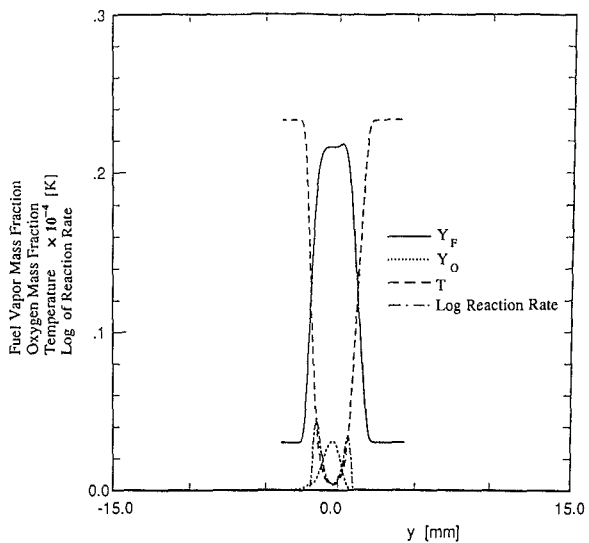


Fig. 25(b)

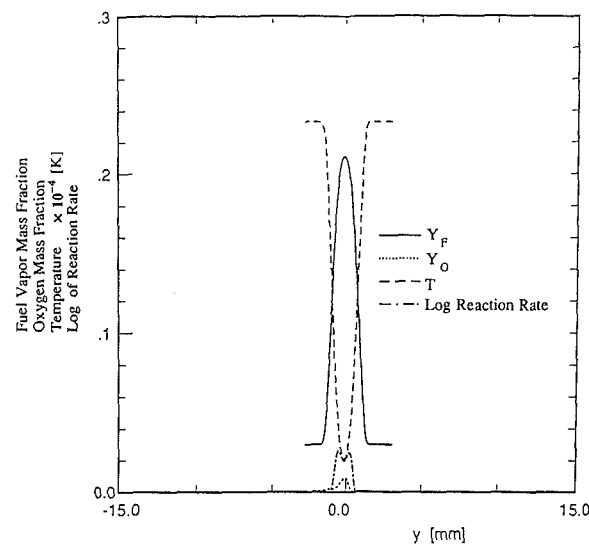


Fig. 25(c)

Fig. 25 Counterflow spray: influence of the strain rate. Profiles of temperature (solid line), fuel vapor mass fraction (dotted line), oxygen mass fraction (dashed line), and log of reaction rate (dot-dash line). Initial droplet diameter = 50  $\mu\text{m}$ . Strain rate = (a) 100  $\text{s}^{-1}$ , (b) 300  $\text{s}^{-1}$ , and (c) 500  $\text{s}^{-1}$ .

on counterflow spray flames include an experimental study by Chen et al. (1988) and theoretical/experimental study by Li et al. (1992). The study by Li et al. predicts the locations of the vaporization zone and the reaction zone as a function of the strain rate for heptane and methanol sprays transported in a nitrogen stream and mixing with a counterflowing oxygen/nitrogen stream. Extinction conditions are also predicted.

The subgrid vaporization models used in these above-maintained spray studies have evolved over the years. Originally, spherically symmetric models with Ranz-Marshall corrections were employed. During the middle 1980's, the Tong and Sirignano model came into use. More recently, the Abramzon and Sirignano model has been employed. Also, experimental drag coefficients such as those of Ingebo (1956) and Renksizbulut and Yuen (1983) have been replaced by computational correlations such as those of Haywood et al. (1989) and Chiang et al. (1992) for input to spray models.

The general conclusions of the one-dimensional planar, two-dimensional planar, and spherically symmetric studies are that: (i) resolution on the scale of the spacing between droplets is important in the determination of ignition phenomena and flame structure, (ii) more than one flame zone can exist at any instant with spray combustion, (iii) an inherent unsteadiness results for the flame structure, (iv) diffusion-like or premixed-like flames can occur, (v) ignition and flame propagation for sprays can sometimes be faster than for gaseous mixtures of identical stoichiometry, and (vi) droplets tend to burn in a cloud or group rather than individually.

**3.5 Probabilistic Formulation.** It is sometimes convenient to employ a probabilistic formulation for the spray analysis. Whenever we have spacial resolution on a scale comparable to or smaller than the averaging spacing between droplets, a given computation cell has a significant probability of not containing any droplet at any particular instant of time. Furthermore, in dealing with a very large number of droplets in a spray, there is no practical way to know exactly where each droplet is located at each instant; a probabilistic formulation is practical therefore in a high resolution analysis.

A probability density function can be defined as  $f(t, x_i, R, u_{ij}, e_l)$  and an infinitesimal hyper-volume in eight-dimensional space is given by

$$dV = dx_1 dx_2 dx_3 du_{i1} du_{i2} du_{i3} dR de_l$$

Then,  $f dV$  is the probability of finding a droplet in the hyper-volume  $dV$  at a particular instant of time. Note that for very fine resolution  $f dV$  is less than unity. However, for very coarse resolution, that product can become much larger than unity since many droplets can be in the hyper-volume; in that case,  $f$  is more commonly named a distribution function. Williams (1985) discusses the distribution function. Sirignano (1986, 1993) extends the independent variable space, relates the probability density function to the distribution function, and separates droplets by class according to initial values.

We can separate the droplets into distinct classes depending upon their initial size, velocity, or composition. Then, a probability density function or a distribution function can be defined for each class of the droplets. Conservation of droplet numbers (neglecting shattering or coalescence) leads to the following equation which governs the probability density function  $f^{(k)}$  for the  $k$ th class of droplets

$$\frac{\partial f^{(k)}}{\partial t} + \frac{\partial}{\partial x_j} (u_{ij} f^{(k)}) + \frac{\partial}{\partial u_{ij}} (a_{ij} f^{(k)}) + \frac{\partial}{\partial R} (\dot{R} f^{(k)}) + \frac{\partial}{\partial e_l} (\dot{e}_l f^{(k)}) = 0 \quad (87)$$

where

$$a_{ij} = \frac{\tilde{F}_{Di}}{\frac{4}{3} \pi \rho_l R^3} + g_i$$

is the droplet acceleration. Note that Eq. (87) is equivalent to the statement that  $f dV$  is a constant.

The characteristics of the hyperbolic partial differential equation (87) are given by

$$\begin{aligned} \frac{d^{(k)}x_i}{dt} &= u_{ti}; \quad \frac{d^{(k)}u_{ti}}{dt} = a_{ti}; \quad \frac{d^{(k)}R}{dt} = \dot{R} = -\frac{\dot{m}}{4\pi\rho_t R^2} \\ \frac{d^{(k)}e_t}{dt} &= \dot{e}_t = \frac{\dot{m}}{4\pi\rho_t R^3} \left[ e_t - e_{ts} + \frac{\dot{q}}{\dot{m}} \right]. \end{aligned} \quad (88)$$

These characteristics define particle paths or probable particle paths for each class of droplet.

Integration of the distribution function gives the averaged values used in the multi-continua approach. The droplet number density  $n^{(k)}$  is given by the five-dimensional integral

$$n^{(k)} = \int f^{(k)} du_{ti} dR de_t \quad (89)$$

Any of the variables  $\varphi = u_{ti}$ ,  $a_{ti}$ ,  $R$ ,  $\dot{R}$ ,  $e_t$ , or  $\dot{e}_t$  can be integrated to give the average quantity

$$\varphi^{(k)} = \left[ \int f^{(k)} \varphi du_{ti} dR de_t \right] / n^{(k)} \quad (90)$$

where  $\varphi^{(k)}$  represents  $u_{ti}^{(k)}$ ,  $a_{ti}^{(k)}$ ,  $R^{(k)}$ ,  $\dot{R}^{(k)}$ ,  $e_t^{(k)}$ , or  $\dot{e}_t^{(k)}$ .

Integration of the divergence form of the equation governing  $f^{(k)}$ , namely Eq. (87), leads to the Eq. (65) for conservation of droplet number which governs droplet number density. Note that, since both  $u_{ti}$  and  $x_i$  are independent variables in Eq. (87), the second term in that equation can be simplified. In particular, within that term,  $u_{ti}$  can be brought forward of the derivative sign.

Equation (87) can be multiplied by  $\varphi$  (term-by-term), rearranged, and integrated over the five-dimensional volume. Here, it is assumed that  $f^{(k)}$  goes to zero as  $u_{ti}$  or  $R$  becomes infinite. Also,  $\dot{R}$  becomes zero when  $R=0$ . Finally, with respect to the averaged quantities defined by Eq. (90), it is assumed that the average of a product of two quantities equals the product of the averages of the two quantities. The error in this assumption reduces as the band of the independent variables ( $u_{ti}$ ,  $R$ ,  $e_t$ ) for a nonzero probability density function in a given class  $k$  is reduced. When  $\varphi=1$ , Eq. (65) is reproduced by this process and when  $\varphi=u_{ti}$ , Eq. (73) is reproduced. With modest effort, use of  $\varphi=R$  and  $\varphi=e_t$  can yield Eqs. (58) and (78), respectively.

The probabilistic formulation or, equivalently, the distribution function formulation is of primary value, because it strengthens the theoretical foundations of the spray equations. In the case where coarse resolution is sought, both gas-phase and liquid-phase properties are averaged over a neighborhood containing many droplets. Then, any uncertainty associated with the precise locations of individual droplets is removed from the final analytical form by the averaging process. In the fine resolution case, uncertainty in droplet position remains a factor; the probability density function describes this uncertainty. There is also an uncertainty in the gas-phase values here on account of the coupling between the phases. For very dilute sprays, the uncertainty in the gas-phase properties can be neglected. In denser sprays, these uncertainties in the gas-phase properties appear in high resolution practical spray problems; theory has not yet fully addressed this interesting problem. Aggarwal and Sirignano (1985a) discuss the uncertainty in ignition delay associated with the uncertain distance of the nearest droplet to the ignition source.

#### 4 Interactions Amongst Droplets

There are three levels of interaction amongst neighboring droplets in a spray. If droplets are sufficiently far apart, the only impact is that neighboring droplets (through their exchanges of mass, momentum, and energy with the surrounding

gas) will affect the ambient conditions of the gas field surrounding a given droplet. As the distance between droplets becomes larger, the influence of neighboring droplets becomes smaller and tends toward zero ultimately. At this first level of interaction, the geometrical configuration of the (mass, momentum, and energy) exchanges between a droplet and its surrounding gas is not affected by the neighboring droplets. In particular, the Nusselt number, Sherwood number, and lift and drag coefficients are identical in values to those for an isolated droplet. This type of interaction has been fully discussed in Section 3.

At the next level of interaction, droplets are closer to each other, on average, and the geometrical configurations of the exchanges with the surrounding gas are modified. In addition to modification of the ambient conditions, the Nusselt number, Sherwood number, and the lift and drag coefficients are modified. Here, a droplet cannot be treated as if it were an isolated droplet; the neighboring droplet(s) are within the gas film or wake of the droplet. In a convective situation, a droplet can influence a second droplet at substantial distances of many tens of droplet radii if the latter is in its wake. If the droplets are placed side by side in a convective situation, significant influence occurs only over short distances of a few droplet radii. This type of interaction will be the major subject of discussion for this section.

The third level of interaction amongst droplets involves collisions whereby the liquids of the different droplets actually make contact with each other. Here, the droplets might coalesce into one droplet or emerge from the collision as two or more droplets. Some discussion of this subject will be made later in this section.

From another perspective, Sirignano (1983) classified interactive droplet studies into three categories: droplet arrays, droplet groups, and sprays. Arrays involved a few interaction droplets with ambient gaseous conditions specified. There are many droplets in a group but gaseous conditions far from the cloud are specified and are not coupled with the droplet calculations. The spray differs from the group in that the total gas field calculation in the domain is strongly coupled to the droplet calculation. In the spray, either the droplets penetrate to the boundaries of the gas or, while the droplets may not penetrate, the impact of the exchanges of mass, momentum, and energy extends throughout the gas. A useful review on droplet interactive processes can be found in Annamalai and Ryan (1992). Note that unpublished information from Annamalai and Ryan indicates that radiative transfer between droplets can be significant even if the separation distance is ten diameters or greater.

The earliest work on droplets that were interactive at the second level was performed for vaporizing droplet arrays without forced convection. Twardus and Brzustowski (1977) considered two vaporizing and burning fuel droplets of equal size with spacing between their centers as a parameter. The vaporization rate decreased monotonically as the spacing decreased. At very large spacing, the droplets achieved the maximum vaporization rate equal to the isolated droplet value for each droplet. When the spacing decreased to the minimum value with the spherical droplet surfaces in contact, the vaporization rate and the Nusselt number were reduced by approximately 31 percent from the isolated droplet values. Clearly, the proximity of another droplet in this stagnant situation inhibited the exchange of mass and energy between the droplet and the gas. Labowsky (1978, 1980) considered several interactive vaporizing droplets in a stagnant domain and found similar reductions in transport rates. More recently, Umemura et al. (1981a, 1981b) have studied this interactive problem. Xiong et al. (1985) argue that diffusion analyses without consideration of natural or forced convection leads to overprediction of the effect of droplet interactions.

Low Reynolds number flow for interacting particles has been

studied by Happel and Brenner (1965), Batchelor and Green (1972), and Jeffrey and Onishi (1984). Nonvaporizing arrays with forced convection at intermediate Reynolds number were studied by Tal and Sirignano (1982) and Tal et al. (1983, 1984a, 1984b). Spherical particles were aligned both in tandem and side-by-side with the gas flowing past them. Relative velocity was held fixed and steady-state solutions were obtained. A cylindrical-cell approach was employed to allow axisymmetric Navier-Stokes calculations to give approximate descriptions of the three-dimensional phenomena. These calculations showed that drag coefficients and Nusselt number decreased for the downstream droplets as the spacing between tandem droplets decreased. In other words, the downstream droplets were partially shielded by the wake of the forward droplet. As spacing between side-by-side droplets decreased, the local relative gas velocity and Reynolds number increases leading to an increase in convective transport and in friction drag. Therefore, the Nusselt number and drag coefficient increase beyond the isolated droplet values as the spacing between side-by-side droplets decreases. Note that surface regression (due to vaporization) and internal circulation were not considered so that the droplets here are essentially equivalent to solid particles. The studies of Tal et al. have considered up to four particles or droplets in tandem. In the case where there are no side-by-side particles and only tandem particles, the drag coefficient and Nusselt number of the first or upstream particle are generally approximately equal to the isolated particle values. In all cases, the downstream particles experience reduced drag coefficient and Nusselt number from the first particle; furthermore, little difference occurs in the values for the second, third, and fourth particles in tandem.

Studies on group vaporization have generally addressed only the first level of interaction. See, for example, Chiu and Liu (1971), Labowsky and Rosner (1978), Chiu et al. (1983), Suzuki and Chiu (1971), and Bellan and Cuffel (1983). Bellan and Harstad (1987, 1988) studied a cluster of droplets in a convective flow focussing on the build-up of fuel vapor and cooling of the gas. The work of Ryan et al. (1990) is an exception wherein correction factors accounted for the second level of interaction. Similarly the spray calculations, such as those addressed in Section 3, have considered only the first level of interaction. A novel approach employing numerical simulations with a cellular automaton for dense sprays was recently introduced by Borghi and Loison (1992).

Patnaik and Sirignano (1986) extended the work of Patnaik et al. (1986) to consider two droplets moving in tandem at constant spacing. The solution of the first droplet was calculated as if that droplet were isolated. Then, that solution for the wake was used as a free stream input to the downstream droplet. The weaknesses of this model are the omission of variation in spacing and upstream influence of the second droplet. Tong and Chen (1988) extended the cylindrical-cell model of Tal and Sirignano (1982) to include vaporization. A three-droplet linear (tandem) array was studied to obtain correlations for the Nusselt number. Kleinstreuer et al. (1989) employed a finite element analysis of the linear array to yield the drag coefficients of interacting spheres. Also, they used a boundary layer analysis for vaporizing droplets to simulate coupled transfer processes for three droplets in tandem. The analysis involves individual computations for the three spheres with coupling only through the determination of an effective temperature for the gas flow approaching the downstream droplets. Tsai and Sterling (1990) determined Nusselt number and drag coefficients for steady flow past a linear array of non-vaporizing spheres. They obtained results that were in qualitative agreement with Tal et al. (1983) and Tong and Chen (1988). All of the above analyses take advantage of axisymmetric flow.

Raju and Sirignano (1990b) developed a transient axisymmetric finite difference analysis with a grid generation scheme

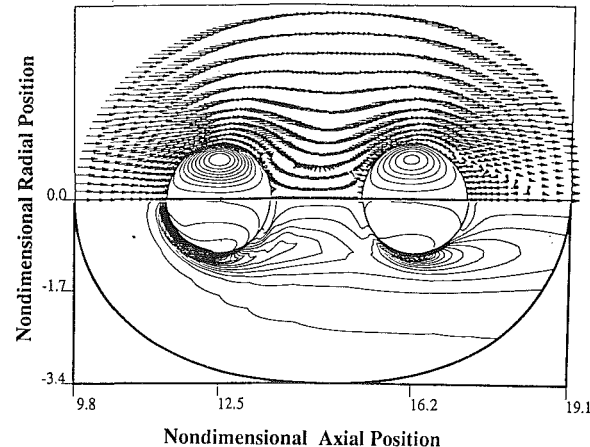


Fig. 26 Two-tandem droplet case: gas-phase velocity vector and liquid-phase stream function (on top), and vorticity contours for both phases (on bottom). Time = 3.00,  $Re_1 = 80.31$ ,  $Re_2 = 85.84$ ,  $R_1 = 1.00$ ,  $R_2 = 1.00$ , nondimensional spacing = 3.71.

for two vaporizing droplets moving in tandem. They considered variable density but otherwise constant thermophysical properties in similar fashion to Patnaik et al. (1986). The extension beyond other studies for tandem droplets involves transient behavior (including unequal regression rates of the two droplet surfaces and temporal variation in droplet spacing due to differences in droplet drag and mass), fully coupled Navier-Stokes solution (allowing for complete coupling of internal liquid flow and gas flow and for complete elliptic behavior with upstream influence), and different initial sizes for the upstream and downstream droplets. They studied a limited range of initial values for Reynolds number, droplet spacing, and droplet radii ratio. The most interesting result was that there exists a critical ratio of the two initial droplet diameters below which droplet collision does not occur. If the ratio of the downstream droplet initial diameter to the upstream initial diameter is larger than the critical ratio, the reduced drag coefficient of the downstream droplet causes less deceleration and greater relative velocity with the gas for the downstream droplet. Therefore, collision is likely since the spacing decreases with time. Below the initial ratio, the reduced inertia of the downstream droplet causes the spacing to increase. The critical ratio is found to be less than unity and very weakly dependent upon initial Reynolds number. Recall, however, that Chiang et al. (1992) showed that constant thermophysical properties could lead to errors in the detailed prediction of the drag coefficients. These errors, of course, make the precise determination of the critical ratio questionable.

More recently, Chiang and Sirignano (1993a) and Chiang (1990) have extended the two-tandem-droplet calculation of Raju and Sirignano (1990b) to account for variable thermophysical properties. A wider range of initial values for Reynolds number, droplet spacing, and droplet radii ratio were considered. Also, correlations of the numerical results for drag coefficient, Nusselt number, and Sherwood number with Reynolds number, transfer number, spacing, and radii ratio were obtained. Furthermore, Chiang and Sirignano (1993b) have extended the analysis to three droplets moving in tandem.

The two-droplet results of Chiang and Sirignano are in qualitative agreement with the findings of Raju and Sirignano. Figure 26 shows gas-phase velocity vector, liquid-phase stream function, and vorticity contours for both phases. The downstream sphere is seen to be within the wake of the upstream sphere. Hence, the effective Reynolds number for the downstream sphere is less than the Reynolds number for the upstream sphere. The strength of the liquid-phase vortex and transport rates on the forward side are less for the downstream droplet than for the upstream droplet. Transport rates on the

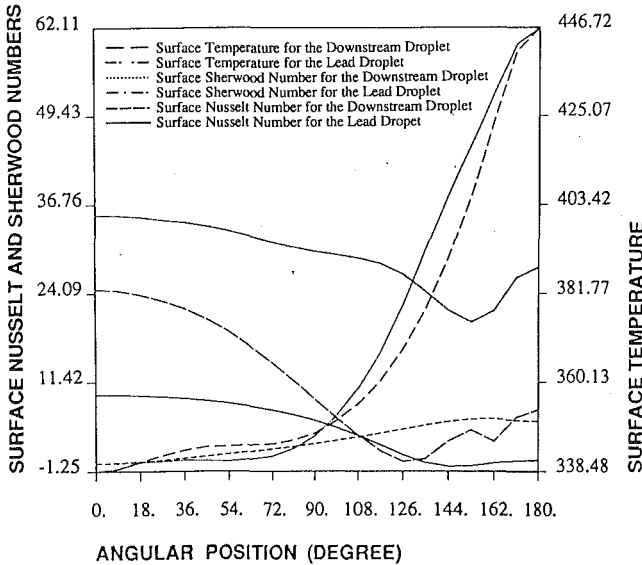


Fig. 27 Surface temperatures, Nusselt number, and Sherwood number versus position on droplet surface for the two-tandem-droplet case. N-decane liquid, 1000 K ambient temperature, 300 K initial droplet temperature, 100 initial Reynolds number, 1.00 initial  $R_1$  and  $R_2$ , 8.0 initial spacing.

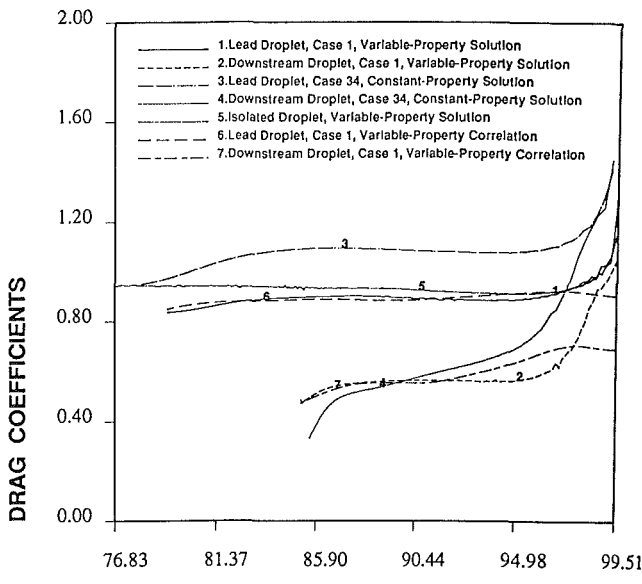


Fig. 28 Drag coefficient versus instantaneous Reynolds number for two-tandem-droplet case

aft side of the droplet are greater for the downstream droplet than for the upstream droplet as shown by Fig. 27.

The drag coefficient is displayed as a function of instantaneous Reynolds number in Fig. 28. The reduction of the drag coefficient for the downstream droplet and the general overprediction of the constant-property solution are shown. The similarity between the drag coefficient of an isolated droplet and that of the lead droplet are shown also. Center-to-center spacing as a function of time is shown in Fig. 29 for various initial spacings  $D$  and various initial droplet radii ratio  $R_2$ . The prediction of strong influence upon the downstream droplet at a spacing of sixteen droplet radii is consistent with the experimental findings of Temkin and Ecker (1989) who found influences up to thirty radii spacing. It is seen that a critical value of  $R_2$  can exist that distinguishes between increasing spacing and decreasing spacing with time.

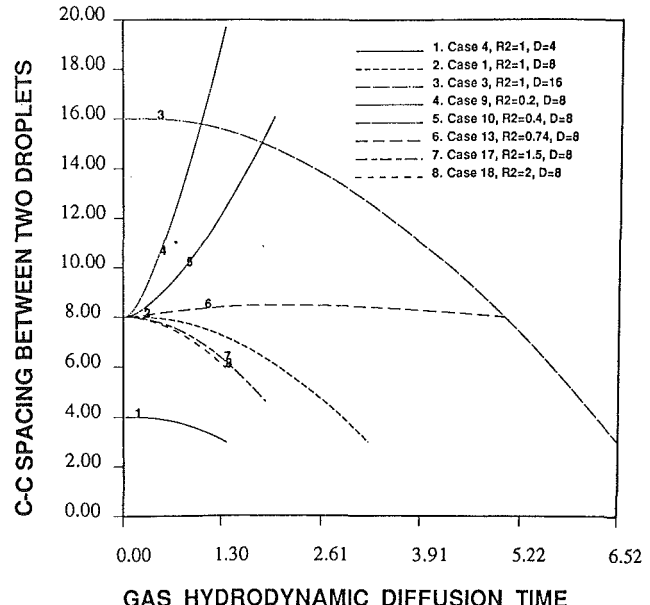


Fig. 29 Center-to-center droplet spacing versus nondimensional time for various initial values for spacing  $D$  and radii ratio  $R_2$

Chiang and Sirignano (1993a) obtained correlations for drag coefficients from their computational results as shown in Fig. 28; also, correlations for Nusselt number and Sherwood number were obtained. A linear regression model was employed to fit over 3000 data points. The correlations are normalized by the isolated droplet correlations given by Eq. (56) of Section 2. The correlations for each of the droplets follow.

For the lead droplet:

$$\begin{aligned} \frac{C_{D1}}{C_{Diso}} &= 0.877 Re_m^{0.003} (1 + B_H)^{-0.040} D^{0.048} (R_2)^{-0.098} \\ \frac{Nu_1}{Nu_{iso}} &= 1.245 Re_m^{-0.073} Pr_m^{0.150} (1 + B_H)^{-0.122} D^{0.013} (R_2)^{-0.056} \\ \frac{Sh_1}{Sh_{iso}} &= 0.367 Re_m^{0.048} Sc_m^{0.730} (1 + B_M)^{0.709} D^{0.057} (R_2)^{-0.018} \end{aligned} \quad (91)$$

where

$$\begin{aligned} 0. \leq B_H &\leq 1.06; 0. \leq B_M \leq 1.29; 11 \leq Re_m \leq 160; \\ 0.68 \leq Pr_m &\leq 0.91; 1.47 \leq Sc_m \leq 2.50; 2.5 \leq D \leq 32; \\ 0.17 \leq R_2 &\leq 2.0 \end{aligned}$$

For the downstream droplet:

$$\begin{aligned} \frac{C_{D2}}{C_{Diso}} &= 0.549 Re_m^{-0.098} (1 + B_H)^{0.132} D^{0.275} (R_2)^{0.521} \\ \frac{Nu_2}{Nu_{iso}} &= 0.528 Re_m^{-0.146} Pr_m^{-0.768} (1 + B_H)^{0.356} D^{0.262} (R_2)^{0.147} \\ \frac{Sh_2}{Sh_{iso}} &= 0.974 Re_m^{0.127} Sc_m^{-0.318} (1 + B_M)^{-0.363} D^{-0.064} (R_2)^{0.857} \end{aligned} \quad (92)$$

where

$$\begin{aligned} 0. \leq B_H &\leq 2.52; 0. \leq B_M < 1.27; 11 \leq Re_m \leq 254; \\ 0.68 \leq Pr_m &< 0.91; 1.48 \leq Sc_m \leq 2.44 \end{aligned}$$

Chiang and Sirignano (1993b) considered three tandem vaporizing droplets of equal initial diameters. The qualitative conclusions of the two-droplet study generally apply to the behavior of the first two droplets. The drag coefficients and transport rates for the second and third droplets are significantly reduced below the lead droplet values which remain close to the isolated droplet values. The transport rates of the

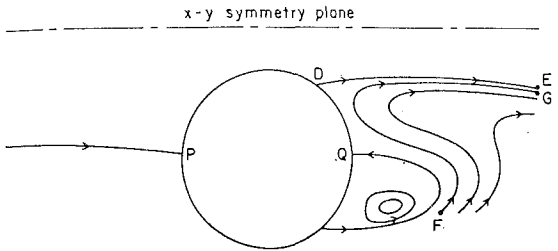


Fig. 30 Streamlines in symmetry plane for flow past two side-by-side spheres

second and third droplets differ by a very small amount in general; however, the second droplet has a slightly lower drag coefficient than the third droplet. Correlations are reported in the paper.

The two-tandem and three-tandem-vaporizing-droplet computational results are consistent with the non-vaporizing sphere results of Tal et al. who found little difference in drag coefficient for downstream particles in a tandem stream. Also, many experimental investigators have found that, in a long stream of equi-sized droplets moving in tandem with uniform initial spacing amongst the droplets, the spacing remains constant with time, implying equal drag coefficients. (Sangiovanni and Kesten, 1976; Nguyen et al., 1991; and Nguyen and Dunn-Rankin, 1992).

Asano et al. (1988) analyzed two tandem spheres in a steady flow with constant properties. The interactions are described in a simple manner using geometric factors. Nguyen et al. (1991) performed a computational and experimental study of droplets moving in tandem. Vaporization was not significant in their experiment due to low ambient temperatures and saturated vapors in the droplet stream vicinity. They found that a lead droplet and a trailing droplet of equal size will collide for small initial spacings which agrees with theoretical predictions including their own prediction. Further experimental studies on drag reduction and collisions for a small number of droplets moving in tandem are reported by Nguyen and Dunn-Rankin (1992).

The interaction of two spheres moving side-by-side in parallel, or approximately in parallel, is a three-dimensional phenomenon. Only a limited number of three-dimensional flow calculations for individual spheres have been made. Dandy and Dwyer (1989) considered steady, uniform shear flow past a heated sphere. Tomboulides et al. (1991) considered flow past a sphere with an unsteady wake.

More recently, Kim et al. (1993) have studied three-dimensional flow over two identical spheres moving in parallel at constant velocity. The separation distance between the two sphere centers is held constant and the line connecting the centers is normal to the free stream velocity vector. Both liquid and solid spheres were considered at Reynolds numbers between 50 and 150. The transient finite-difference calculations were made in one quadrant of the flow field, taking advantage of the two perpendicular planes of symmetry. The asymptotic results yielded the steady flow results.

Figure 30 shows streamlines in the plane of symmetry containing the two sphere centers. In this case, the separation distance is small. It is seen that the flow through the gap between the neighboring spheres has a jetlike character and entrains the outer flow. On the foreside of the sphere in Fig. 30, the stagnation point is perturbed from its position in an axisymmetric flow. As a result, the flow on the side closer to the neighboring sphere has a lower velocity and higher pressure than the axisymmetric case; on the other side, the velocity is higher and the pressure is lower than the axisymmetric reference. On account of asymmetric deviations of pressure and surface friction, the spheres experience lift and torque as well as a modification of the drag due to the mutual interaction.

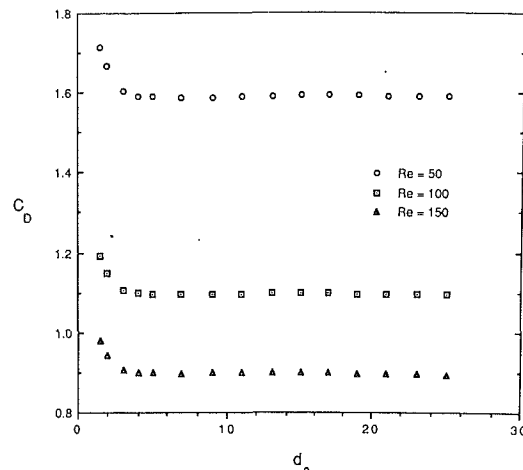


Fig. 31 Drag coefficients versus separation distance at several Reynolds numbers for flow past two side-by-side spheres

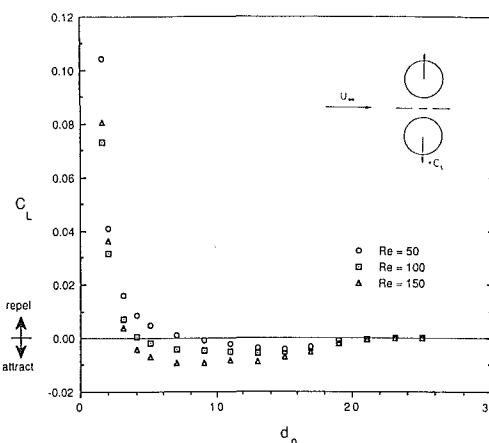


Fig. 32 Lift coefficients versus separation distance at several Reynolds numbers for flow past two side-by-side spheres

The lift forces on the spheres result in a weak attraction at large separation distances and a strong repulsion at small separation distances. The drag coefficient increases as the separation decreases. Figures 31 and 32 display drag and lift coefficients for liquid spheres.

In another recent study, Kim et al. (1992) have considered the effects of drag and lift on the trajectories of two droplets of equal size and equal and parallel initial velocity. At large initial separation, the two droplets move slightly closer while, at small initial separation, the deflection due to repulsion was more significant. In both cases, the translation of the two droplets were nearly parallel.

A general conclusion from the several studies is that collisions amongst droplets seem to have a low probability in a spray where the droplets are moving in a parallel direction or along divergent paths. The stability of droplets in a linear stream and the repulsive lift forces of nearby droplets moving in parallel tend to support this conclusion.

Various types of collisions between two droplets are possible in a spray environment. Weak collisions such as grazing collisions can occur. We can have stronger "head-on" collisions, as determined by relative velocity (i.e., both droplets can be moving in any absolute direction). The stronger collisions can lead to one of several phenomena: permanent coalescence, coalescence with a vibration that leads to separation into two other droplets, coalescence and vibration with separation into two droplets plus smaller satellite droplets, shattering into many smaller droplets, or bouncing. An interesting experimental study of two colliding (water and normal-alkane) droplets has been made by Jiang et al. (1992). The three-droplet collision

is less interesting on account of its lower probability of occurrence.

Arguments are given by O'Rouke and Bracco (1980) that coalescence is an important factor in the dense spray region near the injection point. They developed an elaborate spray model accounting for collision and coalescence of droplets. Bracco (1985) and Reitz (1987) also discuss and employ this model. The model predicts increasing average droplet size with downstream distance from the injector; some experimental evidence of growing droplet size with distance is also cited. This reviewer is, however, rather skeptical because no fundamental experimental study resolving the phenomena on the scale of the droplets within a spray context has been made. The work of Jiang et al. (1992), for example, involved only two droplets deliberately aimed at each other. Several other mechanisms could cause increasing average droplet size with downstream distance: (1) smaller droplets vaporize faster leaving the larger droplets; (2) condensation occurs in the cold, vapor-rich, dense spray region near the injector; and (3) the longer wavelength disturbances on the jet will take a longer Lagrangian time to grow and to yield the larger droplets.

## 5 Droplet Interactions With Turbulence and Vortical Structures

The interactions of a spray with a turbulent gas flow is very important in many applications (e.g., most power and propulsion applications). Two types of studies exist. In one type, the global and statistical properties associated with a cloud or spray with turbulent field are considered. In the other type, detailed attention is given to how an individual particle behaves in a turbulent field. Some studies consider both perspectives. Most of the research work in the field has been performed on the former type of study. Faeth (1987) and Crowe et al. (1988) give helpful reviews of this type of research.

**5.1 Turbulent Spray Flows.** The interactive turbulent fields can be separated into homogeneous turbulent fields and free shear flows (e.g., jets and mixing layers). In some theoretical studies, two-dimensional vortical structures interacting with a spray have been examined. Most of the studies deal with situations where the contribution of the spray to the generation of the turbulence field is secondary. That is, there exists a forced gas flow whose mass flux and kinetic energy flux substantially exceeds the flux values for the liquid component of the dilute flow. The turbulence kinetic energy flux of the gas flow is much less than the mean kinetic energy flux of the gas flow and is comparable to the mean kinetic energy of the liquid flow. Therefore, the turbulent field is much more likely in this situation to receive kinetic energy transferred from the mean gas flow than kinetic energy transferred from the mean liquid flow. An exception to this situation would be a liquid-propellant rocket motor where all of the forced flow is initially in liquid form. In this case, the turbulent kinetic energy appears directly or indirectly through transfer from the mean kinetic energy of the liquid. The direct transfer is defined to be the type where turbulent fluctuations in the liquid flow or boundary layer and wake instabilities in the gas flow past the liquid (e.g., vortex shedding over droplets) cause the gas-phase turbulent fluctuations. Indirect transfer is the case whereby vaporization causes the mean kinetic energy of the liquid to be transformed into mean kinetic energy of the vapor which in turn gets partially transferred to turbulent kinetic energy of the gas.

Dispersion of particles or droplets in a turbulent field has been a subject of major research interest over the past few decades. Hinze (1975) discusses the rudimentary aspects of fluid and particle dispersion. According to Hinze (1975), the first analytical work on particle motion in a turbulent field was performed by Tchen who took the equation for particle

motion derived by Basset, Boussinesq and Oseen and applied it to a particle in a homogeneous turbulent field. Stokes drag, pressure gradient force, virtual mass, and the Basset correction were considered in the analysis. The equation of particle motion will be discussed later in this section. Implicitly, the analysis is limited to low droplet Reynolds number, to cases where the turbulent eddy is large compared to the particle size, and to cases where the particle remains in the same eddy for its lifetime. Hinze explains how others have relaxed the last restriction. Based upon the works discussed in Sections 2 and 3 of this paper, we know how to extend the prediction of droplet or particle motion to higher Reynolds number. The second restriction is a major one; there are practical situations where the droplet or particle size is comparable to the smallest (Kolmogorov) scale of turbulence. Therefore, the droplet experiences not only a temporal variation in its local free stream but nonuniformity as well.

Faeth (1987) has compared three types of two-phase models for turbulent flows: locally homogeneous flow (LHF), deterministic separated flow (DSF), and stochastic separated flow (SSF). He prefers SSF for practical dilute sprays; that model considers finite interphase transport rates and uses random-walk computations to simulate turbulent dispersion for the dispersed phase.

Crowe et al. (1988) review both time-averaged and time-dependent free shear flows of two phases. The time-dependent methods capture the instantaneous flow and can better calculate particle trajectories. In the time-averaged method, a steady flow with gradient diffusion is usually considered.

Elghobashi and Abou-Arab (1983) developed a two-equation turbulence model for two-phase flows that eliminated much of the ad hoc character of simulating the character of the interaction between the two phases in a turbulent flow. While the formulation is derived from continuity and momentum equations, modeling at third order is necessary to achieve closure. The resulting equations describe the turbulent kinetic energy and the dissipation of the turbulent kinetic energy for the continuous phase. Elghobashi et al. (1984) applied the two-equation model to a particle-laden jet calculation and demonstrated respectable agreement with experiment. They showed that additional dissipation of the flow results in this two-phase case. Mostafa and Elghobashi (1985a,b) extended the model to account for vaporization. Rizk and Elghobashi (1985) studied the motion of a spherical particle near a wall accounting for the effects of lift and the modification of drag. Rizk and Elghobashi (1989) extended the two-phase, two-equation turbulence model to account for confined flows with wall effects.

The above mentioned research by Elghobashi and coworkers has employed Eulerian formulations for both the dispersed and continuous phases. Gosman and Ioannides (1981), Mostafa and Mongia (1988), Mostafa et al. (1989), and Berlemont et al. (1991) have employed a stochastic Lagrangian method for the dispersed phase, together with a two-equation turbulence model for the continuous phase. The first study did not account for the modification of the two-equation turbulence model due to the presence of the second phase. MacInnes and Bracco (1992a) have examined stochastic dispersion models for non-vaporizing sprays. They considered several cases of homogeneous turbulence and of shear flows. Concerns were raised about many existing models that predicted eventual non-uniform distribution of particles in a flow that initially possessed a uniform distribution. An approximate correction is derived. The work is extended to include the effects of finite particle response time by MacInnes and Bracco (1992b).

Squires and Eaton (1989, 1991), Elghobashi (1991), and Elghobashi and Truesdell (1991, 1992, 1993) have analyzed two-phase flows by direct numerical simulation (DNS) of isotropic homogeneous turbulent flows. Squires and Eaton used only Stokes drag as the force on the particle and considered both one-way and two-way couplings of the two phases with

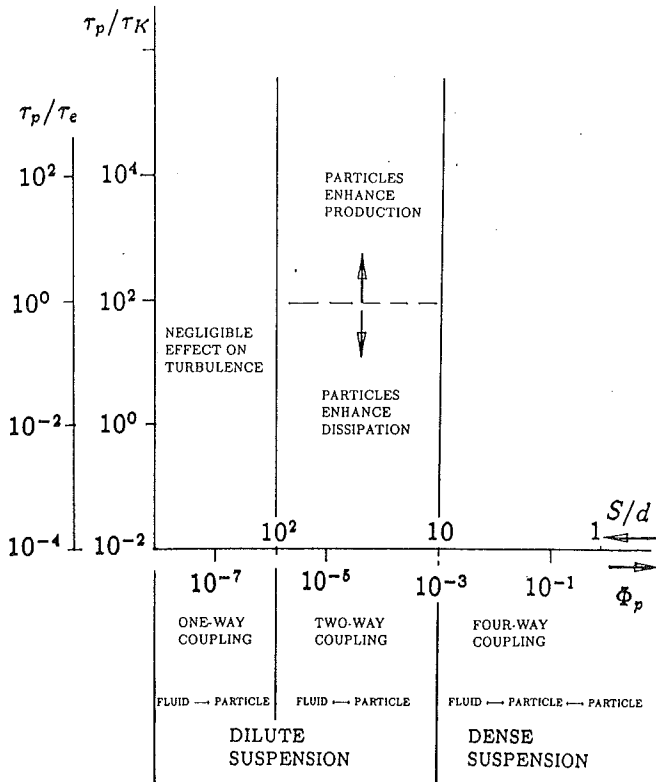


Fig. 33 Map of flow regimes in turbulent particle-laden flows from Elghobashi (1991)

regard to the turbulent field. Figure 33 from Elghobashi (1991) shows the domains of various types of coupling between the phases. The three parameters in the map are the ratio of the droplet kinematic response time to the Kolmogorov time scale, the ratio of the droplet response time to the integral time scale for turbulence, and the ratio of the average distance between neighboring droplets to the droplet diameter. The two time ratios are plotted on the ordinate while the length ratio is plotted on the abscissa. Volume fraction which is immediately determined from the length ratio is also shown. Elghobashi and Truesdell considered viscous and pressure drag, pressure gradient and viscous stress forces on the particle, Basset correction, gravity, and virtual mass. One-way coupling was considered by Elghobashi and Truesdell (1992) while two-way coupling was considered in their other papers (1991, 1993); the particles did not modify the turbulent field substantially for dilute flows. Lagrangian methods were employed to calculate particle trajectories. At zero gravity and short dispersion times, inertia caused particle diffusivity to exceed the fluid diffusivity. Both gravity and inertia reduced lateral dispersion. At low frequencies, particle energy remains higher than the fluid energy. Particle energy is lower than fluid energy in the mid-to-high frequency range. Drag and gravity tended to be the dominant forces. The Basset correction was the next largest force term but generally an order of magnitude smaller.

Some theoretical studies have been performed on time-dependent behavior within mixing layers and jets laden with particles or droplets. Generally, inviscid vortex methods for the dispersed phase are employed. Coupling between the hydrodynamics of the two phases is assumed to be one-way only. Chein and Chung (1987) emphasized the effects of vortex pairing in a mixing layer. The pairing was found to enhance the entrainment and dispersion of the particles. They found optimal dispersion in the mid-range of the Stokes number (ratio of particle aerodynamic response time to the flow characteristic time). Chung and Troutt (1988) extended the method to jet flows. They noted the importance of the large-scale component of turbulence in the dispersion process.

Interesting experimental work on particle dispersion in mixing layers has been performed by Lazaro and Lasheras (1989, 1992a, 1992b) for flows with and without acoustic forcing. In the unforced case, a similarity for particle dispersion independent of particle size is found if the coordinates are normalized by a length proportioned to a density ratio times a Reynolds number times a diameter. Both experimental and theoretical evidence from Lazaro and Lasheras (1989), Chung and Troutt (1988), Chein and Chung (1988), and others indicates that the dispersion of particles with high inertia can exceed that of passive scalars. This agrees with the previously cited DNS results for homogeneous turbulence.

Rangel (1990, 1992) extended the vortex method to consider heat transfer and vaporization of the droplets as well as dispersion. Vortex pairing was also considered in a planar, temporal mixing layer with one-way coupling. The larger droplets tended to be less sensitive to the vortical structure on account of their higher inertia. The smaller droplets were more easily entrained but tended to vaporize completely before vortex pairing had a significant effect. The gas temperature and vapor mass fraction fields were determined by finite-difference Eulerian computations with the droplets serving as sources and sinks. Vortex-dynamical methods were employed to calculate gas velocity while the droplet properties were calculated by Lagrangian discrete-particle methodology. The effects of droplet kinematic inertia were carefully examined. Figure 34 demonstrates the droplet motion and the vapor mass fraction contours in a case where three initially parallel droplet streams are moving through a temporally developing, two-dimensional mixing layer. Droplet and gas properties are averaged in the third dimension. Rangel and Continillo (1992) considered vaporization and ignition for the two-dimensional interaction of a viscous line vortex with a fuel droplet ring or cloud. The effects of chemical kinetic and vaporization parameters on the ignition delay time were determined. Bellan and Harstad (1992) recently modeled a cluster of droplets embedded in a vortical structure. The cluster and the vortex were assumed to convect together which differs from the previous studies. Centrifugal effects caused fuel vapor to accumulate in the vortex core.

In general, much remains to be determined about the modulation of both the mean flow and the turbulent fluctuations or vortical structures by the spray of droplets or cloud of particles. In different situations, the presence of droplets or particles can either enhance or reduce turbulence. More analyses with two-way coupling are necessary.

**5.2 Individual Droplet Behavior in a Turbulent Flow.** Relatively little research has been performed on the interaction of turbulent eddies with individual droplets or particles. An important parameter is the ratio of the turbulent length scale to the droplet diameter. Existing theories typically assume that the droplet is much smaller than the turbulent length scale; i.e.,  $Rk \ll 1$  for all values of the wavenumber  $k$  in the turbulence spectrum. In this limit, a quasi-uniform free stream is experienced by the droplet. Of course, temporal changes can still occur in the free stream. However, it can be shown that, for many flow devices that operate at high Reynolds number, the Kolmogorov scale actually becomes of the order of 100 microns and compares with the droplet size.

A second important parameter is the ratio of the characteristic time for change in the velocity fluctuation to the residence time for the gas (continuous phase) flow past the droplet. If  $U$  is the mean relative droplet velocity and  $u'$  is the velocity fluctuation of the gas, this ratio is given by  $U/u' Rk$ . For values of order unity or smaller, the flow over the droplet is unsteady. Only when the ratio is large compared to unity can the quasi-steady flow assumption be made. In that case and with  $Rk \ll 1$ , the values of the drag and lift coefficients and the Nusselt and Sherwood numbers are not affected by the tur-

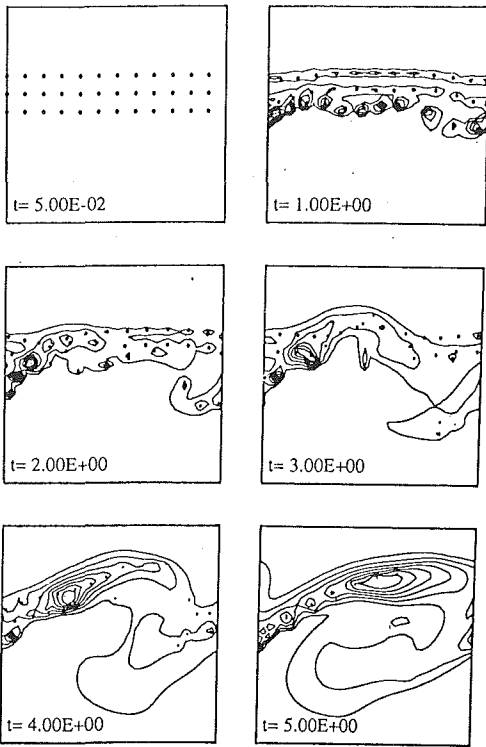


**Fig. 34 Temporal development of vapor mass fraction contours and droplet position with three droplet streams moving through a temporally developing two-dimensional mixing layer**

bulent flow. (Note that the aerodynamic forces and the transport rates would still be affected by the turbulent fluctuations.)

The conventional practice is to use certain corrections on the drag force for unsteadiness in the relative droplet velocity. Neglecting gravity, we can write

$$\frac{4\pi}{3}\rho_1 R^3 \frac{du_p}{dt} = 6\pi\mu R(u - u_p) + \frac{2}{3}\pi\rho R^3 \left( \frac{du}{dt} - \frac{du_p}{dt} \right) + 6R^2\sqrt{\pi\rho\mu} \int_{t_0}^t \frac{\left( \frac{du}{dt} - \frac{du_p}{dt} \right)}{\sqrt{t-t'}} dt' \quad (93)$$

The second term is the apparent mass term that accounts for the inertia of the gas in the boundary layer and wake of the droplet. It is negligible when the gas density is much smaller than the liquid density (which is usually the case). The third term is the Bassett correction force; within the context of a low Reynolds number flow, it corrects for temporal variations in the relative velocity. It can be shown by an order of magnitude argument that this correction is negligible if the second (time ratio) parameter mentioned above is large compared to unity.

Equation (93) is seriously flawed for application to sprays in turbulent flows in spite of its extensive use. It does not account for situations with high wavenumber where  $Rk$  is of order unity or larger. It also requires correction for higher Reynolds number, correction for effects of vaporization and Stefan flow, and corrections for the proximity of other droplets. In the quasi-steady and quasi-uniform limit, these corrections have been discussed in Sections 2, 3, and 4. If values of both the first and second parameters are large, a nonuniform but quasi-steady flow is obtained. As discussed in Section 4, some studies of these three-dimensional flows have been made. However, in general, substantially more research is required here.

It should be understood that some velocity fluctuations in the wavenumber range where  $Rk$  is of order unity will be

generated at sufficiently high droplet Reynolds number. We can expect that vortex shedding of the flow over a droplet can occur producing eddies of a size of the same order of magnitude as the droplet.

Little research has been performed on convective heat and mass transport in turbulent spray flows. On account of its relevance to combustion instability in liquid-fueled and liquid-propellant systems, a substantial amount of research has been performed on the impact of long wavelength ( $Rk \ll 1$ ) fluctuations on a spray (Strahle, 1964, 1965a, 1965b, 1966; Priem, 1963; Priem and Heidmann, 1960; Heidmann and Wieber, 1965, 1966; Harrje and Reardon, 1972; Tong and Sirignano, 1989). The fluctuations of transport rates in this case with uniform but temporally varying free streams approaching the droplet has been found to be significant. Extension of these analyses to the high wavenumber domain is necessary to understand fully the behavior of sprays involved in heat and mass exchange with a turbulent flow.

## 6 Concluding Remarks

Engineering design can benefit from the advances of the past decade discussed in this review. For example, the models for droplet vaporization, heating, and acceleration can be added to existing codes. While droplet lifetimes do not vary substantially from one model to the next, the instantaneous vaporization and heating rates and the acceleration do vary significantly. Therefore, the trajectories and vapor concentration as a function of time and position within a flow chamber or flow field can vary substantially depending on the particular model. The accuracy of the model becomes more important in situations where multicomponent liquids are present, local heat losses to the walls must be predicted, or flammability limits in a combustion chamber must be predicted.

The spray formulations discussed in Section 3 provide mechanisms for developing scientific insight and for improvements in engineering analysis and design. Numerical errors can be diminished following the guidelines. Also, resolution can be optimized with consideration given to the various trade-offs. It still remains for issues of droplet interactions in dense sprays and of turbulence-droplet interactions to be completely included in the spray analysis. It is expected that, in the not-too-distant future, a fuller spectrum of these types of interactions can be addressed in the formulations of the spray equations to be used in practice.

The behavior of a spray flow has been shown to be complex and to involve many length and time scales. There are many distinct subdomains in the flow and many challenging analytical and computational issues. The topic of spray flow still requires more research. Some comments and suggestions on these needs follow.

There is a glaring lack of experimental data that resolves the flow in the boundary layer, wake, and internal liquid of a droplet. One promising development is the laser based technique (Melton and Winter, 1990) that demonstrates qualitatively the presence of the internal circulation of the droplets. It can provide the basis for further experimental developments. Recently, interesting non-intrusive liquid interior temperature measurements have been made by Wells and Melton (1990), Hanlon and Melton (1992), and Zhang and Melton (1993). There is qualitative agreement between theory and experiment on these measurements.

In all analyses and calculations to date, only spherical droplets have been considered. The more realistic situation is that the larger droplets (more precisely droplets with large Weber numbers) will distort and the solution requires the determination of the interface shape and location. Droplet distortion and possible break-up into smaller droplets is a problem of major practical importance, demanding substantial advances in computational methodologies. Droplet distortion results

when the surface-tension force becomes smaller than the pressure and shear forces on the droplet surface. The issue of the determination of the liquid-gas interface is one of the major analytical challenges in the field of nonlinear mechanics. In the extreme of droplet distortion, the issue of the droplet break-up into smaller droplets becomes important.

Another challenge concerns droplet vaporization at near-critical and supercritical pressures. The critical point for a mixture depends strongly upon the composition and critical pressure values can be greater for a mixture than for any of its components. Therefore, certain portions of the field can be supercritical while other portions are subcritical even when the pressure is uniform. Droplets can exist therefore even if the pressure is higher than the critical pressure for any of the gas or liquid components. These calculations are very sensitive to the approximations employed for the equation of state and for the thermodynamic properties. A limited number of studies at spherically symmetric conditions exist but extensive study of the axisymmetric droplet and of the spray situation are needed.

The surface tension becomes greatly reduced as the critical point is approached; therefore, the near-critical behavior is complicated by the distortion of the droplet shape. Also, ambient gases more readily dissolve in the liquid as the critical point is reached. The liquid phase becomes multicomponent and liquid-phase mass diffusion becomes important.

More than one species can be present in the liquid phase either on account of initial conditions or due to absorption from the gas phase. In such cases, the liquid-phase mass diffusion must be considered through species-continuity equations for the liquid. In addition, a phase-equilibrium interface condition is required for each liquid component. The major computational complication is not the addition of another equation but rather the addition of a new and longer characteristic time. The Lewis number for a common liquid is typically greater than ten. Therefore, finer spatial and temporal resolution is required for the liquid phase when mass diffusion becomes important there.

One of the computational challenges before us involves the study of split operators that will expedite these spray calculations wherein the liquid-phase characteristic time can be much larger than the gas-phase times. The liquid-phase calculations could be performed with larger time steps than for the gas-phase calculations.

Another challenge relates to the nucleation of vapor within the droplet. This internal gasification becomes possible with a multicomponent mixture when the phase equilibrium at some internal point yields a vapor pressure (for a given local temperature and liquid composition) that exceeds the total pressure at the point of nucleation. This gasification, at the extreme, could result in a destruction of the droplet into smaller droplets. In order to analyze this gasification and microexplosion, the ability to treat moving nonspherical boundaries must be developed. Even then, the phenomenon might occur on such a fine scale that subgrid modeling is required.

Another interesting challenge involves slurry droplets wherein solid particles exist in the liquid. Often, small metal or coal particles are mixed with liquid fuels to obtain very high energy densities. These particles have kinematic and thermal inertias so that momentum and energy exchanges with the liquid are nontrivial.

One important need is to address further corrections with the point-source approximation. First, correction is needed in the dense spray situation where total liquid volume in a given domain is not negligible compared to the gas volume. Second, the correct application of the ambient conditions for the subgrid droplet model must be pursued.

The full two-way coupling of turbulent gas flows with the spray must be studied further. Only limited studies of this important interaction have been made. Another key problem

in certain applications involves the distortion, shattering, or coalescence of droplets. Spray calculation methodology should be developed to treat this phenomenon. While some studies of radiative heating of a spray have been performed, there is a need for further study.

Other interesting extensions involve three-dimensional configurations and highly compressible (including supersonic) gas behavior. Little or nothing has been analyzed for sprays in these situations.

Typically, liquid is injected as a jet to form the spray. Our current analytical capability allows only for the prescription of some upstream boundary conditions giving initial droplet sizes and velocities. There is a major need to develop a predictive capability for the primary atomization process. This would allow for the analysis of the spray formation processes.

Another major challenge involves our capability to determine spacing between neighboring droplets in a computationally efficient manner. Currently, the only clear option is to scan the positions of all droplets in a calculation and, thereby, tediously determine minimum distances. This tedious route has not been followed in practice. The need exists in a dense spray to determine these spacings since the droplet drag, lift, torque, heating rate, and vaporization rate will depend upon this spacing.

## Acknowledgments

Interactions over the past two decades with ten postdoctoral associates and fourteen graduate students on the subject of sprays have been very productive, stimulating, and instructive. Nearly all of these junior collaborators are identified in the references. Exciting interactions with senior collaborators are also recognized; Drs. H. A. Dwyer, S. E. Elghobashi, G. J. Fix, B. R. Sanders, E. Suuberg, and S. C. Yao are identified here. Several federal funding agencies and industrial organizations have been supportive of my spray research; special recognition for continuing support goes to Dr. Julian Tishkoff of AFOSR and Dr. Gabriel Roy of ONR. Ms. Sue Kanda and Ms. Lisa Rehbaum are acknowledged for their outstanding word processing efforts. Finally, the ASME Fluids Engineering Division and the Freeman Scholar Award Committee are thanked for their support of the exercise that resulted in this review paper.

## References

- Abramzon, B., and Sirignano, W. A., 1989, "Droplet Vaporization Model for Spray Combustion Calculations," *International Journal of Heat and Mass Transfer*, Vol. 32, pp. 1605-1618.
- Acritov, A., and Taylor, T. D., 1962, "Heat and Mass Transfer from Single Spheres in Stokes Flow," *Physics of Fluids*, Vol. 5, pp. 387-394.
- Acritov, A., and Goddard, J., 1965, "Asymptotic Expansion for Laminar Forced Convection Heat and Mass Transfer," *Journal of Fluid Mechanics*, Vol. 23, pp. 273-291.
- Aggarwal, S. K., Lee, D. N., Fix, G. J., and Sirignano, W. A., 1981, "Numerical Computation of Fuel Air Mixing in a Two-Phase Axisymmetric Coaxial Free Jet Flow," *Proceedings Fourth IMACS Int'l. Symposium on Computer Methods for Partial Differential Equations*, IMACS.
- Aggarwal, S. K., Fix, G. J., Lee, D. N., and Sirignano, W. A., 1983, "Numerical Optimization Studies of Axisymmetric Unsteady Sprays," *Journal of Computational Physics*, Vol. 50, pp. 101-115.
- Aggarwal, S. K., and Sirignano, W. A., 1984, "Numerical Modeling of One-Dimensional Enclosed Homogeneous and Heterogeneous Deflagrations," *Computer and Fluids*, Vol. 12, pp. 145-158.
- Aggarwal, S. K., Tong, A. Y., and Sirignano, W. A., 1984, "A Comparison of Vaporization Models in Spray Calculations," *AIAA Journal*, Vol. 22, pp. 1448-1457.
- Aggarwal, S. K., Fix, G. J., and Sirignano, W. A., 1985, "Two-Phase Laminar Axisymmetric Jet Flow: Explicit, Implicit, and Split-Operator Approximations," *Numerical Methods in Partial Differential Equations*, Vol. 1, pp. 279-294.
- Aggarwal, S. K., and Sirignano, W. A., 1985a, "Ignition of Fuel Sprays: Deterministic Calculations for Idealized Droplet Arrays," *Twentieth Symposium (International) on Combustion*, The Combustion Institute, pp. 1773-1780.
- Aggarwal, S. K., and Sirignano, W. A., 1985b, "Unsteady Spray Flame Propagation in a Closed Volume," *Combustion and Flame*, Vol. 62, pp. 69-84.

- Aggarwal, S. K., and Sirignano, W. A., 1986, "An Ignition Study of Polydisperse Sprays," *Combustion Science and Technology*, Vol. 46, pp. 289-300.
- Aggarwal, S. K., 1987, "Modeling of Multicomponent Fuel Spray Vaporization," *International Journal of Heat and Mass Transfer*, Vol. 30, pp. 1949-1961.
- Aggarwal, S. K., 1988, "Ignition Behavior of a Dilute Multicomponent Fuel Spray," AIAA 26th Aerospace Sciences Meeting, Paper 88-0635.
- Annamalai, K., and Ryan, W., 1992, "Interactive Processes in Gasification and Combustion. Part I: Liquid Drop Arrays and Clouds," *Progress in Energy Combustion and Science*, Vol. 18, pp. 221-295.
- Asano, K., Taniguchi, I., and Kawahara, T., 1988, "Numerical and Experimental Approaches to Simultaneous Vaporization of Two Adjacent Volatile Drops," *Proceedings of the 4th International Conference on Liquid Atomization and Sprays*, pp. 411-418.
- Batchelor, G. K., and Green, J. T., 1972, "The Hydrodynamic Interaction of Two Small Freely-moving Spheres in a Linear Flow Field," *Journal of Fluid Mechanics*, Vol. 56, pp. 375-400.
- Batchelor, G. K., 1990, *An Introduction to Fluid Dynamics*, Cambridge University Press.
- Bellan, J., and Cuffel, R., 1983, "A Theory of Non-dilute Spray Evaporation Based Upon Multiple Drop Interactions," *Combustion and Flame*, Vol. 51, pp. 55-67.
- Bellan, J., and Harstad, K., 1987, "Analysis of the Convective Evaporation of Non-dilute Clusters of Drops," *International Journal of Heat and Mass Transfer*, Vol. 30, pp. 125-136.
- Bellan, J., and Harstad, K., 1988, "Turbulence Effects During Evaporation of Drops in Clusters," *International Journal of Heat and Mass Transfer*, Vol. 31, pp. 1655-1668.
- Bellan, J., and Harstad, K., 1992, "Evaporation of Steadily Injected, Identical Clusters of Drops Embedded in Jet Vortices," *Twenty-Fourth Symposium (International) on Combustion*, Poster Session.
- Berlemon, A., Grancher, M., and Gousset, G., 1991, "On the Lagrangian Simulation of Turbulence Influence on Droplet Evaporation," *International Journal of Heat and Mass Transfer*, Vol. 34, pp. 2805-2812.
- Bhatia, R., and Sirignano, W. A., 1991, "A One-Dimensional Analysis of Liquid-Fueled Combustion Instability," *Journal of Propulsion and Power*, Vol. 7, pp. 953-961.
- Borghi, R., and Loison, S., 1992, "Studies of Dense Sprays Combustion by Numerical Simulation with a Cellular Automaton," *Twenty-Fourth Symposium (International) on Combustion*, The Combustion Institute, in press.
- Bracco, F. V., 1985, "Modeling of Engine Sprays," SAE Preprint 850394.
- Chein, R., and Chung, J. N., 1987, "Effects of Vortex Pairing on Particle Dispersion in Turbulent Shear Flows," *International Journal of Multiphase Flow*, Vol. 13, pp. 785-802.
- Chein, R., and Chung, J. N., 1988, "Simulation of Particle Dispersion in a Two-Dimensional Mixing Layer," *AIChE Journal*, Vol. 34, pp. 946-954.
- Chen, Z. H., Lin, T. H., and Sohrab, S. H., 1988, "Combustion of Liquid Fuel Sprays in Stagnation-Point Flow," *Combustion Science and Technology*, Vol. 60, pp. 63-77.
- Chiang, C. H., 1990, "Isolated and Interacting, Vaporizing Fuel Droplets: Field Calculation with Variable Properties," Ph.D. dissertation, University of California, Irvine.
- Chiang, C. H., and Sirignano, W. A., 1991, "Axisymmetric Vaporizing Oxygen Droplet Computations," Preprint 91-0281, AIAA 29th Aerospace Sciences Meeting, Reno, NV.
- Chiang, C. H., Raju, M. S., and Sirignano, W. A., 1992, "Numerical Analysis of Convecting, Vaporizing Fuel Droplet with Variable Properties," *International Journal of Heat and Mass Transfer*, Vol. 35, pp. 1307-1324.
- Chiang, C. H., and Sirignano, W. A., 1993a, "Interacting, Convecting, Vaporizing Fuel Droplets with Variable Properties," *International Journal of Heat and Mass Transfer*, in press.
- Chiang, C. H., and Sirignano, W. A., 1993b, "Axisymmetric Calculations of Three-Droplet Interactions," *Atomization and Sprays*, Vol. 3, pp. 91-107.
- Chigier, N. A., 1981, *Energy, Combustion, and Environment*, McGraw-Hill, New York.
- Chiu, H. H., and Liu, T. M., 1971, "Group Combustion of Liquid Droplets," *Combustion Science and Technology*, Vol. 17, pp. 127-131.
- Chiu, H. H., Kim, H. Y., and Croke, E. J., 1983, "Internal Group Combustion of Liquid Droplets," *Nineteenth Symposium (Int'l.) on Combustion*, The Combustion Institute, pp. 971-980.
- Chung, P. M., 1965, "Chemically Reacting Nonequilibrium Boundary Layers," *Advances in Heat Transfer*, Vol. 2, Hartnett, J. P., and Irvine, T. F., eds., Academic Press.
- Chung, J. N., Ayyaswamy, P. S., and Sadhal, S. S., 1984a, "Laminar Condensation on a Moving Drop. Part I. Singular Perturbation Technique," *Journal of Fluid Mechanics*, Vol. 139, pp. 105-130.
- Chung, J. N., Ayyaswamy, P. S., and Sadhal, S. S., 1984b, "Laminar Condensation on a Moving Drop. Part 2. Numerical Solutions," *Journal of Fluid Mechanics*, Vol. 139, pp. 131-144.
- Chung, J. N., and Troutt, T. R., 1988, "Simulation of Particle Dispersion in an Axisymmetric Jet," *Journal of Fluid Mechanics*, Vol. 186, pp. 199-227.
- Clift, R., Grace, J. R., and Weber, M. E., 1978, *Bubbles, Drops, and Particles*, Academic Press.
- Conner, J. M., and Elghobashi, S. E., 1987, "Numerical Solution of Laminar Flow Past a Sphere with Surface Mass Transfer," *Numerical Heat Transfer*, Vol. 122, pp. 57-82.
- Continillo, G., and Sirignano, W. A., 1988, "Numerical Study of Multicomponent Fuel Spray Flame Propagation in a Spherical Closed Volume," *Twenty-Second Symposium (International) on Combustion*, The Combustion Institute, pp. 1941-1949.
- Continillo, G., and Sirignano, W. A., 1990, "Counterflow Spray Combustion Modelling," *Combustion and Flame*, Vol. 81, pp. 325-340.
- Continillo, G., and Sirignano, W. A., 1991, "Unsteady, Spherically Symmetric Flame Propagation Through Multicomponent Fuel Spray Clouds," *Modern Research Topics in Aerospace Propulsion*, G. Angelino, L. DeLuca, and W. A. Sirignano, eds., Springer-Verlag.
- Crowe, C. T., Sharma, M. P., and Stock, D. E., 1977, "The Particle-Source-in Cell (PSI-CELL) Model for Gas-Droplet Flows," *ASME JOURNAL OF FLUIDS ENGINEERING*, Vol. 99, p. 325.
- Crowe, C. T., Chung, J. N., and Troutt, T. R., 1988, "Particle Mixing in Free Shear Flows," *Progress in Energy and Combustion Science*, Vol. 14, pp. 171-199.
- Crowe, C. T., 1978, "On the Vapor Droplet Flows Including Boundary Droplet Effects," *Two-Phase Transport and Reactor Safety*, Vol. 1, pp. 385-405.
- Crowe, C. T., 1982, "Numerical Models for Dilute Gas-Particle Flows," *ASME JOURNAL OF FLUIDS ENGINEERING*, Vol. 104, pp. 297-301.
- Dandy, D. S., and Dwyer, H. H., 1990, "A Sphere in Shear Flow at Finite Reynolds Number: Effect of Shear on Particle Lift, Drag, and Heat Transfer," *Journal of Fluid Mechanics*, Vol. 216, pp. 381-410.
- Delplanque, J.-P., Rangel, R. H., and Sirignano, W. A., 1990, "Liquid-Waste Incineration in a Parallel-Stream Configuration: Effect of Auxiliary Fuel," *Dynamics of Deflagrations and Reactive Systems: Heterogeneous Combustion, Progress in Astronautics and Aeronautics*, Vol. 132, AIAA, pp. 164-186.
- Delplanque, J.-P., and Rangel, R. H., 1991, "Droplet Stream Combustion in the Steady Boundary Layer Near a Wall," *Combustion Science and Technology*, Vol. 78, pp. 97-115.
- Delplanque, J.-P., and Sirignano, W. A., 1993, "Numerical Study of the Transient Vaporization of an Oxygen Droplet at Sub- and Super-critical Conditions," *International Journal of Heat and Mass Transfer*, in press.
- Dukowicz, J. K., 1980, "A Particle-Fluid Numerical Model for Liquid Sprays," *Journal of Computational Physics*, Vol. 35, pp. 229-253.
- Dwyer, H. A., and Sanders, B. R., 1984a, "Detailed Computation of Unsteady Droplet Dynamics," *Twenty-Sixth Symposium (International) on Combustion*, The Combustion Institute, pp. 1743-1749.
- Dwyer, H. A., and Sanders, B. R., 1984b, "Comparative Study of Droplet Heating and Vaporization at High Reynolds and Pecllet Numbers," *Dynamics of Flames and Reactive Systems, Progress in Astronautics and Aeronautics*, Vol. 95, AIAA, pp. 464-483.
- Dwyer, H. A., and Sanders, B. R., 1984c, "Droplet Dynamics and Vaporization with Pressure as a Parameter," ASME Winter Annual Meeting, paper 84-WA-HT-20.
- El-Wakil, M. M., Priem, R. J., Brikowski, H. J., Meyer, P. S., and Uyehara, O. A., 1956, "Experimental and Calculated Temperature and Mass Histories of Vaporizing Fuel Drop," NACA TN 2490.
- Elghobashi, S. E., and Abou-Arab, T. W., 1983, "A Two-Equation Turbulence Model for Two-Phase Flows," *The Physics of Fluids*, Vol. 26, pp. 931-938.
- Elghobashi, S. E., Abou-Arab, T., Rizk, M., and Mostafa, A., 1984, "Prediction of the Particle-Laden Jet with a Two-Equation Turbulence Model," *International Journal of Multiphase Flow*, Vol. 10, pp. 697-710.
- Elghobashi, S. E., and Truesdell, G. C., 1991, "On the Interaction Between Solid Particles and Decaying Turbulence," *Eighth Symposium on Turbulent Shear Flows*, Munich.
- Elghobashi, S. E., 1991, "Particle-Laden Turbulent Flows: Direct Simulation and Closure Models," *Applied Scientific Research*, Vol. 48, pp. 301-314.
- Elghobashi, S. E., and Truesdell, G. C., 1992, "Direct Simulation of Particle Dispersion in a Decaying Isotropic Turbulence," *Journal of Fluid Mechanics*, Vol. 242, pp. 655-706.
- Elghobashi, S. E., and Truesdell, G. C., 1993, "On the Two-Way Interaction Between Homogeneous Turbulence and Dispersed Solid Particles: Part I: Turbulence Modification," to appear in *Physics of Fluids*, Vol. A5.
- Faeth, G. M., 1983, "Evaporation and Combustion of Sprays," *Progress in Energy Combustion Science*, Vol. 9, pp. 1-76.
- Faeth, G. M., 1987, "Mixing, Transport, and Combustion in Sprays," *Progress in Energy and Combustion Science*, Vol. 13, pp. 293-345.
- Frossling, N., 1938, "Evaporation of Falling Drops," *Gelands Beitr. Geophys.*, Vol. 52, p. 170.
- Glassman, I., 1987, *Combustion*, 2nd edition, Academic Press.
- Gosman, A. D., and Ioannides, E., 1981, "Aspects of Computer Simulation of Liquid-fuelled Combustors," AIAA Preprint 81-0323.
- Hadamard, J. S., 1911, "Mouvement Permanent Lent d'une Sphere Liquide et Visqueuse dans Une Liquid Visqueuse," *C. R. Acad. Sci.*, Vol. 152, pp. 1735-1738.
- Hanlon, T. R., and Melton, L. A., 1992, "Exciplex Fluorescence Thermometry of Falling Hexadecane Droplets," *ASME Journal of Heat Transfer*, Vol. 114, pp. 450-457.
- Happel, J., and Brenner, H., 1965, *Low Reynolds Number Hydrodynamics*, Prentice Hall.
- Harper, J. F., and Moore, D. W., 1968, "The Motion of a Spherical Liquid Drop at High Reynolds Number," *Journal of Fluid Mechanics*, pp. 367-391.
- Harper, J. F., 1970, "Viscous Drag in Steady Potential Flow Past a Bubble," *Chemical Engineering Science*, Vol. 25, pp. 342-343.
- Harje, D. T., and Reardon, F. H., editors, 1972, *Liquid Propellant Rocket Combustion Instability*, NASA SP194, Government Printing Office.

- Haywood, R. J., and Renksizbulut, M., 1986, "On Variable Property, Blowing and Transient Effects in Convective Droplet Evaporation with Internal Circulation," *Proceedings of the Eighth International Heat Transfer Conference*, pp. 1861-1866.
- Haywood, R. J., Nafziger, N., and Renksizbulut, M., 1989, "A Detailed Examination of Gas and Liquid Phase Transient Processes in Convective Droplet Evaporation," *ASME Journal of Heat Transfer*, Vol. 111, pp. 495-502.
- Heidmann, M. F., and Wieber, P. R., 1965, "Analysis of n-heptane Vaporization in Unstable Combustor with Travelling Transverse Oscillations," NASA TN-3424.
- Heidmann, M. F., and Wieber, P. R., 1966, "Analysis of Frequency Response Characteristics of Propellant Vaporization," NASA TM-X-52195.
- Hinze, J. O., 1972, "Turbulent and Fluid Particle Interaction," *Progress in Heat and Mass Transfer*, Vol. 6, pp. 433-452.
- Hinze, J. O., 1975, *Turbulence*, McGraw-Hill.
- Howarth, L. (ed.), 1964, *Modern Developments in Fluid Dynamics-High Speed Flow*, Vol. 1, Clarendon Press.
- Ingebo, R. D., 1956, "Drag Coefficients for Droplets and Solid Spheres in Clouds Accelerating in Airstreams," NACA Technical Note 3762.
- Jeffrey, D. J., and Onishi, Y., 1984, "Calculation of the Resistance and Mobility Functions for Two Unequal Rigid Spheres in Low Reynolds Flow," *Journal of Fluid Mechanics*, Vol. 139, pp. 261-290.
- Jiang, Y. J., Umemura, A., and Law, C. K., 1992, "An Experimental Investigation on the Collision Behaviour of Hydrocarbon Droplets," *Journal of Fluid Mechanics*, Vol. 234, pp. 171-190.
- Johns, L. E., and Beckman, R. B., 1966, "Mechanism of Dispersed-Phase Mass Transfer in Viscous, Single-Drop Extraction System," *AICHE Journal*, Vol. 12, pp. 10-16.
- Kanury, A. M., 1975, *Introduction to Combustion Phenomena*, Gordon and Breach, New York.
- Kim, I., Elghobashi, S. E., and Sirignano, W. A., 1992, "Three-Dimensional Flow Computation for Two Interacting, Moving Droplets," Preprint 92-0343, AIAA 30th Aerospace Sciences Meeting, Reno, NV.
- Kim, I., Elghobashi, S. E., and Sirignano, W. A., 1993, "Three-Dimensional Flow Over Two Spheres Placed Side-by-Side," *Journal of Fluid Mechanics*, Vol. 246, pp. 465-488.
- Kleinstreuer, C., Chiang, H., and Wang, Y. Y., 1989, "Mathematical Modelling of Interacting Vaporizing Fuel Droplets," *Heat Transfer Phenomena in Radiation, Combustion and Fire*, Vol. 106, ASME Heat Transfer Division, pp. 469-477.
- Kuo, K. K., 1986, *Principles of Combustion*, John Wiley and Sons.
- Labowsky, M., 1978, "A Formalism for Calculating the Evaporation Rates of Rapidly Evaporating Interacting Particles," *Combustion Science and Technology*, Vol. 18, pp. 145-151.
- Labowsky, M., and Rosner, D. C., 1978, "Group Combustion of Droplets in Fuel Clouds. I. Quasi-steady Predictions," *Evaporation-Combustion of Fuels*, J. T. Zung, ed., *Advances in Chemistry Series*, Vol. 166, pp. 63-79.
- Labowsky, M., 1980, "Calculation of Burning Rates of Interacting Fuel Droplets," *Combustion Science and Technology*, Vol. 22, pp. 217-226.
- Landau, L. D., and Lifshitz, E. M., 1987, *Fluid Mechanics*, 2nd Edition, Pergamon Press.
- Lamb, Sir H., 1945, *Hydrodynamics*, Dover.
- Landis, R. B., and Mills, A. F., 1974, "Effects of Internal Diffusional Resistance on the Vaporization of Binary Droplets," Paper B7.9, *Fifth Int. Heat Transfer Conf.*, Tokyo, Japan.
- Lara-Urbaneja, P., and Sirignano, W. A., 1981, "Theory of Transient Multicomponent Droplet Vaporization in a Convective Field," *Eighteenth Symposium (Intl.) on Combustion*, The Combustion Institute, pp. 1365-1374.
- Law, C. K., 1976, "Unsteady Droplet Combustion with Droplet Heating," *Combustion and Flame*, Vol. 26, pp. 17-22.
- Law, C. K., Prakash, S., and Sirignano, W. A., 1977, "Theory of Convective, Transient, Multicomponent Droplet Vaporization," *Sixteenth Symposium (Int'l.) Combust.*, The Combustion Institute, pp. 605-617.
- Law, C. K., and Sirignano, W. A., 1977, "Unsteady Droplet Combustion With Droplet Heating II: Conduction Limit," *Combustion and Flame*, Vol. 28, pp. 175-186.
- Law, C. K., 1982, "Recent Advances in Droplet Vaporization and Combustion," *Progress Energy Combustion Science*, Vol. 8, pp. 171-201.
- Lazaro, B. J., and Lasheras, J. C., 1989, "Particle Dispersion in a Turbulent, Plane, Free Shear Layer," *Physics of Fluids*, Vol. A1, pp. 1035-1044.
- Lazaro, B. J., and Lasheras, J. C., 1992a, "Particle Dispersion in the Developing Free Shear Layer. Part 1. Unforced Flow," *Journal of Fluid Mechanics*, Vol. 235, pp. 143-178.
- Lazaro, B. J., and Lasheras, J. C., 1992b, "Particle Dispersion in the Developing Free Shear Layer. Part 2. Forced Flow," *Journal of Fluid Mechanics*, Vol. 235, pp. 179-221.
- Lefebvre, A. H., 1989, *Atomization and Sprays*, Hemisphere.
- Lees, L., 1956, "Laminar Heat Transfer Over Blunt-Nosed Bodies at Hypersonic Flight Speeds," *Jet Propulsion*, Vol. 26, pp. 259-269.
- Levich, V. G., 1962, *Physicochemical Hydrodynamics*, Prentice Hall.
- Li, S. C., Libby, P. A., and Williams, F. A., 1992, "Experimental and Theoretical Studies of Counterflow Spray Diffusion Flames," *Twenty-Fourth Symposium (International) on Combustion*, The Combustion Institute, in press.
- MacInnes, J. M., and Bracco, F. V., 1992a, "Stochastic Particle Dispersion Modelling and the Tracer-Particle Limit," *Physics of Fluids*, A (in press).
- MacInnes, J. M., and Bracco, F. V., 1992b, "A Stochastic Model of Turbulent Drop Dispersion in Dilute Sprays," ILASS-Europe Conference, Amsterdam.
- Megaridis, C. M., and Sirignano, W. A., 1991, "Numerical Modelling of a Vaporizing Multicomponent Droplet," *Twenty-Third Symposium (International) on Combustion*, The Combustion Institute, pp. 1413-1421.
- Megaridis, C. M., and Sirignano, W. A., 1992, "Multicomponent Droplet Vaporization in a Laminar Convecting Environment," *Combustion Science and Technology*, Vol. 87, pp. 27-44.
- Melton, L. A., and Winter, M., 1990, "Measurement of Internal Circulation in Droplets Using Laser-Induced Fluorescence," *Applied Optics*, Vol. 29, pp. 4574-4577.
- Molavi, K., and Sirignano, W. A., 1988, "Computational Analysis of Acoustic Instabilities in Dump Combustor Configurations," Preprint 88-2856, AIAA/ASME 24th Joint Propulsion Conference, Boston, MA.
- Mostafa, A. A., and Elghobashi, S. E., 1985a, "A Two-Equation Turbulence Model for Jet Flows Laden with Vaporizing Droplets," *International Journal of Multiphase Flow*, Vol. 11, pp. 515-533.
- Mostafa, A. A., and Elghobashi, S. E., 1985b, "A Study of the Motion of Vaporizing Droplets in a Turbulent Flow," *Dynamics of Flames and Reactive Systems, Progress in Astronautics and Aeronautics*, Vol. 95, J. R. Bowen, N. Mason, A. K. Oppenheim, R. I. Soloukhin, eds., pp. 513-529.
- Mostafa, A. A., and Mongia, H. C., 1988, "On the Interaction of Particles and Turbulent Fluid Flow," *International Journal of Heat and Mass Transfer*, Vol. 31, pp. 2063-2075.
- Mostafa, A. A., Mongia, H. C., McDonell, V. G., and Samuels, G. S., 1989, "Evolution of Particle Laden Jet Flows: A Theoretical and Experimental Study," *AIAA Journal*, Vol. 27, pp. 167-183.
- Naber, J. D., and Reitz, R. D., 1988, "Modelling Engine Spray/Wall Impingement," Preprint 88-0107, SAE Congress and Exposition, Detroit, Feb. 29-Mar. 4.
- Nguyen, Q. V., and Dunn-Rankin, D., 1992, "Experiments Examining Drag in Linear Droplet Packets," *Experiments in Fluids*, Vol. 12, pp. 157-165.
- Nguyen, Q. V., Kangel, R. H., and Dunn-Rankin, D., 1991, "Measurement and Prediction of Trajectories and Collision of Droplets," *International Journal of Multiphase Flow*, Vol. 17, pp. 159-177.
- O'Rourke, P. J., and Bracco, F. V., 1980, "Modeling of Drop Interactions in Thick Sprays and a Comparison with Experiments," Stratified Charge Automotive Engines Conference, The Institution of Mechanical Engineers.
- Patnaik, G., Sirignano, W. A., Dwyer, H. A., and Sanders, B. R., 1986, "A Numerical Technique for the Solution of a Vaporizing Fuel Droplet," *Dynamics of Reactive Systems, Progress in Astronautics and Aeronautics*, Vol. 105, AIAA, pp. 253-266.
- Patnaik, G., and Sirignano, W. A., 1986, "Axisymmetric, Transient Calculation for Two Vaporizing Fuel Droplets," Western States Section/Combustion Institute Technical Meeting, Banff, Alberta, Canada.
- Prakash, S., and Sirignano, W. A., 1978, "Liquid Fuel Droplet Heating with Internal Circulation," *International Journal of Heat and Mass Transfer*, Vol. 21, pp. 885-895.
- Prakash, S., and Sirignano, W. A., 1980, "Theory of Convective Droplet Vaporization with Unsteady Heat Transfer in the Circulating Liquid Phase," *International Journal of Heat and Mass Transfer*, Vol. 23, pp. 253-268.
- Priem, R. J., and Heidmann, M. F., 1960, "Propellant Vaporization as a Design Criterion for Rocket Engine Combustion Chambers," NASA Report TR-R67.
- Priem, R. J., 1963, "Theoretical and Experimental Models of Unstable Rocket Combustors," *Ninth Symposium (International) on Combustion*, The Combustion Institute, pp. 982-992.
- Raju, M. S., and Sirignano, W. A., 1989, "Spray Computations in a Centerbody Combustor," *ASME Journal of Engineering for Gas Turbines and Power*, Vol. 111, pp. 710-718.
- Raju, M. S., and Sirignano, W. A., 1990a, "Multicomponent Spray Computations in a Modified Centerbody Combustor," *Journal of Propulsion and Power*, Vol. 6, pp. 97-105.
- Raju, M. S., and Sirignano, W. A., 1990b, "Interaction Between Two Vaporizing Droplets in an Intermediate-Reynolds-Number-Flow," *Physics of Fluids*, Vol. 2, pp. 1780-1796.
- Rangel, R. H., and Fernandez-Pello, A. C., 1984, "Mixed Convective Droplet Combustion with Internal Circulation," *Combustion Science and Technology*, Vol. 42, pp. 47-65.
- Rangel, R. H., and Sirignano, W. A., 1986, "Rapid Vaporization and Heating of Two Parallel Fuel Droplet Streams," *Twenty-First Symposium (International) on Combustion*, The Combustion Institute, pp. 617-624.
- Rangel, R. H., and Sirignano, W. A., 1988a, "Unsteady Flame Propagation in a Spray with Transient Droplet Vaporization," *Twenty-Second Symposium (International) on Combustion*, The Combustion Institute, pp. 1931-1939.
- Rangel, R. H., and Sirignano, W. A., 1988b, "Two-Dimensional Modeling of Flame Propagation in Fuel Stream Arrangements," *Dynamics of Reactive Systems Part II: Heterogeneous Combustion and Applications*, A. L. Kuhl, J. R. Bowen, J. S. Leyfer and A. Borisov, eds., *Progress in Astronautics and Aeronautics*, Vol. 113, AIAA, pp. 128-150.
- Rangel, R. H., and Sirignano, W. A., 1989a, "Combustion of Parallel Fuel Droplet Streams," *Combustion and Flame*, Vol. 75, pp. 241-254.
- Rangel, R. H., and Sirignano, W. A., 1989b, "An Evaluation of the Point-Source Approximation in Spray Calculations," *Numerical Heat Transfer, Part A*, Vol. 16, pp. 37-57.
- Rangel, R. H., 1990, "Spray Entrainment and Mixing in a Temporally-Growing Shear Layer," ASME Winter Annual Meeting, HTD 148, pp. 11-18.
- Rangel, R. H., and Sirignano, W. A., 1991, "Spray Combustion in Idealized Configurations: Parallel Droplet Streams," *Numerical Approaches to Com-*

- bustion Modeling, Progress in Astronautics and Aeronautics*, Vol. 135, E. S. Oran and J. P. Boris, eds., pp. 585-613.
- Rangel, R. H., 1992, "Heat Transfer in Vertically Enhanced Mixing of Vaporizing Droplet Sprays," *Annual Review of Heat Transfer*, Vol. 4, C. L. Tien, ed., Hemisphere, pp. 331-362.
- Rangel, R. H., and Continillo, G., 1992, "Theory of Vaporization and Ignition of a Droplet Cloud in the Field of a Vortex," *Twenty-Fourth Symposium (International) on Combustion*, The Combustion Institute (in press).
- Ranz, W. E., and Marshall, W. R., 1952, "Evaporation from Drops," *Chemical Engineering Progress*, Vol. 48, pp. 141-146 and pp. 173-180.
- Reitz, R. D., 1987, "Modeling Atomization Processes in High-Pressure Vaporizing Sprays," *Atomisation and Spray Technology*, Vol. 3, pp. 309-337.
- Renksizbulut, M., and Haywood, R. J., 1988, "Transient Droplet Evaporation With Variable Properties and Internal Circulation at Intermediate Reynolds Numbers," *International Journal of Multiphase Flow*, Vol. 14, pp. 189-202.
- Renksizbulut, M., and Yuen, M. C., 1983, "Experimental Study of Droplet Evaporation in High Temperature Air Stream," *ASME Journal of Heat Transfer*, Vol. 105, pp. 384-388.
- Rizk, M. A., and Eighobashi, S. E., 1985, "The Motion of a Spherical Particle Suspended in a Turbulent Flow Near a Plane Wall," *The Physics of Fluids*, Vol. 28, pp. 806-817.
- Rizk, M. A., and Elghobashi, S. E., 1989, "A Two-Equation Turbulence Model for Dispersed Dilute Confined Two-Phase Flows," *International Journal of Multiphase Flow*, Vol. 15, pp. 119-133.
- Ryan, W., Annamalai, K., and Caton, J., 1990, "Relation Between Group Combustion and Drop Array Studies," *Combustion and Flame*, Vol. 80, pp. 313-321.
- Rybczynski, W., 1911, "On the Translatory Motion of a Fluid Sphere in a Viscous Medium," *Bull. Int. Acad. Pol. Sci., Lett. A. Sci. Math. Natur. Series A*, pp. 40-46.
- Sangiovanni, J. J., and Kesten, A. S., 1976, "Effect of Droplet Interaction on Ignition in Monodispersed Droplet Streams," *Sixteenth Symposium (International) on Combustion*, The Combustion Institute, pp. 577-592.
- Seth, B., Aggarwal, S. K., and Sirignano, W. A., 1978, "Flame Propagation Through an Air-Fuel Spray with Transient Droplet Vaporization," *Combustion and Flame*, Vol. 32, pp. 257-270.
- Sherman, F. S., 1990, *Viscous Flow*, McGraw-Hill.
- Shuen, J. S., Yang, V., and Hsiao, C. C., 1992, "Combustion of Liquid Fuel Droplets in Supercritical Conditions," *Combustions and Flame*, Vol. 89, pp. 299-319.
- Sirignano, W. A., 1972, "Introduction to Analytical Models of High Frequency Combustion Instability," *Liquid Propellant Rocket Combustion Instability*, D. T. Harrje and F. H. Reardon, eds., NASA SP194, U.S. Government Printing Office.
- Sirignano, W. A., and Law, C. K., 1978, "Transient Heating and Liquid Phase Mass Diffusion in Droplet Vaporization," *Evaporation-Combustion of Fuels*, J. T. Zung, ed., *Adv. in Chemistry Series 166*, ACS, pp. 1-26.
- Sirignano, W. A., 1979, "Theory of Multicomponent Fuel Droplet Vaporization," *Archives of Thermodynamics and Combustion*, Vol. 9, pp. 235-251.
- Sirignano, W. A., 1983, "Fuel Droplet Vaporization and Spray Combustion," *Progress Energy Combustion Science*, Vol. 9, pp. 291-322.
- Sirignano, W. A., 1985a, "Spray Combustion Simulation," *Numerical Simulation Combustion Phenomena*, R. Glowinski, B. Larroutrou, and R. Teman, eds., Springer-Verlag, Heidelberg.
- Sirignano, W. A., 1985b, "Linear Model of Convective Heat Transfer in a Spray," *Recent Advances in Aerospace Science*, C. Casci, ed., Plenum Press.
- Sirignano, W. A., 1986, "The Formulation of Spray Combustion Models: Resolution Compared to Droplet Spacing," *ASME Journal of Heat Transfer*, Vol. 108, pp. 633-639.
- Sirignano, W. A., 1988, "An Integrated Approach to Spray Combustion Model Development," *Combustion Science and Technology*, Vol. 58, No. 1-3, pp. 231-251.
- Sirignano, W. A., 1993, "Computational Spray Combustion," *Numerical Modeling in Combustion*, T. J. Chung, ed., Hemisphere Publications, in press.
- Squires, K. D., and Eaton, J. K., 1989, "Study of the Effects of Particle Loading on Homogeneous Turbulence Using Direct Numerical Simulation," *Proceedings International Symposium on Turbulence Modification in Dispersed Multiphase Flows*, San Diego, CA.
- Squires, K. D., and Eaton, J. K., 1991, "Preferential Concentration of Particles by Turbulence," *Physics of Fluids A*, Vol. 3, pp. 1169-1178.
- Strahle, W. C., 1964, "Periodic Solutions to a Convective Droplet Burning Problem: the Stagnation Point," *Tenth Symposium (International) on Combustion*, The Combustion Institute, pp. 1315-1325.
- Strahle, W. C., 1965a, "Unsteady Reacting Boundary Layer on a Vaporizing Flat Plate," *AIAA Journal*, Vol. 3, pp. 1195-1198.
- Strahle, W. C., 1965b, "Unsteady Laminar Jet Flames at Large Frequencies of Oscillation," *AIAA Journal*, Vol. 3, pp. 957-960.
- Strahle, W. C., 1966, "High Frequency Behavior of the Laminar Jet Flame Subjected to Transverse Sound Waves," *Eleventh Symposium (International) on Combustion*, The Combustion Institute, pp. 747-754.
- Sundararajan, T., and Ayyaswamy, P. S., 1984, "Hydrodynamics and Heat Transfer Associated with Condensation on a Moving Drop: Solutions for Intermediate Reynolds Number," *Journal of Fluid Mechanics*, Vol. 149, pp. 33-58.
- Suzuki, T., and Chiu, H. H., 1971, "Multi Droplet Combustion on Liquid Propellants," *Proc. Ninth International Symposium on Space Technology and Science*, AGNE Publishing Co., Tokyo, Japan, pp. 145-154.
- Tal, R., and Sirignano, W. A., 1982, "Cylindrical Cell Model for the Hydrodynamics of Particle Assemblages at Intermediate Reynolds Numbers," *AIChE Journal*, Vol. 28, pp. 233-237.
- Tal, R., Lee, D. M., and Sirignano, W. A., 1983, "Hydrodynamics and Heat Transfer in Sphere Assemblages-Cylindrical Cell Models," *International Journal of Heat and Mass Transfer*, Vol. 26, pp. 1265-1273.
- Tal, R., Lee, D. N., and Sirignano, W. A., 1984a, "Periodic Solutions of Heat Transfer for Flow Through a Periodic Assemblage of Spheres," *International Journal of Heat and Mass Transfer*, Vol. 27, pp. 1414-1417.
- Tal, R., Lee, D. A., and Sirignano, W. A., 1984b, "Heat and Momentum Transfer Around a Pair of Spheres in Viscous Flow," *International Journal of Heat and Mass Transfer*, Vol. 27, pp. 1953-1962.
- Talley, D. G., and Yao, S. C., 1986, "A Semi-Empirical Approach to Thermal and Composition Transients Inside Vaporizing Fuel Droplets," *Twenty-First Symposium (International) on Combustion*, The Combustion Institute, pp. 609-616.
- Temkin, S., and Ecker, G. Z., 1989, "Droplet Pair Interactions in a Shock-wave Flow Field," *Journal of Fluid Mechanics*, Vol. 202, pp. 467-497.
- Tomboulides, A. G., Orszag, S. A., and Karniadakis, G. E., 1991, "Three-dimensional Simulation of Flow Past a Sphere," *ISOPe Proceedings*, Edinburgh.
- Tong, A. Y., and Sirignano, W. A., 1982a, "Transient Thermal Boundary Layer in Heating of Droplet with Internal Circulation: Evaluation of Assumptions," *Combustion Science and Technology*, Vol. 11, pp. 87-94.
- Tong, A. Y., and Sirignano, W. A., 1982b, "Analytical Solution for Diffusion and Circulation in a Vaporizing Droplet," *Nineteenth Symposium (International) on Combustion*, The Combustion Institute, pp. 1007-1020.
- Tong, A. Y., and Sirignano, W. A., 1983, "Analysis of Vaporizing Droplet with Slip, Internal Circulation, and Unsteady Liquid-Phase and Quasi-Steady Gas-Phase Heat Transfer," *ASME-JSME Thermal Joint Engineering Conference*.
- Tong, A. Y., and Sirignano, W. A., 1986a, "Multicomponent Droplet Vaporization in a High Temperature Gas," *Combustion and Flame*, Vol. 66, pp. 221-235.
- Tong, A. Y., and Sirignano, W. A., 1986b, "Multicomponent Transient Droplet Vaporization with Internal Circulation: Integral Equation Formulation and Approximate Solution," *Numerical Heat Transfer*, Vol. 10, pp. 253-278.
- Tong, A. Y., and Chen, S. J., 1988, "Heat Transfer Correlations for Vaporizing Liquid Droplet Arrays in a High Temperature Gas at Intermediate Reynolds Number," *International Journal of Heat and Fluid Flow*, Vol. 9, pp. 118-130.
- Tong, A., and Sirignano, W. A., 1989, "Oscillatory Vaporization Fuel Droplets in Unstable Combustor," *Journal of Propulsion and Power*, Vol. 5, pp. 257-261.
- Tsai, J. S., and Sterling, A. M., 1990, "The Application of an Embedded Grid to the Solution of Heat and Momentum Transfer for Spheres in a Linear Array," *International Journal of Heat and Mass Transfer*, Vol. 33, pp. 2491-2502.
- Twardus, E. M., and Brzustowski, T. A., 1977, "The Interaction Between Two Burning Fuel Droplets," *Archiwum Processor Spalania*, Vol. 8, pp. 347-358.
- Umemura, A., Ogawa, A., and Oishiwa, N., 1981a, "Analysis of the Interaction Between Two Burning Droplets," *Combustion and Flame*, Vol. 41, pp. 45-55.
- Umemura, A., Ogawa, A., and Oishiwa, N., 1981b, "Analysis of the Interaction Between Two Burning Droplets with Different Sizes," *Combustion and Flame*, Vol. 43, pp. 111-119.
- Wells, M. R., and Melton, L. A., 1990, "Temperature Measurements of Falling Droplets," *ASME Journal of Heat Transfer*, Vol. 112, pp. 1008-1013.
- Williams, F. A., 1985, *Combustion Theory; The Fundamental Theory of Chemically Reacting Flow Systems*, Second Edition, Benjamin/Cummings, Menlo Park, CA.
- White, F. M., 1991, *Viscous Fluid Flow*, McGraw-Hill.
- Xiong, T. Y., Law, C. K., and Miyasaka, K., 1985, "Interactive Vaporization and Combustion of Binary Droplet System," *Twentieth Symposium (International) on Combustion*, The Combustion Institute, pp. 1781-1787.
- Zhang, J., and Melton, L. A., 1993, "Potential System Errors in Droplet Temperatures Obtained by Fluorescence Methods," *ASME Journal of Heat Transfer*, in press.